Jül-4286

Institute of Chemistry and Dynamics of the Geosphere (ICG)
Stratosphere (ICG-1)

Water and nitric acid in cirrus clouds: microphysical kinetical modeling and a closure to field observations

Iulia Gensch

Mitglied der Helmholtz-Gemeinschaft

JÜLICH
FORSCHUNGSZENTRUM

Water and nitric acid in cirrus clouds: microphysical kinetical modeling and a closure to field observations

Iulia Gensch

Berichte des Forschungszentrums Jülich; 4286
ISSN 0944-2952
Institute of Chemistry and Dynamics of the Geosphere (ICG)
Stratosphere (ICG-1) Jül-4286

D 5 (Diss., Bonn, Univ., 2008)

Vollständig frei verfügbar im Internet auf dem Jülicher Open Access Server (JUWEL) unter
http://www.fz-juelich.de/zb/juwel

Zu beziehen durch: Forschungszentrum Jülich GmbH · Zentralbibliothek, Verlag
D-52425 Jülich · Bundesrepublik Deutschland
☎ 02461 61-5220 · Telefax: 02461 61-6103 · e-mail: zb-publikation@fz-juelich.de

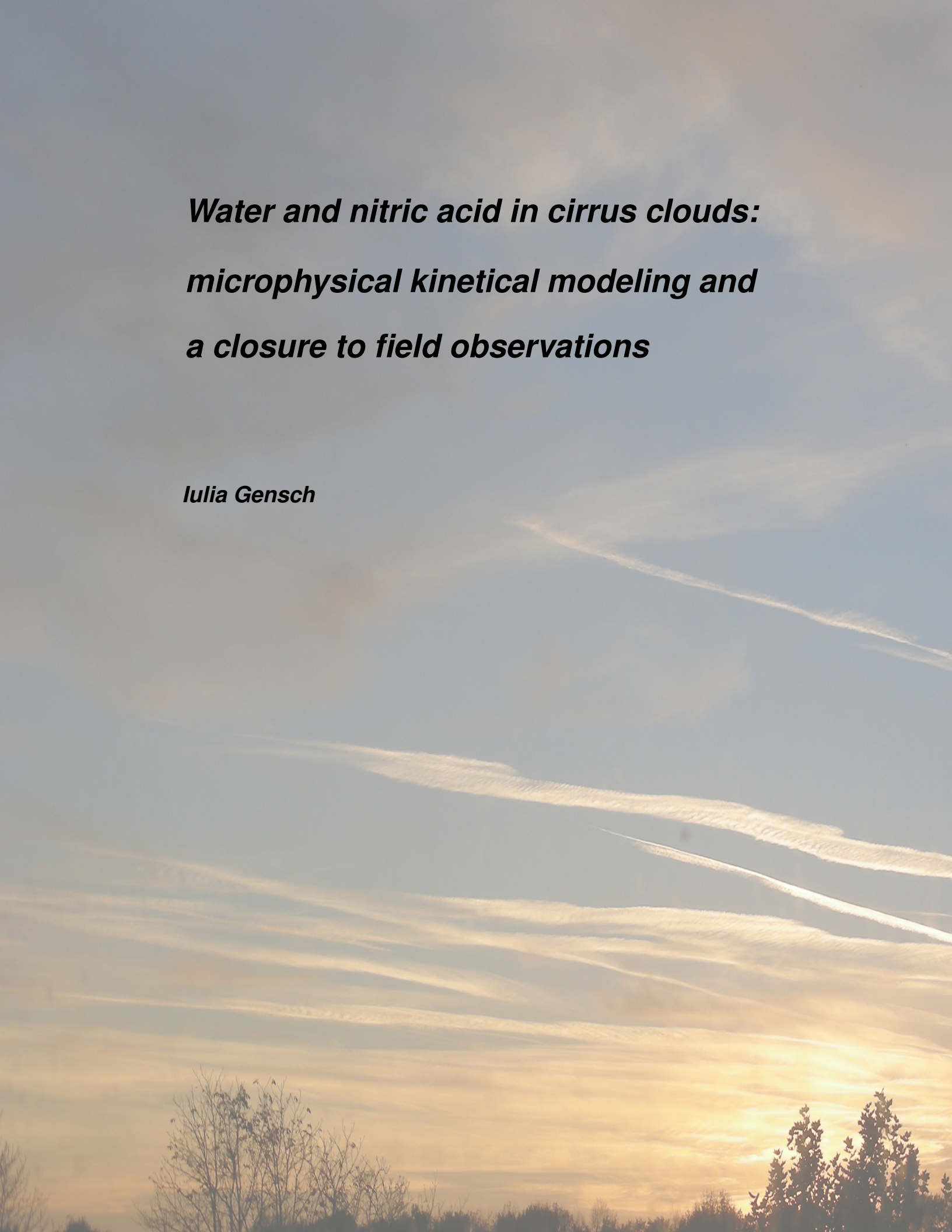

Water and nitric acid in cirrus clouds: microphysical kinetical modeling and a closure to field observations

Iulia Gensch

Învăţat e omul care nu termină niciodată de învăţat.

Lucian Blaga (1895-1961)

Abstract

Upper tropospheric relative humidities over ice (RH_{ice}) of up to 200 % have been reported frequently in recent times. This unexpectedly high supersaturation out- and inside of cold cirrus clouds may have significant impact on the Earth's climate. In the first case, clear sky supersaturation could be justified when the critical supersaturation for ice cloud formation is higher than until now assumed. This would lead to a decrease in high cloud cover and thus impact on the radiation budget. In the second case, high supersaturation inside of cirrus clouds could suggest the existence of unknown microphysical and radiative properties with consequences for climate and the vertical redistribution of water and nitric acid. *Peter et al.* (2006) summarized possible reasons for the observed supersaturation in a 'supersaturation puzzle', calling into question whether this puzzle can be solved by solely using the conventional ice cloud microphysics. Another important question raised in this study is whether the supersaturation may result from uncertainties or flaws in the water measurements. The aim of this PhD thesis is to puzzle out these questions. Therefore upper tropospheric field observations are simulated with an adequate conventional kinetic model in order to analyze the origin and persistence of high ice supersaturation, particularly inside cold cirrus clouds.

The proposed **M**odel for **A**erosol and **I**ce **D**ynamics (MAID) handles widely aerosol and ice microphysics, including: gas-diffusive particle growth and evaporation, homogeneous and heterogeneous ice nucleation, water vapor deposition and nitric acid uptake on growing ice crystal. Special emphasis of MAID is the exact balancing of chemical species among different physical states. MAID is validated here, based on observations during the field campaign POLSTAR–1 1997 (Polar Stratospheric Aerosol Experiment). Further, a detailed analysis of cirrus cloud observations during CR-AVE 2006, the tropical Costa Rica – Aura Validation Experiment, is performed with MAID. The model is initialized with different aerosol properties, water mixing ratios, accommodation factors of water on ice and amplitudes of mesoscale temperature fluctuations. A notable feature here is to vary the freezing mechanism in the simulations. The model results indicate high sensitivity of the cloud microphysical evolution to the freezing pathway. The ice microphysics, as well as the partitioning of water and nitric acid inside the cloud derived from all sensitivity studies are compared at last with the the microphysical and chemical in-situ observations, to determine the most probable constellation of initial conditions and processes that led to the very cold, sub-visible tropical cirrus cloud observed during CR–AVE. The best agreement between model results and measurements is given when the cirrus cloud forms heterogeneously, with total accommodation of water on ice. By varying the freezing pathway, the accommodation factor of water on ice, or the amount of available water, clouds with completely different microphysical properties form.

As a summary, this work demonstrates that it is possible to simulate significant supersaturation inside cold cirrus ($T < 200$ K) with conventional microphysics when assuming heterogeneous ice nucleation as the freezing mechanism. Thus, heterogeneous freezing appears to be an important pathway for cold cirrus cloud formation. More generally, a freezing mechanism producing low number densities of ice crystals could explain the frequent high supersaturation inside cirrus clouds observed in this temperature range.

Acknowledgments

Many people deserve my gratitude for joining and supporting me throughout this exciting and fulfilling, but also now – and – again exhausting journey.

I deeply thank my supervisor, guide and friend Martina Krämer to first open the door for me to become a Ph.D. candidate. She was for me an invaluable source for academic counseling, but also for tranquility and regeneration during most hectic times.

I acknowledge Martin Riese and Joachim Treusch for their confidence and solidarity, to secure the financial support that allowed me to start and complete my Ph.D. work. Their positive – thinking and stand against cut-and-dried mentality were especially helpful in fostering my self-esteem, indispensable to overcome the severe changes caused by the altered doctoral work regime and life style.

I owe Helmut Bunz a lot for sharing with me his thoroughly elaborated model as a wonderful theoretical instrument to explore the hights.

A big thank you goes also to all the people who make up the Department of Chemistry and Dynamics of Geosphere ICG – 1 at the Research Center Jülich, for always providing a stimulating scientific environment. I value the time, knowledge and experiences we have shared together. Andreas Bott contributed to this thesis as examiner. His questions clarified issues and more often than not made me re – think parts of my work.

Thank you! / Danke!

Dedication

My deep love and gratitude go to my family in Romania: to my parents whose love and support always sustained me; they gave me a home where excellence was encouraged and stimulated every day; to my brother Emil for being my best friend over the years. Thank you! / Vă mulţumesc!

My most loving thanks are dedicated to the little German – Romanian family around me for being such a long lasting source of energy and inspiration throughout these exhausting years: to Thomas, who gave me affection and emotional support, but also critical feedback whenever I sought his opinion; to my daughters Maria and Elena, to have brought a deeper sense of completion in my life than I ever had imagined possible. I am very grateful to them for showing me how proud of their 'mami' they were from beginning to the end. I dedicate this thesis to them.

Contents

List of Figures

List of Tables

Chapter 1

Introduction

It is nowadays evident that water, aerosols and hence the clouds in the upper troposphere play an increasing role in many so called 'strategic' climate discussions, challenging the present - day society. A deeper understanding of how high - altitude clouds form, evolve and impact their environment is therefore highly required.

The second assessment report of the Intergovernmental Panel of Climate Change (IPCC) introduced the cirrus clouds among the major contributors to the radiative forcing of the climate, pointing out their warming effect, at the same time admitting the very low level of scientific understanding in evaluating 'the forcing, the degree of knowledge of the physical / chemical mechanisms determining the forcing and the uncertainties surrounding the quantitative estimate of the forcing' (Figure 1.1). In the fourth IPCC assessment report the cirrus clouds are withdrawn from the newer version of the chart. The reason for it is by no means that these clouds do not play any role in the climate system. On the contrary, Chapter 7 of *IPCC Fourth Assessment Report* (2007) gives an extensive analysis of processes that give feedback between climate and clouds, atmospheric water and aerosols, such as the cloud albedo and cloud lifetime effect, as well as the semi - direct effect of the aerosols. Despite of the detailed qualitative analysis, it is recognized that the magnitude and even trends of these interactions are not yet fully understood and steadily undergo changes (Chapter 2).

The atmospheric constituents – gases (especially water vapor), aerosols and clouds – are closely linked through chemistry as well as dynamics and radiation:

- High water vapor supersaturation with respect to ice in clear air have been frequently observed in the past years (e.g *Jensen et al.* (2005)). The increase of the ice supersaturation threshold for cirrus formation may cause a decrease of the

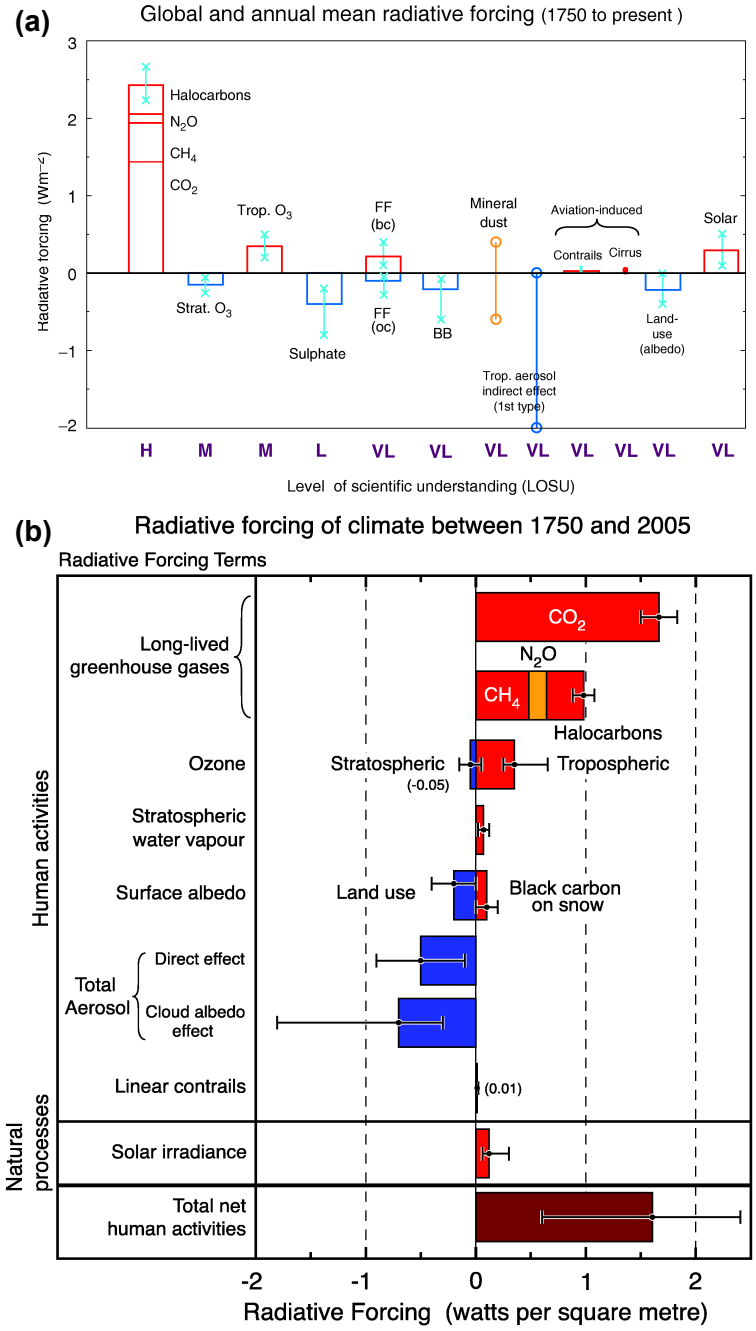

Figure 1.1: Summary of the principal components of the radiative forcing of climate (colored bars: contribution of different elements to the radiative forcing; colored / black lines: uncertainty range). Source - a: Figure 6.6, Chapter 6 of *IPCC Second Assessment Report* (2001); (LOSU: level of scientific understanding, with H, M, L and VL denoting high, medium, low and very low levels, respectively). b: Figure 2 / FAQ 2.1, Chapter 2 of *IPCC Fourth Assessment Report* (2007)

high - cloud cover. This may impact on the radiation balance of the atmosphere (*Gettelman and Kinnison* (2007));

- The ice supersaturation threshold for cirrus formation and the microphysics of the evolving cloud are sensitive to alterations in the aerosol population. Injection of heterogeneous ice nuclei (IN) into the UT region, especially of aircraft generated soot, may significantly impact on the formation and evolution of natural cirrus clouds (e.g. *Anderson et al.* (1999), *Hendricks et al.* (2004) and *Kärcher et al.* (2007));
- The partitioning of water and other chemical components among phases influences the exchange between upper troposphere and lower stratosphere. The fluxes of water + long - lived greenhouse gases into the stratosphere, and the other way round, of ozone + NO_x downward into the troposphere can change. Due to strong uptake of nitric acid on ice at low temperatures, the microphysics in the ice cloud will influence its vertical distribution, which further influences the heterogeneous chemistry on cirrus particles (e.g. *Borrmann et al.* (1997), *Meilinger et al.* (2001) and *von Hobe* (2008)).

These interactions are subject of recent investigations, both individually and as an ensemble, in order to understand and predict how each of the constituents affect the Earth's climate.

High supersaturation inside of cloud free air masses was measured often during field campaigns, which goes well with the theory. This implies that relative humidity with respect to ice can increase up to 140 - 170 %, depending on temperature, earlier than the ice nucleation initiates (*Koop et al.* (2000)). More problematic is to explain substantial and persistent supersaturation inside cirrus clouds, since the formed ice crystals are expected to deplete very fast the ambient water vapor. *Peter et al.* (2006) reviewed some of the arised open questions in a 'supersaturation puzzle'. The major formulated uncertainties, which are to be solved in this PhD thesis are:

- Is it possible to reproduce observed supersaturation, microphysics and nitric acid uptake inside cirrus clouds with the conventional knowledge of ice cloud microphysical processes?
- Can simulated cirrus microphysical properties and water vapor supersaturation give 'guidelines' in case of strong discrepancies in the in - situ measurements, for example when different instruments repeatedly show divergent measurements of the same parameter: water vapor mixing ratios, or microphysics of ice crystals?

For this purpose, the detailed microphysical **M**odel for **A**erosol and **I**ce **D**ynamics, **MAID**, was established at Forschungszentrum Jülich, ICG1, further developed and employed to simulate condensation and freezing of UT aerosol particles, microphysics and partitioning of water and nitric acid in ice clouds. MAID is based on an existing microphysical model (*Bunz and Dlugi* (1991)), which was developed at Forschungszentrum Karlsruhe (Institut für Meteorologie und Klima) to simulate aerosol and ice processes in the aerosol chamber AIDA. The model was first adapted for Lagrangian atmospheric cirrus cloud calculations. The new version of MAID was then extended by a new ice microphysics scheme simulating:

- the freezing mechanism in aerosol particles containing a non - soluble part (heterogeneous ice nucleation);
- the nitric acid uptake on growing ice crystals ('trapping').

MAID was validated subsequently for UT calculations. For this purpose, the model was initialized using measurements in an Arctic cirrus cloud, probed during the POLar STratospheric AeRosol Experiment, POLSTAR – 1 1997. This cirrus cloud had been already modeled by *Meilinger et al.* (1999), using another ice nucleation scheme. Moreover, for the POLSTAR – 1 case first sensitivity studies are performed with MAID, by employing the lately developed freezing modules, to investigate the impact of the ice nucleation pathway on the cloud microphysics.

Finally, MAID was employed to reproduce the microphysics, supersaturation and the nitric acid partitioning in a thin tropical cirrus cloud observed during the Costa Rica – Aura Validation Experiment, CR – AVE 2006. Therefore, parameters and processes, crucial for the formation and evolution of the cloud, were varied in the model initialization. Multiple 'scenarios' for the cloud formation and evolution were thus created. A comparison between the output sets, resulted from the simulations of these different scenarios, and the observations in the cirrus cloud (as closure) showed that it is possible to reproduce observed ice cloud properties with the conventional microphysics.

Chapter 2 of this work provides a general description of the different entities, water vapor – aerosol – ice clouds, interacting in the upper troposphere, possibly affecting the climate. Chapter 3 describes the theoretical background of MAID, as well as an approach for its application in sensitivity and closure studies. The POLSTAR – 1 study for MAID validation is also here presented. The CR – AVE detailed sensitivity and closure studies are subject of Chapter 4. In conclusion, chapter 5 summarizes the results and gives an outlook on future challenges in the cirrus cloud research field.

Chapter 2

Cirrus clouds, Aerosols and Climate

Cirrus clouds cover on average $\approx 30\,\%$ of the Earth surface and play an important role in the climate system (*Lynch et al.* (2002)). Evaluating the net radiative and chemical impact of cirrus clouds in the upper troposphere depends on an appropriate understanding of the processes that determine their frequency, spatial distribution and lifetime. The formation and evolution of cirrus clouds are determined by environmental conditions – e.g. temperature, ambient water vapor, background aerosol –, as well as the interactions among these elements. The complexity and non - linearity of the linked processes acting together in the UT (Figure 2.1) complicate the understanding of cirrus clouds microphysics.

Upper tropospheric low temperatures are often connected with relative humidity with respect to ice far higher than 100 %. The initially cloud free air masses make up the so - called 'ice - supersaturated regions' (ISSRs, see *Gierens et al.* (1999)). The cirrus clouds arise embedded into these ISSRs, once the relative humidity with respect to ice exceeded the ice saturation threshold and ice nucleated in the aerosol particles. The relative humidity with respect to ice, RH_{ice} and the ice saturation ratio, S_{ice}, are defined in the Equations 3.23 and 3.24. Since the main part of UT aerosol consists of soluble - supercooled - aqueous sulphuric acid particles, it is generally assumed that the homogeneous freezing (Section 3.1.2), at RH_{ice} of 140 - 170 % and temperatures of 240 - 180 K (*Koop et al.* (2000)), is the most likely pathway for the cirrus cloud formation. The so arised clouds are optically 'thick', they consist of many small ice crystals, with a strong albedo effect. Fewer particles containing a non-soluble impurity (heterogeneous ice nuclei, IN) freeze heterogeneously at a lower S_{cr}^{het} (Section 3.1.2). As a result, the injection of soot particles into the upper tropospheric ISSRs by aircrafts for example, may cause the extension

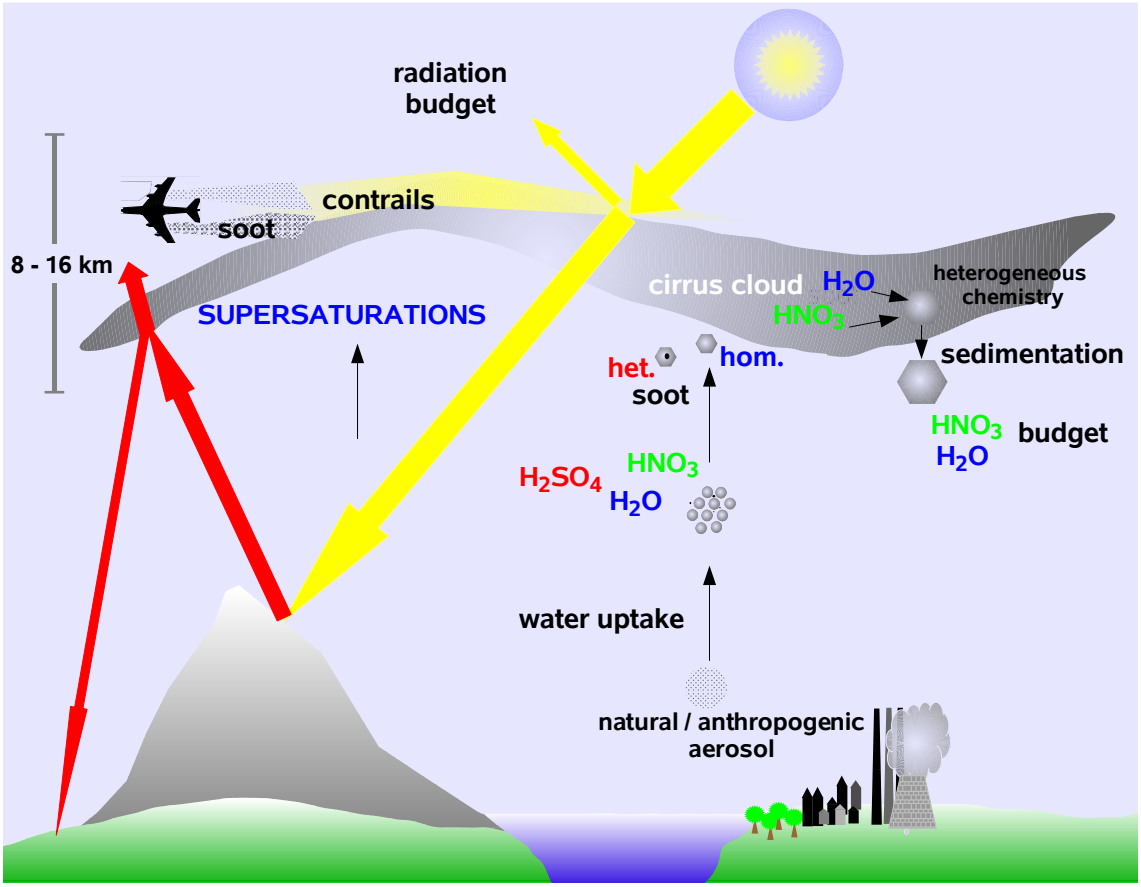

Figure 2.1: Schematic of cirrus clouds and their role in the climate (for details, see text).

of the high – altitude cloud cover by lowering the ice nucleation threshold, thus impacting on the radiation budget. In addition, the heterogeneous ice nucleation produces less ice crystals than the homogeneous one, the clouds are optically 'thin'. Consequently, the alteration of the ice nucleation pathway leads to clouds with different radiative properties. The ice clouds trap outgoing long-wave radiation (greenhouse effect) and reflect the solar radiation (albedo effect). Depending on their optical thickness and cloud - top - hight, the net effect of cirrus clouds at the Earth's surface may be cooling, neutral or even warming (Figure 2.2). Low, thick clouds reflect solar radiation and cool primarly the surface of the Earth. High, thin cirrus clouds, emphasized in this work, allow most sun radiation to reach the Earth's surface. Besides, infrared radiation outgoing from Earth is efficiently absorbed by cirrus cloud ice particles and re - emitted at very low radiation temperature. It is therefore generally assumed that the greenhouse effect of high - thin - very cold - ice

clouds is stronger than their albedo effect and thus, they have a net warming effect at the Earth's surface. The contribution of this cirrus type to the radiative forcing of the atmosphere is once again evident. However, estimating of warming and cooling effects is yet highly uncertain, since the ice - phase cloud processes, which govern the microphysical and radiative properties of cirrus clouds are poorly characterized at this time (*IPCC Fourth Assessment Report* (2007)).

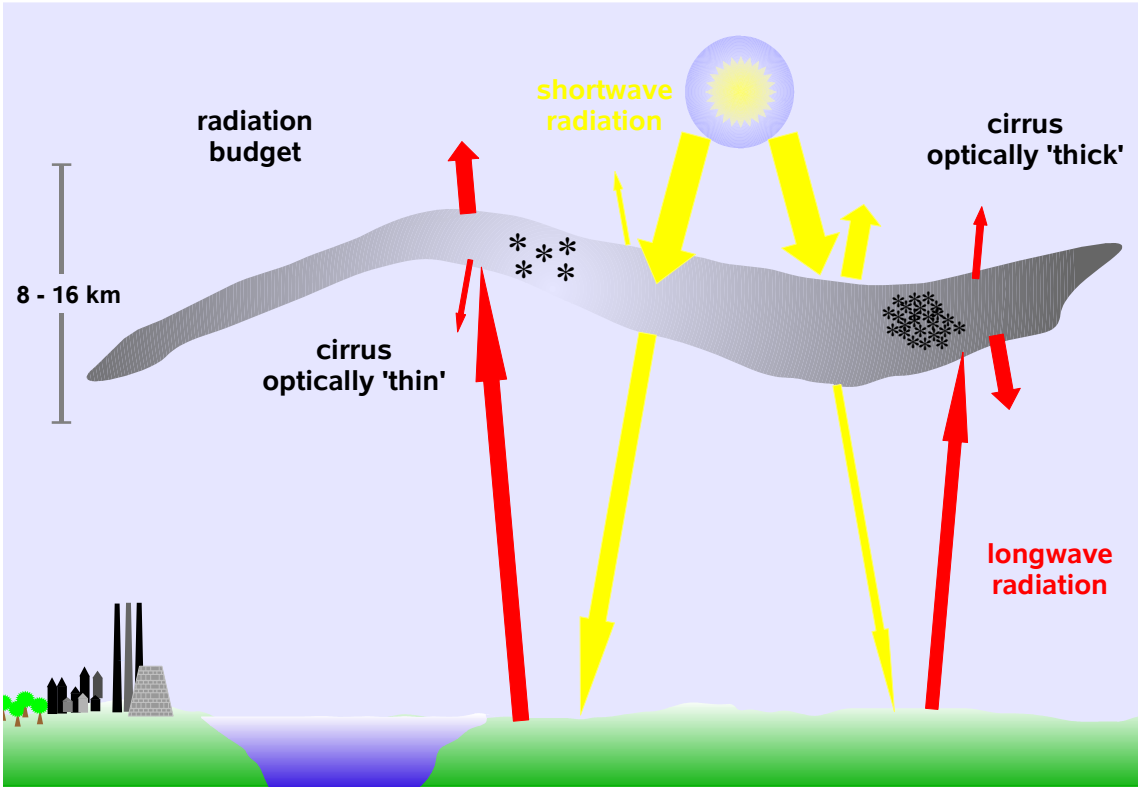

Figure 2.2: Net radiative impact of different cirrus cloud types: 'thick' cirrus may have a cooling net effect, whereas 'thin high' cirrus may have a warming net effect at the Earth's surface.

A better understanding of the cloud microphysics, enclosing the partitioning of atmospheric chemical species among different physical states and particle sedimentation, is also needed to assess the role of cirrus clouds in the vertical redistribution of water vapor

and other UT trace gases. Deep convection can lead to hydration of under - saturated UT via the rapid evaporation of entrained ice crystals. Conversely, convection may provide the cold super - saturated UT with ice nuclei and thus lead to dehydration via freezing, growth and sedimentation of ice particles. Cirrus in the UT may also provide surface area for heterogeneous chemistry. Thus, a detailed determination of the competition between homogeneous / heterogeneous ice nucleation modes is essential for an accurate characterization of the arised cloud microphysics. Here, the chemical composition and freezing behaviour of the various types of ice nuclei in the upper troposphere are required. This chapter describes potential feedback processes among aerosols, water vapor / supersaturation and clouds.

2.1 Impact of aerosols on clouds

Recent studies revealed a dissimilarity in the distributions of RH_{ice} outside the cirrus clouds between the Southern (SH) and Northern Hemisphere (NH) (*Ovarlez et al.* (2002) and *Gayet et al.* (2004)), showing higher frequency of higher supersaturation in the SH. This difference was attributed to the different pollution levels of NH / SH. RH_{ice} in clear air is limited to values below the ice supersaturation threshold (Equation 3.23), since at this level ice nucleation initiates and cloud forms – in other words the maximum clear air relative humidity defines a lower limit for the ice nucleation threshold, providing information on the mode of ice nucleation. Since there are less ice nuclei in the cleaner Southern Hemisphere, the high homogeneous freezing thresholds are reached more often, prior the clouds form. This emphasizes the role of aerosols as contributors to climate change. Aerosol particles influence climate in many ways (*Ramanathan et al.* (2001)). Directly, increased aerosol leads to lower net surface solar radiation (see negative forcing in Figure 1.1). Indirectly, aerosols act as ice nuclei and modify optical properties and lifetimes of clouds:

- the more smaller liquid / ice particles exist in a cloud, the more solar radiation is reflected (Twomey effect)
- smaller cloud particles reduce precipitation efficiency; in case of cirrus clouds, smaller ice crystals settle down slower ('cloud lifetime effect')
- absorption of solar radiation by embedded soot may cause particle evaporation / sublimation ('semi – direct effect')

The atmospheric cycles of two radiatively important species, sulfate and soot, which are major components of the UT aerosol, have been significantly perturbed by anthropogenic activities, for instance by incomplete combustion processes, aviation, or industrial activities. These aerosols may change the balance between homogeneous and heterogeneous freezing (Figure 2.1), potentially impacting on clouds and climate.

Upper tropospheric aerosol particles

In the upper troposphere, individual aerosol particles may contain chemically distinct species, or exist as composite mixtures of a core refractory material (soot, dust and seldom, sea salt) with a coating of sulfates, nitrates and organics. Background UT aerosols that can form ice crystals consist of preponderantly sulfates, very often nitrates, sometimes organics and soot and rarely of meteoritic dust (*Murphy et al.* (2007)). Measurements of upper tropospheric ice nuclei show that many particles contain mixed phases and compositions of the simple classes mentioned above (e.g. *DeMott et al.* (2003), *Cziczo et al.* (2004a,b, 2006) and *Richardson et al.* (2007)). The complexity of these mixtures may lead to a complexity of cloud forming mechanisms.

General information about size and number densities of liquid aerosol particles in the UT, as well as concentrations of non-soluble cores are given for instance by *Seifert et al.* (2003) and *Minikin et al.* (2003). At this point it is appropriate to accentuate that only a minor part of the total aerosol contains non-soluble cores (there are at least two orders of magnitude between the total aerosol number density and the number density of non-soluble cores, coated with liquid shells, *Blake and Kato* (1995)). This circumstance could be of special importance for the cirrus cloud formation and thus, for this work. Non-soluble cores may essentially reduce the ice nucleation threshold (Section 3.1.2). Therefore, partly non-soluble particles possess the ability to change the predominant freezing mechanism in the cloud formation. Moreover, the number density of non-soluble ice nuclei may limit the number density of the raised ice crystals (see the estimation of Twomey effect of different freezing pathways in Figure 2.6). The alteration of the cirrus cloud microphysics may have, as showed above, a strong impact on the climate.

2.2 Cirrus cloud impact on climate

Understanding the ice initiation in cirrus clouds and their evolution is critical to accurately quantify future climate changes. Firstly, recent studies showed that the cirrus cover might increase because of human activities, e.g. due to air traffic *Minnis et al.* (2004), with implications for the radiative forcing of the atmosphere. But then again, there is still a question whether cirrus clouds have a negative or a positive net effect at the Earth surface. Therefore, investigating the formation mechanism and the microphysics of these clouds becomes an important issue in determining the anthropogenic contribution to the changes in the atmosphere. Secondly, cirrus clouds may play an important role in the water vapor distribution. The formation of cirrus clouds is often associated with advection / convection of moist air masses in colder regions (Figure 2.1). RH_{ice} in clear air increases with decreasing temperature, until the freezing threshold is reached and ice nucleates. The nature of the freezing aerosol particles may determine the prevailing freezing mechanism, which in turn has a strong impact on the cloud microphysics. Ice crystall growth and sedimentation influences the vertical distribution of water vapor and also of other UT trace gases (Figure 2.1), such as nitric acid (see Section 2.3).

Thin cirrus clouds

Cirrus are high altitude clouds, composed of small ice crystals, arised at temperatures lower then 240 K. Properties associated to cirrus clouds are comprehensively defined and described for example by *Pruppacher and Klett* (1997), *Gayet et al.* (2002) and *Lynch et al.* (2002). Cirrus clouds, depending on the ratio of their shortwave 'visible' to longwave 'infrared' optical depth, can act to either cool or warm the planet. 'Thin' (low optical depths in the visible) cirrus stand for a distinct type of ice clouds, with special importance in the radiaton budget, since their infrared heat trapping exceeds their solar shading effect. Linear contrails and sub-visible cirrus clouds (SVC) are examples of this cloud species.

- linear contrails (Figure 2.3) are condensation trails behind high-flying aircrafts. The impact of persistent linear contrails from aviation on the radiative forcing is referred in Chapter 2 of *IPCC Fourth Assessment Report* (2007). These have a positive contribution to radiative forcing of 0.01 W/m^2 (Figure 1.1), 'with a low level of scientific understanding'. Compared to *IPCC* (1999), the impact of contrails on the

radiative forcing is considered less important in *IPCC Fourth Assessment Report* (2007). Despite of this, contrails studies are helpful for a better understanding of the formation of natural cirrus clouds in supersaturated regions.

- sub-visible natural cirrus clouds have low optical depths in the visible. For instance, the optical depth (OD) of SVC is lower than 0.03 at the wavelength of 694 nm (*Lynch et al.* (2002)). Consequently, more than 93.3 % of the light is passing through the cloud. Therefore, these clouds are usually invisible for the naked eye. The SVCs are though detected with the infrared imagery and appear here on white because their tops are very cold. They form frequently in the tropical tropopause layer (TTL). These SVCs are particularly important for the cloud radiative forcing signal. Since the tropopause is very high and cold at the Tropics, the top of these ice clouds is exceptionally cold. Therefore, their greenhouse effect is accordingly strong. Measurements show mostly that the TTL sub-visible cirrus clouds contain few, relatively small ice crystals. Such a cloud is the subject of a detailed analysis in Chapter 4.

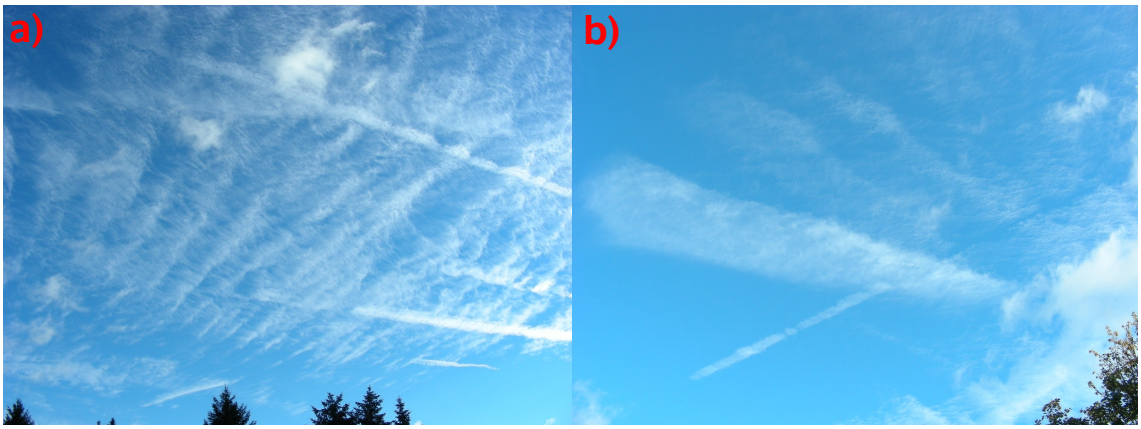

Figure 2.3: Natural cirrus clouds and contrails on Jülich's sky (a: gravity wave cirrus clouds and fresh contrails; b: fresh and aging contrails that develop to spread cirrus clouds).

Cirrus cloud formation

The cirrus cloud–generating mechanisms are described in detail by *Lynch et al.* (2002). Key issues in the cirrus cloud initiating are the aerosol composition (Section 2.1) and the ice nucleation mechanisms. The nucleation pathway is crucial for the microphysical

properties of cirrus. Cirrus modeling studies (*Hoyle et al.* (2005)) indicate that variations in the factors driving the ice nucleation, such as temperature and relative humidity evolution, determined by the water vapor and cooling rates, lead to formation of cirrus clouds with totally different microphysical characteristics. Also the background aerosol influences significantly the freezing process. However, the relation between aerosol composition and ice nucleating properties is not well understood. Ice nucleation may occur homogeneously in liquid aerosol particles or heterogeneously, if non-soluble particles are involved in the freezing process. Figure 2.4 depicts in schematic form both pathways of ice formation. Ice number densities are always some orders of magnitude lower than the ambient aerosol number densities at the location where the cirrus cloud forms. Due to difficulties in measuring volatile components of aerosol and ice particles, there is no information about the aerosol fraction that freezes homogeneously or heterogeneously. Therefore, systematic laboratory experiments are very important to test and describe the freezing behavior of different aerosol types and aerosol mixtures.

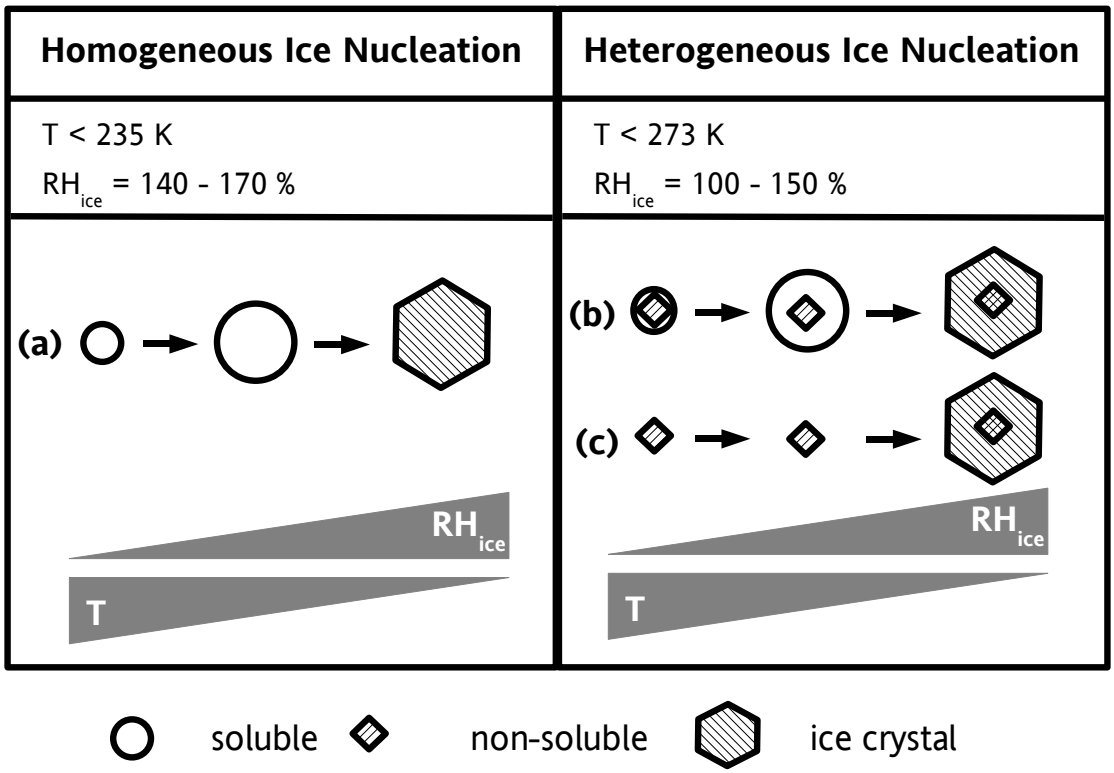

Figure 2.4: Pathways to ice nucleation in UT (a: homogeneous; b / c: heterogeneous immersion / deposition freezing, respectively)

Homogeneous freezing

Homogeneous freezing of supercooled water droplets (panel a of Figure 2.4) is a stochastic process, which depends strongly on temperature. The condition of nucleation of a stable phase from a metastable parent phase is that a germ forms and reaches a critical size, when its growth is favored. This critical embryo initiates the freezing of the whole droplet. At a given temperature, there is a certain probability that the critical germ develops, expressed as the freezing rate. The freezing rate in the droplets depends on the nucleation rate coefficient J, defined as the number of critical germs formed per time and liquid volume. The definition of the nucleation rate coefficient J assumes that the probability of droplet freezing is proportional to the droplet volume.

The homogeneous freezing threshold, S_{cr}^{hom} and the nucleation rate coefficient, J, have been assessed theoretically by *Koop et al.* (2000), derived from laboratory studies using different techniques. According to this, S_{cr}^{hom} and J are expressed as functions of the solution water activity (a_w, Equations 3.25–3.27) alone.

Heterogeneous freezing

Heterogeneous freezing occurs when the aerosol particles include non-soluble components. The immersion and deposition freezing are possible mechanisms for the heterogeneous ice nucleation (panels b and c of Figure 2.4). Immersion freezing occurs in solution droplets bearing a non-soluble inclusion. In case of the deposition freezing, water vapor transforms directly to ice by deposition on a suitable non-soluble nucleus. Non-soluble substrates, embedded or not in supercooled liquid droplets, provide the possibility that an ice embryo forms and may reach the critical size with a lower free energy barrier than in the case of homogeneous ice nucleation. The degree of this energy reduction and thus, the temperature at which ice nucleation initiates depend strongly on the substrate properties.

The reduction of the heterogeneous freezing threshold can be described in process models using the 'shifted' activity method proposed by *Kärcher and Lohmann* (2003). The heterogeneous nucleation rate coefficient, J_{het} is calculated similar to the homogeneous nucleation rate coefficient, J_{hom}, using the 'shifted' activity, $a_w + \delta a_w$ instead of a_w. In this concept, the particles containing heterogeneous ice nuclei freeze at a critical ice sat-

uration ratio, S_{cr}^{het}. This value is shifted downwards from S_{cr}^{hom} by the quantity of δa_w. Consequently, the nucleation rate j (number of critical germs formed per time), changes as depicted in panel a of Figure 2.5.

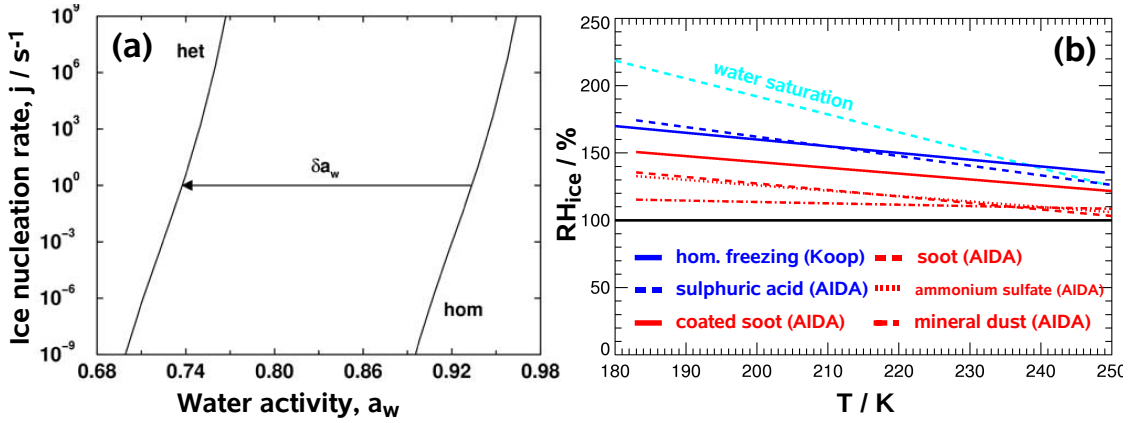

Figure 2.5: 'Shifted' activity method, suggested by *Kärcher and Lohmann* (2003) for the heterogeneous freezing (a: example of shifted water activity with the quantity δa_w, used to determine the heterogeneous ice nucleation rate; b: experimental parametrisations of homogeneous (blue) and heterogeneous (red) freezing behavior for different aerosols; the AIDA parametrisations are taken from *Schlicht* (2006); liquid water saturation (turquoise); saturation with respect to ice, $RH_{ice} = 100\,\%$ (black); for details see text).

Parametrisations of S_{cr}^{het} and S_{cr}^{hom}, necessary to determine the quantity of δa_w (see Equation 3.28) are given in panel b of Figure 2.5. *Koop et al.* (2000) gives S_{cr}^{hom} (blue solid line) for different aqueous solutions, depending only on temperature and aerosol particle size. Numerous measurements of freezing behavior of different aerosols were also carried out in the aerosol chamber AIDA (Forschungszentrum Karlsruhe). *Mangold et al.* (2005) and *Möhler et al.* (2005) supplied a representative set of experimental data. These data have been used to develop parametrisations of S_{cr} for several significant aerosols in the UT region: aqueous sulphuric acid droplets, soot, soot coated with sulphuric acid, particles containing crystallized ammonium sulphate and mineral dust. An overview of these parametrisations is given in *Schlicht* (2006). S_{cr}^{hom} for aqueous sulphuric acid droplets (blue dashed line) shows good agreement with the parametrisation of *Koop et al.* (2000). The heterogeneous ice nuclei (red lines) freeze at lower RH_{ice} than in the homogeneous case (blue), but still higher than $RH_{ice} = 100\,\%$ (black). It is evident that mineral dust particles (red dot–dashed line) act as very efficient heterogeneous ice nuclei. Soot coated with sulphuric acid (red solid line) is believed to be an important ice nucleus in the upper

tropospheric region. Compared to other heterogeneous ice nuclei, coated soot catalyzes ice formation at lower temperature or higher RH_{ice}. On the other hand, its freezing threshold is slightly lower than the homogeneous one. All parametrisation are well below the liquid water saturation line (turquoise) at T = 180–235 K. Through the implementation of these new parametrisations into process models, the impact of different ice nuclei on the ice cloud formation can be investigated.

Parametrisation of cirrus cloud formation in modeling studies

Model studies show that the number density of the ice crystals formed homogeneously depend only on temperature and cooling rates, i.e. on the relative humidity evolution (*Tabazadeh et al.* (1997) and *Kärcher and Lohmann* (2002a)). Figure 2.6 (panel a, *Kärcher and Lohmann* (2002b)) shows that at low temperatures (open circles, T = 196.4 K) and high vertical velocities w, the highest number of ice crystals nucleates. The simulations at each temperature are performed for three different starting aerosol number densities (1000, 2500 and 8000 cm^{-3}), therefore three symbols for each temperature. Since the symbols overlap more or less, the simulated ice number densities are very similar. Accordingly, the dependence of the homogeneously arised ice crystal number densities on the aerosol is very weak. *Kärcher and Lohmann* (2002b) extends this conclusion to analyse a natural event, the Pinatubo volcanic eruption in 1991. The study shows that even dramatically enhanced sulphate aerosol number densities, observed afterwards, do not strongly impact on the formation of cirrus clouds. At this point, it should be noted that the Pinatubo event had altered only the aerosol that freeze homogeneously. In addition, global climate model simulations (*Lohmann et al.* (2003)) show that the Pinatubo volcanic eruption had no significant effect on cirrus cloud coverage and optical thickness, in agreement with satellite observations presented by *Luo et al.* (2002). These studies underline that the homogeneous ice cloud formation is determined only to a minor extent by the number densities of supercooled liquid aerosol particles. Consequently, the Twomey effect (see aerosol section) is, other than in warm clouds, not relevant in homogeneously arised cirrus clouds.

The Twomey effect is also estimated in case of heterogeneous freezing by *Kärcher and Lohmann* (2003). Panel b of Figure 2.6 depicts the ice number density vs. vertical velocity for the heterogeneous freezing (solid line), paralell to the homogeneous freezing (dashed line, see also panel a of Figure 2.6). Three regions can be defined here: on the

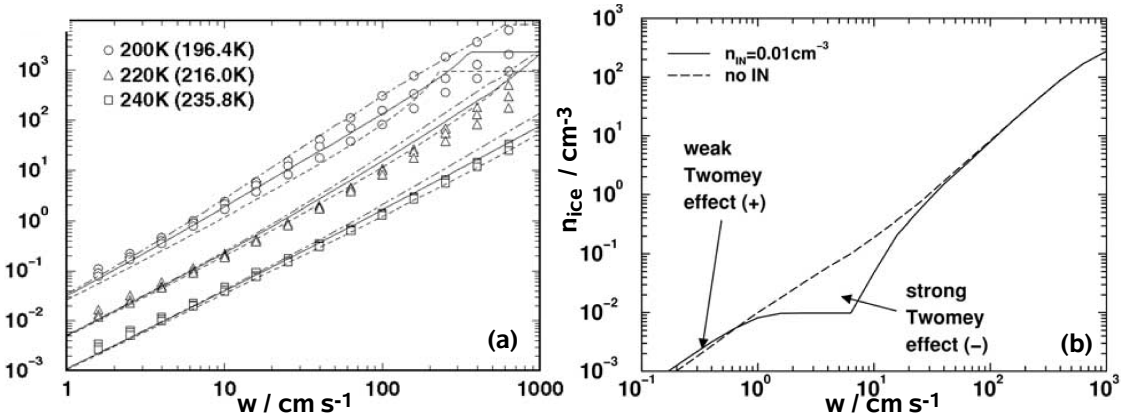

Figure 2.6: Ice crystal number densities as function of the vertical velocity of air parcels at different initial values of T (a: for the homogeneous freezing from numerical simulations (symbols) and from the analytical parametrisations (curves) *Kärcher and Lohmann* (2002b); b: for the heterogeneous freezing; the heterogeneous ice nuclei number density is set here to 0.01 cm^{-3} *Kärcher and Lohmann* (2003)).

left side of vertical velocity range ($w < 1\,cm\,/\,s$) the heterogeneous freezing has a weak Twomey effect. A positive change in the ice number density is caused by adding of ice nuclei. This is also accompanied by a decrease of the freezing threshold. The number of heterogeneously formed ice crystals increases with the vertical velocity as long as ice nuclei are still 'available'. Once all prescribed ice nuclei have been activated, the heterogeneous ice nucleation mode is blocked. By further cooling , no new ice nucleates until the homogeneous freezing threshold, S_{cr}^{hom}, is reached and the homogeneous ice nucleation mode is activated. This represents the second region, at vertical velocities of 2 to 10 cm / s, found in gravity waves for instance. The Twomey effect becomes negative and is very pronounced. On the right side of vertical velocity range ($w > 30\,cm\,/\,s$), the aerosol freezes homogeneously, so the Twomey effect becomes unimportant.

However, the use of parametrisations in case of the heterogeneous freezing is problematic. The high complexity of factors and processes that lead to this ice nucleation pathway in the UT region is not well enough understood to exactly describe cirrus cloud formation. There is few information on the chemical composition of atmospheric ice nuclei and laboratory studies show that each aerosol type has very different freezing properties.

'Supersaturation Puzzle'

In warm liquid clouds condensation occurs when the water vapor partial pressure exceeds the saturation water vapor pressure. Consequently, supersaturation of more than a fraction of 1 % persists rarely. In case of ice clouds, high supersaturation develops prior to ice nucleation. This could be explained by the condensation of water vapor to ice, which may be seen as a two step process: firstly water vapor condenses to water, afterwards the liquid freezes (*Koop et al.* (2000)). Since the saturation water vapor pressure over ice is lower than over liquid water, ice supersaturation is expected before condensation occurs. Explicitly, in clear air, which is saturated or supersaturated with respect to ice ($RH_{ice} \geqslant 100\,\%$), the water vapor partial pressure might be still lower than the saturation water vapor pressure over liquid water and consequently, the water remains in gas phase. Ice initiates first when a certain saturation threshold have been reached.

Accordingly, the clasical mycrophysical theory shows that in cooling cloud free air masses the relative humidity with respect to ice increases, reaching values far higher than 100 %, as long as the freezing threshold (S_{cr}) has been not attained. At S_{cr} (yellow star in panel a of Figure 2.7) ice nucleation initiates and the cloud forms. Inside the arised cloud the ice crystals grow by water vapor deposition. In the beginning the few ice crystals do not deplete yet the water vapor efficiently. Consequently, by further cooling (green arrow shows the ascending moving of the air) RH_{ice} still increases. After a while, there are enough ice particles that act as a strong sink for the water vapor. Therefore, inside the ice cloud RH_{ice} decreases rapidly to thermodynamic equilibrium value of 100 %. Big crystals can be eventually removed from the cloud by sedimentation, the rest sublimate. The cloud disappers finally.

Because of the rapid relaxation, RH_{ice} distribution in the ice clouds is expected to be centred around saturation or lower. With more reason, the unlikely high supersaturation with respect to ice and its persistence measured during field campaigns put under question the degree of understanding of the microphysical processes that influence the ice cloud formation and evolution. Panels e and f of Figure 2.7 depict measurements collected during 28 flights in Arctic + mid-latitudes + tropical regions, covering a broad range of climatological conditions (*Krämer et al.* (2008b)). The two diagrams show a very comprehensive data set of relative humidities in clear air and inside cirrus clouds. The field observations were processed to obtain the frequency of RH_{ice} in a data contingent within defined temperature intervals (in this case, in bins of 1 K between $180-250$ K). The method for

distinguishing clear air from data measured inside the clouds is explained by *Krämer et al.* (2008b). Besides, special features are analysed in both data sets by dividing the above refered temperature range in 'cold' ($T < 200$ K) and 'warm' ($T > 200$ K) regions. The liquid water saturation line and the thresholds for the homogeneous and heterogeneous freezing of coated soot, as important UT ice nucleus, are also shown, as references for a comparison with the field observational data (see panel b of Figure 2.5).

Panel e of Figure 2.7 shows that RH_{ice} up to the homogeneous freezing threshold are not uncommon in the cloud free upper troposphere. Additionally, the RH_{ice} show a very random distribution. The reddish points, signifying high data frequencies, are spread all over the RH_{ice}/T range, from unsaturated to supersaturated, at low and high temperatures. This could be explained by the high variability of temporal and geographic conditions, under which the air was sampled. A special feature in this analysis is the concentration of high data frequencies between the dashed lines at $T < 200$ K, representing RH_{ice} as function of temperature for water vapor mixing ratios of 2 and 3 ppmv, respectively. This indicates that in the tropical UT (high altitudes, very low temperatures) water mixing ratios of $2-3$ ppmv are commonly present. These very low water vapor mixing ratios are a chalenge for the instrumants. Clear air measurements in the 'cold' region of the temperature range show in few cases RH_{ice} slightly higher than the homogeneous freezing threshold. Since the maximum clear air relative humidity is, by definition, limited to values corresponding to the homogeneous ice nucleation threshold, these points suggest that under very cold conditions, the ice nucleation may be hindered by yet unknown processes, which may be reproduced by the 'suppressed nucleation' depicted in panel b of Figure 2.7 (red arrow). By continuous cooling of an air parcel the relative humidity with respect to ice increases unceasingly even then, when the homogeneous freezing threshold have been reached. No ice nucleates in aerosol particles. The water vapor can not be depleted by aerosol so efficiently like by ice, it remains in gas phase. High RH_{ice} persists for long time (red curve in panel d) in clear air.

In panel f of Figure 2.7, RH_{ice} occurence inside cirrus clouds as a function of temperature is shown. The highest frequencies of RH_{ice} concentrate around 100 % in the case of 'warmer' ice clouds ($T > 200$ K). This suggests that most measurements were carried out in old clouds after reaching their equilibrium steady state. The narrower distribution at higher temperature indicates that this state is reached faster in 'warmer' clouds. In 'cold' cirrus clouds ($T < 200$ K), the frequencies of RH_{ice} show a broader distribution around the

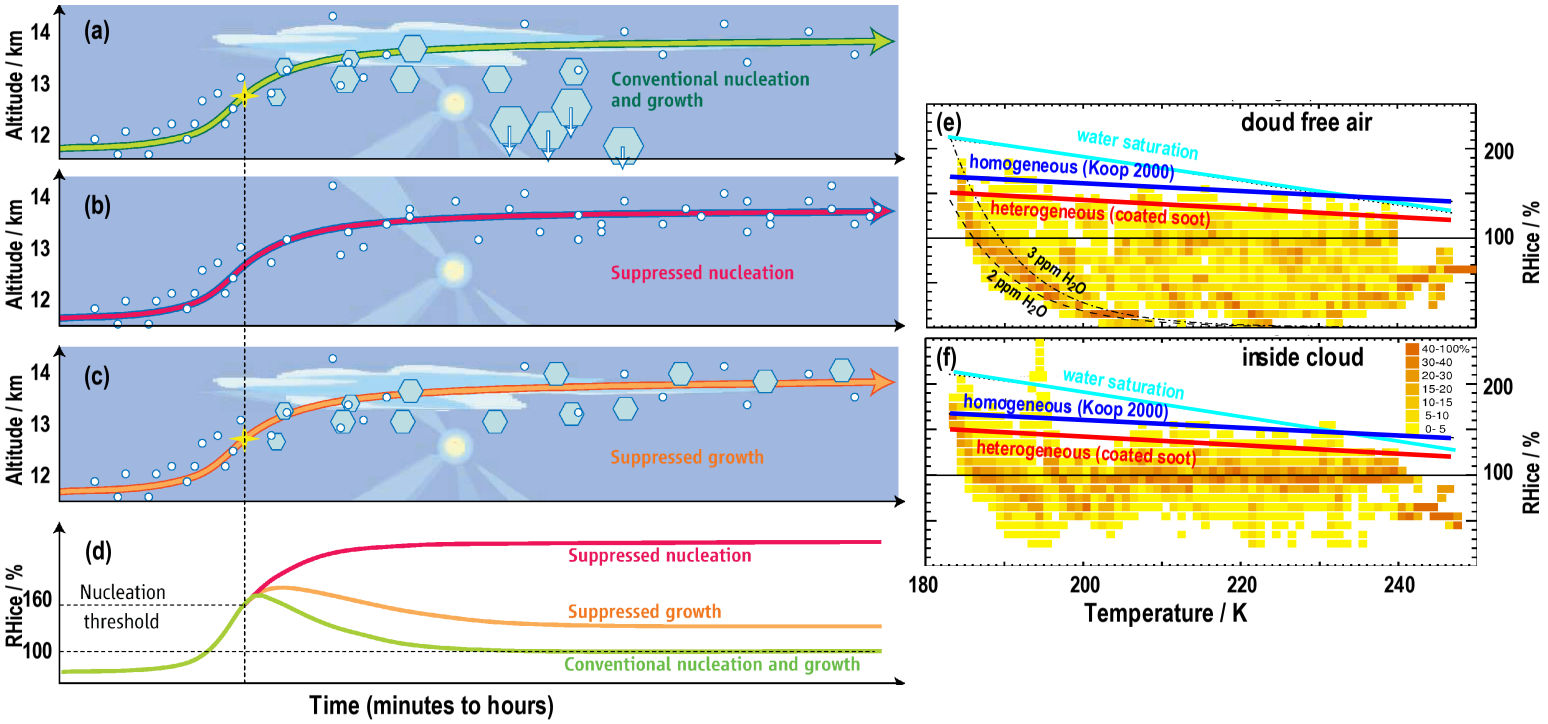

Figure 2.7: Ice supersaturation in a cirrus life cycle: different scenarios and experimental data (panels a–c: three scenarios for the formation of ice clouds in rising / cooling air masses; d: effect of these scenarios on ice supersaturation evolution *Peter et al.* (2006); e and f: field observations of relative humidities in clear air and inside cirrus clouds, respectively; yellow to red colored spots: frequency of measured RH_{ice} in the data contingent within defined temperature intervals, in % (*Krämer et al.* (2008b)); black dashed and dot–dashed lines: relative humidities with respect to ice as function of temperature for water vapor mixing ratios of 2 and 3 ppmv; solid lines: liquid water saturation (turquoise), ice saturation (black), parametrisations for the homogeneous (blue) and coated–soot– heterogeneous (red) freezing). According to conventional understanding, ice particles nucleate (star), grow, reduce the supersaturation (green curves) and settle down. Frequentt observations suggest suppressed nucleation (red curves) in cloud–free air or suppressed growth (orange curves) inside clouds.

100 % level. High supersaturation may be a sign of slower water kinetics at very low temperatures and could be described by the 'suppressed growth' case from panel c of Figure 2.7. Contrarly to the former case, the cloud arises when RH_{ice} exceeds the freezing threshold. Yet, for some reason, the ice crystals do not deplete effectively the ambient water vapor. The relative humidity is not so high like in the 'suppressed nucleation' case, but still persistently higher than 100 % (orange curve in panel d). Because of the suppressed growth, the ice crystals stay small and are not displaced, so the cloud persists for longer time.

This extreme RH_{ice} temporal evolution in a cooling air parcel, illustrated in panel d by both, red and orange curve are against the basic principles of the clasical theory of cloud formation and developing, represented by the green curve. Furthermore, panel f shows that in few cases RH_{ice} exceeds even the liquid water saturation threshold, which is definitely a violation of the physical laws. In the past years, there were lot of discussions, whether the very high cloud free relative humidities, respectively the persistent relative humidities inside clouds at $T < 200$ K could be attributed to instruments inaccuracy, or whether they really exist. The next emerging question, in case they exist, is whether they can be explained with the conventional microphysics. These questions are the quintessence of the 'supersaturation puzzle' by *Peter et al.* (2006).

2.3 Partitioning of water and nitric acid in cirrus clouds

As mentioned in Section 2.1, under UT conditions (very cold temperatures and relatively dry air), background aerosol particles are believed to be mainly composed of aqueous solutions of sulfuric acid, concentrated up to 90 % (binary solution aerosol). Because the vapor pressure of H_2SO_4 is extremely low at temperatures of 180 – 240 K (e.g. $1.5 \cdot 10^{-13}$ hPa at 200 K), sulfuric acid resides practically completely in the condensed phase. Another important component present in this region is nitric acid (see also Figure 2.1). The temporal evolution of an aerosol population, consisting initially of binary solution particles and following an ascending trajectory (e.g. in case of a lee – wave cloud) is depicted in Figure 2.8. When forced to rise, the air expands and cools adiabatically. Ambient H_2SO_4 / H_2O aerosols take up an increasing amount of H_2O and HNO_3 by condensation from the gas phase and grow. The aerosol composition changes to supercooled ternary solutions (STS) – H_2SO_4 / H_2O / HNO_3.

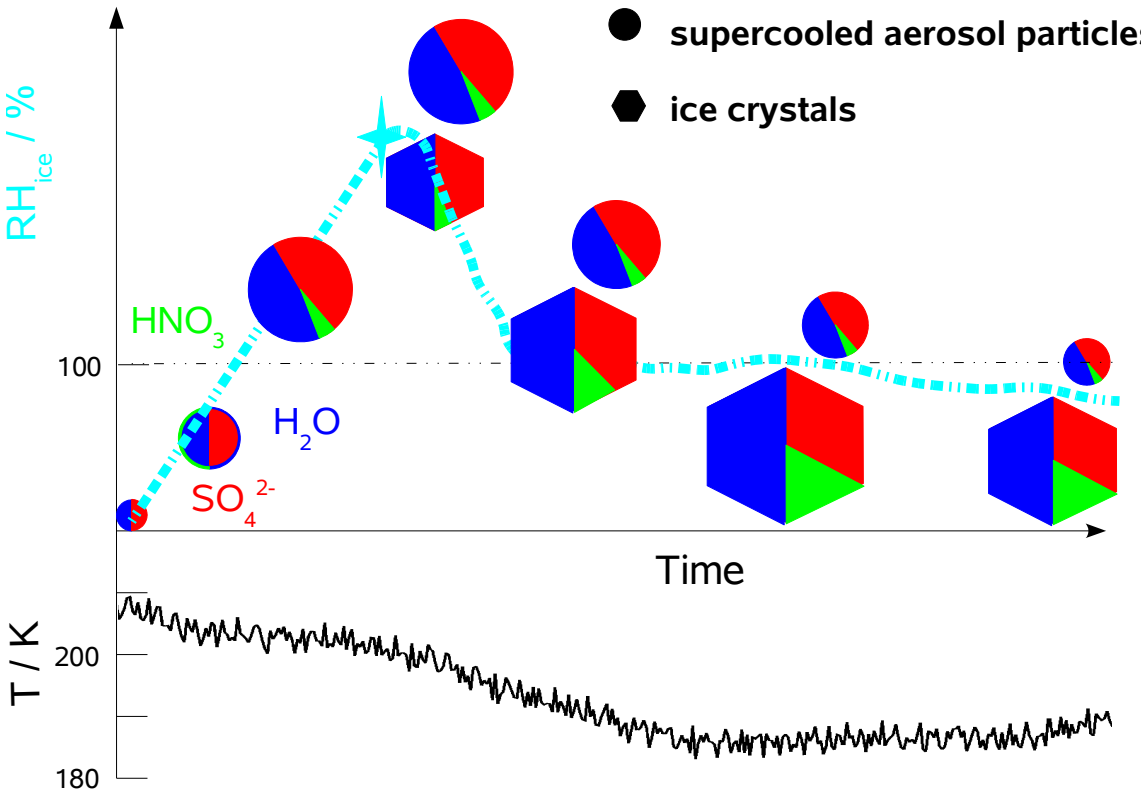

Figure 2.8: Life cycle of a cirrus cloud: aerosol and ice crystal time evolution by cooling / heating of an atmospheric air parcel (turquoise line: RH_{ice}; black line: temperature; circles: aerosol particles; hexagons: ice crystals; red / blue / green colors: H_2SO_4 / H_2O / HNO_3 species.)

Due to the temperature decrease, the relative humidity with respect to ice increases. When RH_{ice} reaches the homogeneous, respectively the heterogeneous (in the presence of ice nuclei) freezing threshold ice starts to nucleate. From this point on, interstitial liquid aerosol particles coexist with the ice crystals. The nitric acid included in the freezing aerosol is retained in the forming ice. Ambient water vapor deposits on the newly formed crystals and the ice particles grow rapidly. Gaseous nitric acid surrounding the ice germ may simply be adsorbed onto the ice germ surface and become buried by subsequent ad – layers of molecules ('trapping effect', *Kärcher and Basko* (2004)). By further cooling, RH_{ice} keeps raising until the water depletion by ice from gas phase compensates the temperature decrease. At that moment RH_{ice} drops, either fast or slow, towards equilib-

rium values, depending on the microphysical properties of the ice cloud. The interstitial particles shrink with the RH_{ice} decrease. Water and nitric acid are released from the liquid particles in the gas phase. The ice crystals grow by the uptake of the water and nitric acid from the gas phase. When reaching a certain size, ice particles may settle down. As a consequence, water and other trace gases may be vertically redistributed. Important chemical atmospheric components that may be transported downward with the falling ice crystals are water and nitric acid. The differences in the partitioning of water and nitric acid in homogeneously or heterogeneously formed ice clouds are subject of the work presented here and will be shown in Sections 3.3.2 and 4.3.2. Figure 2.8 shows at the latest times a temperature increase, causing the RH_{ice} decrease under 100 %. The cirrus cloud approaches the end of its life. The ice crystals become smaller due to water sublimation and after a while, the cloud disappears completely.

Nitric acid in cirrus clouds

Some studies (e.g. *Borrmann et al.* (1997), *Solomon et al.* (1997) and *von Hobe* (2008)) propose that cirrus clouds in the cold tropopause region may play an important role in the chlorine activation through heterogeneous reactions of $ClONO_2$ and HCl at the surface of the ice particles (see Figure 2.1). Therefore the examination of nitric acid uptake onto cirrus cloud ice particles is very important to quantify the potential role of cirrus clouds in the upper tropospheric chemistry, especially for the UT ozone chemistry (*Krämer et al.* (2008a)).

Ullerstam and Abbatt (1997) have shown in laboratory experiments that HNO_3 is rapidly taken up by ice surfaces. The results were confirmed by field experiments that investigated the uptake of HNO_3 on cirrus cloud ice particles (*Popp et al.* (2006) and *Meilinger et al.* (1999)). The first study shows nitric acid measurements in a TTL sub-visible cirrus. When entering the cloud, particulate (liquid + ice) HNO_3 increased rapidly, being associated with corresponding changes in the gas phase. This can be explained by an efficient HNO_3 uptake on ice crystals. In the second study, particulate and gas-phase reactive nitro – oxides (NO_y) measurements were made while passing through an Arctic ice cloud near the tropopause at 196 K (*Meilinger et al.* (1999)). The nitric acid concentrations in the ice were significantly smaller than one would have expected. A possible explanation is that the depletion of gas-phase HNO_3 had occurred by efficient uptake onto the ternary

supercooled droplets. Consequently, only little amounts of nitric acid have remained available for uptake by ice particles. Measurements of condensed nitric acid in cirrus cloud particles observed during various airborne field campaigns showed very high HNO_3 / H_2O molar ratios, in a negative correlation with the ambient temperature (*Voigt et al.* (2006)). *Krämer et al.* (2008a) found that in the whole UT temperature range (T = 185–240 K), the HNO_3 fractions in ice can widely vary, from 0.01 up to 100 %. The same study shows also that the ice water content (IWC) in a cirrus cloud is a major parameter determining the content of HNO_3 at given temperatures. Neither the nitric acid retention in the particles at the moment of freezing, nor solely pure surface adsorption (*Tabazadeh et al.* (1999)) can explain the magnitude and the variability of the nitric acid content in ice crystals (*Popp et al.* (2004)). Moreover, recent laboratory investigations indicate a larger uptake of trace gases by growing ice films compared to experiments with static ice (*Ullerstam and Abbatt* (2005)). Consequently, the nitric acid uptake simulation must be reassessed, based on the fact that the ice surface as reference frame is not static.

Nitric acid, with by far lower partial vapor pressures than water at same temperature, deposits on growing ice crystals. Because of the very low molecular diffusion of nitric acid within the bulk – ice under UT conditions, the HNO_3 uptake is restricted to the surface layer. Additionally, it is proved that the major part of the adsorption is irreversible. Temperature fluctuations in the UT make ice crystals successively undergoing cycles of condensation Section 3.1.2growth / evaporation in a highly dynamic cirrus cloud environment. Hence, the nitric acid is literally encapsulated into the particle. When ice sublimates, the trapped nitric acid escapes in the gas phase. The 'trapping' of nitric acid on growing ice particles was implemented for the first time in a process model by *Kärcher and Voigt* (2006), yielding good results for the modeling of HNO_3 partitioning in cirrus clouds.

Further observations of nitric acid in the UT region are needed in order to resolve some of the outstanding questions concerning the mechanism and efficiency of HNO_3 uptake on ice clouds. Better prediction of the freezing pathways is necessary, since the partitioning of HNO_3 between ice and interstitial aerosol is very sensitive to the microphysical processes evolving in homogeneously / heterogeneously formed cirrus clouds (Sections 3.3 and 4.3.2).

Chapter 3

Modeling Aerosol and Ice Particles Dynamics

In this chapter, the theoretical and numerical requirements for the detailed microphysical aerosol and ice model MAID (*Bunz et al.* (2008)) are presented. In addition, the operational approach of MAID in sensitivity and closure studies is described. Finally, a study to validate MAID for UT calculations is carried out: a cirrus cloud already modeled by *Meilinger et al.* (1999) is reprocessed with MAID. Moreover, the results of *Meilinger et al.* (1999) are extended by detailed simulations: sensitivity studies are performed to test the revised modules of homogeneous and heterogeneous freezing implemented in MAID. The results are shown in Section 3.3.

3.1 Theoretical background

Figure 3.1 shows a flow chart of the major microphysical processes that govern aerosol and ice particles dynamics in the UT region and which are implemented in the model in form of numerical algorithms. Each element of this flow chart is described in the corresponding section, marked in reddish in Figure 3.1. A changing thermodynamic environment controls the behavior of the aerosol particle population, therefore processes like condensation growth vs. shrinkage due to evaporation, ice forming by homogeneous / heterogeneous freezing, water and nitric acid uptake on ice crystals vs. sublimation are simulated. Processes, like aerosol particle nucleation and coagulation are not considered here (*Bunz and Dlugi* (1991)). Since MAID is employed as a zero-dimensional model, following the evolution of an aerosol / ice population inside an atmospheric parcel that moves along a trajectory, sedimentation of ice particles is not described here.

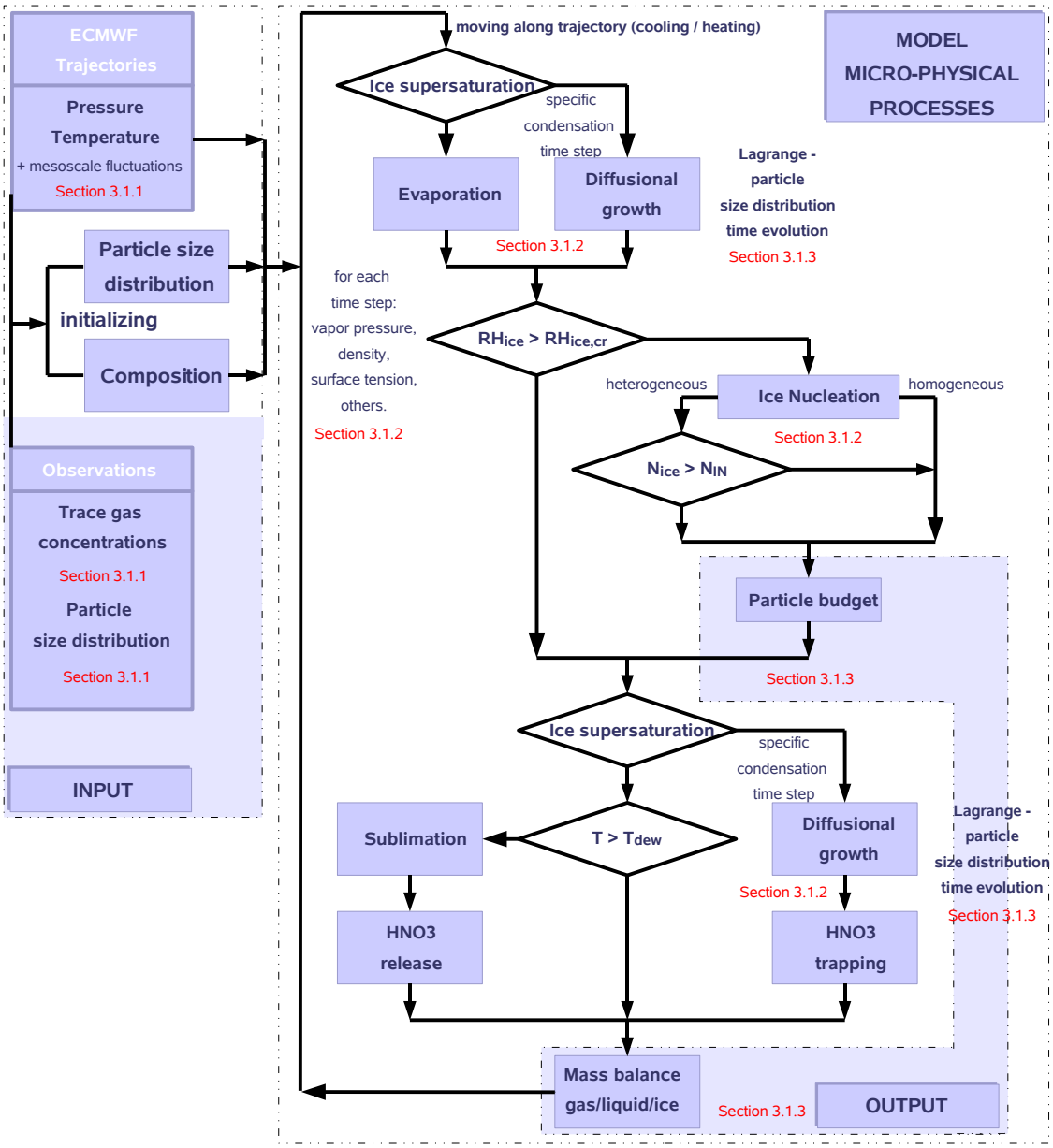

Figure 3.1: Flow chart of MAID (description of each element of the chart is given in the corresponding section, marked in reddish).

3.1.1 Model initialization

Thermodynamic variables

Under UT conditions, it is assumed that particle and ambient air temperature are the same. The model is forced with temperatures and pressures along atmospheric trajectories, as described in Section 4.2.1.

Chemistry and physical state of aerosol particles

Information about the physical state and the chemical composition of the aerosols is necessary when initializing the model. Under different ambient conditions, soluble aerosols of different sizes can be liquid or mixed (liquid + solid). Non-soluble solid cores, e.g. soot, can be embedded in liquid aerosols. Even if measurements of the chemical composition of aerosol particles in the upper troposphere show significant mass fraction of organic compounds (*Murphy et al.* (2006)), there is still almost no information about their thermodynamical behavior under UT conditions. Therefore, only inorganic species are considered here. The background aerosol particles consist of supercooled ternary solutions H_2SO_4 /H_2O / HNO_3.

Because of the very low surface vapor pressure at the low UT temperatures (Section 2.3), the sulphuric acid is completely incorporated in the solution droplets. Thus, it is treated as a part of the non-volatile core of the particle. Initial H_2SO_4 is calculated with the *Tabazadeh et al.* (1997) parametrisation, described in the box below.

***Tabazadeh et al.* (1997) parametrisation**

The UT background aerosols consist mainly of aqueous sulphuric acid particles (Section 2.1). The equilibrium composition of binary aerosols H_2SO_4 /H_2O under UT conditions depends on the temperature and relative humidity over ice (RH_{ice}) in accordance with *Tabazadeh et al.* (1997) parametrisation, based on the thermodynamic model of *Carslaw et al.* (1995):

$$m_{H_2SO_4}(a_w, T) = y_1(a_w) + \frac{(T-190)\cdot(y_2(a_w) - y_1(a_w))}{70} \tag{3.1}$$

where

$m_{H_2SO_4}$ – sulphuric acid molality in mol $\cdot$ kg^{-1};

a_w	– water activity of the H_2SO_4 /H_2O solution;
T	– temperature in K;
y_1, y_2	– polynomial functions $y = A \cdot a_w^B + C \cdot a_w + D$;
A, B, C, D	– coefficients in the polynomial composition functions y for binary solutions H_2SO_4 /H_2O.

Equation 3.1 is valid for temperatures between 185 and 260 K and a wide range of droplet solution composition, and therefore for a wide range of water activities.

The nitric acid starts, other than the sulphuric acid, completely in the gaseous state and is partitioning during the simulation between gas and aerosol / ice particles depending on temperature and composition of phases. Mixing ratios of HNO_3 and H_2O observed during field campaigns are utilized to initialize the model.

Particle size distribution

For a detailed simulation of aerosol dynamics and thermodynamics, the particle population is represented in the model using a sectional approximation. The size distribution is therefore divided in discrete 'bins', each section contains internally mixed particles (i.e. all the particles in a bin have the same composition). Aerosol measurements during field campaigns provide the information about the size distribution of the simulated particle population, such as shape of the particle size distribution (i.e. how many modes) and characteristics of each particle mode (total number densities, geometrical mean radii and standard deviations). The initial aerosol population is created as described in the box.

Aerosol particle representation

The atmospheric aerosol ensemble is simulated by a density function $n(\vec{R}, r, t)$. where

$\vec{R}$	– location of the particle;
r	– a particle property, e.g. size, composition or shape;
t	– time.

$\vec{R}$ can be neglected if it is assumed that the box is homogenized by convective mixing.

The space independent density function $n(r,t)$ is described by:

$$n(r,t) = \int_{x_k-\frac{1}{2}\Delta x}^{x_k+\frac{1}{2}\Delta x} n(x,t)dx \tag{3.2}$$

x – dimension describing the bin;
Δx – bin width.

The atmospheric aerosol size distribution covers many orders of magnitude in its dimensions (radii, number densities). Consequently:

$$x_k = \ln(v_k) \tag{3.3}$$

$$x_k = x_1 + (k-1)\Delta x \qquad k = 1,...,N_b \tag{3.4}$$

k – indices describing the bin;
v_k – volume of single particles in the size bin k in m^3.

In order to generate a discrete size distribution, the model uses the method of volume ratio size distribution (e.g. *Jacobson* (2005)):

$$v_k = V_{rat} \cdot v_{k-1} \qquad k = 1,...,N_b \tag{3.5}$$

where

v_{k-1} – volume of single particles in the next smaller size bin (k^{th}-1) in m^3;
V_{rat} – volume growth factor.

$$V_{rat} = \exp(\Delta x) \tag{3.6}$$

$$v_k = V_{rat}^{k-1} \cdot v_1 \qquad k = 1,...,N_b \tag{3.7}$$

$$V_{rat} = \left(\frac{v_{N_b}}{v_1}\right)^{\frac{1}{N_b-1}} = \left(\frac{r_{N_b}}{r_1}\right)^{\frac{3}{N_b-1}} \tag{3.8}$$

where

r_1 – particle radius in the first bin in m;
r_{N_b} – particle radius in the highest bin in m.

The total volume concentration in a size bin is (see also 3.1.3):

$$V_k = \sum_{kk} V_{kk,k} \qquad k = 1,...,N_b \qquad kk = 1,...,N_v \tag{3.9}$$

where

kk – indices describing the chemical component;
$V_{kk,k}$ – component volume concentration in a size bin in $m^3 \cdot m^{-3}$;
N_b – total number of size sections;
N_v – total number of components.

Since the atmospheric aerosol is assumed to be a continuum, the model computes an initial size distribution based on the above described information using analytical functions, see e.g. *Jänicke* (1998). Three superimposed logarithmic normal distributions can be simulated:

$$\frac{dN}{d\log r} = \sum_{m=1}^{m=3} \frac{N_m}{\sqrt{2\cdot\pi}\cdot\log\sigma_m} \cdot \exp\left(-\frac{1}{2}\cdot\frac{\log^2\left(\frac{r}{\bar{r}_m}\right)}{\log^2\sigma_m}\right) \tag{3.10}$$

where

N – particle number densities in m^{-3};
r – particle radius in m;
m – indices for the three modes;
$\log\sigma_m$ – standard deviation of $\log r$;
$\bar{r}_m$ – geometrical mean radius in m.

3.1.2 Microphysical aerosol processes in the model

Condensation growth and evaporation

The mass transfer between the bulk gas phase and the surface of the aerosol particles is treated explicitly, using a kinetic approach: equilibrium prevails only within the particles, not between bulk gas and condensed phase. The gradient between the ambient vapor pressure of the condensable components and that at the particle surface is the driving force for the mass transfer (e.g. *Wexler and Potukuchi* (1998)). When the gradient is positive, particles grow due to a mass flux of the condensing vapor to the aerosol. In the case of a negative gradient, the mass flux is directed from the condensed phase

towards the gas phase, and then evaporation causes particle shrinkage. The numerical algorithms used to simulate the condensation growth are shown in the box.

Numerical formulations for the mass transfer

The mass change of a single particle, due to condensation of the kkth gaseous compound is:

$$\frac{dm_{kk}}{dt} = 4 \cdot \pi \cdot D_{kk} \cdot \frac{M_{kk}}{R \cdot T} \cdot r_p \cdot f(K_n, \alpha) \cdot (p_{kk,\infty} - p_{kk,s}) \tag{3.11}$$

where

kk	– indices for the kkth component;
D_{kk}	– diffusion coefficient of vapor in m$^2 \cdot$ s^{-1} (see Eq.3.12 and 3.13);
M_{kk}	– molecular weight in kg $\cdot$ mol^{-1};
R	– gas constant = 8.3143 J $\cdot$ mol^{-1} $\cdot$ K^{-1};
r_p	– particle radius in m;
$f(K_n, \alpha)$	– correction factor to continuum diffusion (see Eq.3.14);
K_n	– Knudsen number (see Eq.3.15);
α	– accommodation factor;
$p_{kk,\infty}$	– partial pressure of the condensable gas far from the particle in Pa;
$p_{kk,s}$	– vapor pressure at the curved particle surface in Pa (see Eq.3.19).

The accommodation factor represents the fraction of molecules sticking onto the particle when colliding with it.

Diffusivity coefficients of vapors in the air are parameterized as follows:

$$D_{H_2O} = 21.1 \cdot 10^{-6} \cdot \left(\frac{T}{T_0}\right)^{1.94} \cdot \left(\frac{p_0}{p}\right) \tag{3.12}$$

Pruppacher and Klett (1997)

$$D_{HNO_3} = 13.13 \cdot 10^{-6} \cdot \left(\frac{T}{T_0}\right)^{1.75} \cdot \left(\frac{p_0}{p}\right) \tag{3.13}$$

VDI–Wärmeatlas (2006)

where

D_{H_2O}	– diffusivity coefficient of water vapor in air in m$^2 \cdot$ s^{-1} ;
D_{HNO_3}	– diffusivity coefficient of nitric acid in air in m$^2 \cdot$ s^{-1};
T	– air temperature in K, T_0 = 273.15 K;
p	– ambient pressure in Pa , p_0 = 1.01325 Pa.

In the transition regime (i.e. between continuum and free molecular flow), the diffusion of particles with diameters smaller or in the same range with the mean free path of the gas molecules is corrected with the

factor $f(K_n, \alpha)$ (*Dahneke* (1983)), considering an imperfect surface accommodation:

$$f(K_n, \alpha) = \frac{1 + K_n}{1 + \frac{2 \cdot K_n \cdot (1 + K_n)}{\alpha}} \tag{3.14}$$

$$K_n = \frac{\lambda}{r_p} \tag{3.15}$$

where

λ – mean free path in m;

The Knudsen number can be expressed by means of diffusivity coefficient and mean velocity of the vapor molecules:

$$K_n \cong 2 \cdot \frac{D_{kk}}{\overline{c_{kk}}} \tag{3.16}$$

where

$\overline{c_{kk}}$ – mean velocity of the vapor molecules in $m \cdot s^{-1}$ (see Eq.3.17).

$$\overline{c_{kk}} = \sqrt{\frac{8 \cdot R \cdot T}{\pi \cdot M_{kk}}} \tag{3.17}$$

Parametrisations for the vapor pressures of the trace gases over plain solutions containing mixtures of H_2SO_4 / H_2O / HNO_3 in equilibrium with ice at very low temperatures were made by *Luo et al.* (1995):

$$\ln p = A(wt) + \frac{B(wt)}{T} + \ln C(wt) \tag{3.18}$$

where

p – saturation vapor pressure over supercooled solutions in Pa;
A, B, C – correlation coefficients depending of the solution concentration;
wt – weight fraction of the component.

The saturation vapor pressures over curved particle surfaces are corrected with the Kelvin factor:

$$p_{kk,s} = p_{kk,s,pl} \cdot \exp\left(\frac{2 \cdot \sigma \cdot M_{kk}}{\rho \cdot R \cdot T \cdot r_p}\right) \tag{3.19}$$

(e.g. *Pruppacher and Klett* (1997))

where

$p_{kk,s,pl}$ – saturation vapor pressure over plain solutions in Pa (see Eq.3.18);
σ – average particle surface tension in $kg \cdot s^{-2}$ (see Eq.3.20);
M_{kk} – molecular weight in $kg \cdot mol^{-1}$;
ρ – particle density in $kg \cdot m^{-3}$ (see Eq.3.21).

Further, densities and surface tensions of ternary solutions H_2SO_4 / H_2O / HNO_3 at upper tropospheric temperatures are described in the parametrisation by *Martin et al.* (2000):

$$\sigma(x,y) = \frac{\sum_{i=0}^{5}\sum_{j=0}^{5}\sigma_{i,j}\cdot x^i \cdot y^j}{\sigma_0 + \sigma_1 \cdot x + \sigma_2 \cdot y} \tag{3.20}$$

$$\rho(x,y) = \sum_{i=0}^{4}\sum_{j=0}^{3}\rho_{i,j}\cdot x^i \cdot y^j \tag{3.21}$$

where

x – weight percent of H_2SO_4;
y – weight percent of HNO_3;
σ – coefficients in a polynomial expansion of surface tension of ternary solutions H_2SO_4 / H_2O / HNO_3;
ρ – coefficients in a polynomial expansion of density of ternary solutions H_2SO_4 / H_2O / HNO_3.

Homogeneous and heterogeneous ice nucleation and sublimation

The model describes the phase transition from metastable STS droplets to ice as an important process in the formation of ice clouds. Other than in warm clouds, very high water supersaturation with respect to ice have to be reached before exceeding the nucleation threshold (Section 2.2). The saturation water vapor pressure over ice is described in the parametrisation by *Marti and Mauersberger* (1993), given in the box below.

***Marti and Mauersberger* (1993) parametrisation**

$$p_{sat,ice} = \exp\left(\frac{A}{T} + B\right) \tag{3.22}$$

where

$p_{sat,ice}$ – saturation water vapor pressure over ice in Pa;
A – parametrisation coefficient, A=-6132.935395;
B – parametrisation coefficient, B=28.867509.

The relative humidity with respect to ice RH_{ice} is:

$$RH_{ice} = \frac{p_{H_2O}}{p_{sat,ice}} * 100. \tag{3.23}$$

where

p_{H_2O} – water partial vapor pressure in Pa.

The ice saturation ratio S_{ice} is:

$$S_{ice} = \frac{RH_{ice}}{100} = \frac{a_w}{a_w^{ice}} \tag{3.24}$$

where

a_w – water activity in a liquid solution;
a_w^{ice} – water activity in a solution in equilibrium with ice.

The critical ice saturation ratios S_{cr}^{hom} and S_{cr}^{het} represent the S_{ice} threshold for the homogeneous and heterogeneous ice nucleation, respectively.

Homogeneous freezing of the supercooled aerosol particles is simulated using the parametrisation by *Koop et al.* (2000), based on experimental data, where the nucleation rate coefficients of supercooled aqueous solutions depend only on water activity and temperature. The box below details the parametrisation by *Koop et al.* (2000).

***Koop et al.* (2000) parametrisation for the homogeneous ice nucleation**

The homogeneous ice nucleation rate is proportional to the particle volume:

$$j_{hom} = V_p \cdot J_{hom}(a_w, T) \tag{3.25}$$

where

j_{hom} – homogeneous ice nucleation rate in s^{-1};
J_{hom} – homogeneous ice nucleation rate coefficient in $m^{-3} \cdot s^{-1}$;
V_p – particle volume in m^3.

The parametrisation for $J_{hom}(a_w, T)$, given by *Koop et al.* (2000) is:

$$\log\left(J_{hom}(a_w, T)\right) = -906.7 + 8502 \cdot \Delta a_w - 26924 \cdot (\Delta a_w)^2 + 29180 \cdot (\Delta a_w)^3 \tag{3.26}$$

with

$$\Delta a_w = a_w - a_w^{ice} \qquad 0.26 < \Delta a_w < 0.34 \tag{3.27}$$

Heterogeneous freezing may be a very important pathway for cirrus clouds formation (*Jensen et al.* (1998)). Therefore, this mechanism had to be introduced in MAID. The formulations used in the model and detailed in the box describe the 'shifted' activity method, proposed by *Kärcher and Lohmann* (2003). All parametrisations shown in panel b of Figure 2.5 were lately implemented in MAID.

In the sensitivity and closure studies, presented in this chapter and also in Chapter 4, the ice nuclei are represented by soot particles coated with sulphuric acid. For this ice nuclei type, the parametrisation of critical saturation ratios S_{cr}^{het} as a function of temperature have been implemented in the model, based on experiments in the AIDA aerosol chamber (*Möhler et al.* (2005)). The heterogeneous ice nuclei number density is set using the study by *Blake and Kato* (1995), who sampled and characterized black carbon soot aerosols from the upper troposphere and lower stratosphere and derived latitudinal number densities, as well as total mass and total surface area.

The approach used in MAID is to let ice nucleate until all insoluble cores are consumed. At that moment, heterogeneous ice nucleation is suppressed and, if further cooling of the air parcel occurs, two alternatives for the later cloud evolution are open:

- water vapor depletion by deposition on the ice can compensate an increase of relative humidity; the few existing crystals grow; the cloud remains 'thin';
- relative humidity increases continously and exceeds the threshold for a subsequent homogeneous ice nucleation; supercooled ternary droplets freeze; the 'homogeneous' cloud consists in this case of many small ice crystals.

'Shifted activity' method for the heterogeneous ice nucleation

In order to force in the simulations the particles to freeze at these prescribed values, it is necessary to 'shift' the water activity with a certain amount δa_w.

$$\delta a_w = \left(S_{cr}^{hom}(T, r_p) - S_{cr}^{het} \right) \cdot a_w^{ice} \tag{3.28}$$

where

S_{cr}^{hom} – homogeneous critical freezing saturation;
S_{cr}^{het} – heterogeneous critical freezing saturation.

The critical freezing saturation of homogeneous ice formation S_{cr}^{hom} is computed depending on temperature and liquid aerosol size by choosing an ice nucleation rate of 1 min^{-1} (*Koop et al.* (2000)).

The critical freezing saturation of heterogeneous ice formation S_{cr}^{het} is derived from AIDA ice nucleation measurements of soot particles coated with sulfuric acid (*Möhler et al.* (2005)), which are believed to be important ice nuclei in the upper tropospheric region.

The heterogeneous ice nucleation rate is given by:

$$j_{het} = A_c \cdot J_{het}(a_w, T, Z) \tag{3.29}$$

where

j_{het} – heterogeneous ice nucleation rate in s^{-1};
J_{het} – heterogeneous ice nucleation rate coefficient in $m^{-2} \cdot s^{-1}$;
Z – a set of factors that determine the freezing behavior of the ice nuclei;
A_c – ice nuclei surface in m^2.

$$J_{het}(a_w, T, Z) = \Delta \cdot J_{hom}((a_w + \delta a_w), T) \tag{3.30}$$

where

Δ – ratio of kinetic pre-factors of homogeneous / heterogeneous freezing mechanisms; $\Delta \approxeq 30 \cdot 10^{-9}$ in m *Kärcher and Lohmann* (2003).

In mixed phase particles both mechanisms, heterogeneous freezing and homogeneous freezing in the liquid shell coating the ice nuclei, contribute in the calculations of ice nucleation rates, as shown in the box.

Ice nucleation in mixed phase particles

While Equations 3.29 and 3.30 could well describe the deposition freezing, the next formulation is used in case of the immersion freezing (see heterogeneous freezing in Section 2.2). The ice nucleation rate is then given by:

$$\begin{aligned} j_{mix} = (V_p - V_c) \cdot J_{hom}(a_w, T) + A_c \cdot J_{het}(a_w, T, Z) = \frac{4 \cdot \pi \cdot r_c^3}{3} \\ \cdot \left(\left(\left(\frac{r_p}{r_c} \right)^3 - 1 \right) \cdot J_{hom}(a_w, T) + \frac{3 \cdot \Delta}{r_c} \cdot J_{hom}((a_w + \delta a_w), T) \right) \end{aligned} \tag{3.31}$$

where

j_{mix} – ice nucleation rate in mixed phase particles in s^{-1};
r_c – radius of insoluble core, embedded in liquid aerosol particle in m;
$\frac{r_p}{r_c}$ – e.g. H_2SO_4 coating fraction of the soot cores (*Möhler et al.* (2005)).

The nucleation rates influence the probability that liquid particles freeze in a bin. The concentrations of the aerosol components are conserved at each time step, they only pass from the liquid to the ice phase. The retention fraction of the described volatile species are reported to be near unity (*Yin et al.* (2002)), so that the molecules dissolved in the liquid phase are considered to be entirely retained in the ice particles upon freezing.

The ice crystals are supposed to sublimate, if the ambient temperature is higher then their dew point ($T > T_{dew}$). In that case, any contained soluble trace species will evaporate at a rate consistent to the mass transfer law, depending on the partial vapor pressures in the system.

Trace gases uptake on ice particles – nitric acid 'trapping'

The ice crystal growth due to water vapor deposition is treated in the same manner as for aerosols (see box '**Numerical formulations for the mass transfer**'). The investigation of nitric acid partitioning in cirrus clouds is one of the goals of this work. Therefore the implementation of the HNO_3 'trapping' on growing ice crystals in MAID was necessary. At the moment, this is considered the best mechanism to describe the nitric acid uptake on cirrus ice particles (Section 2.3). The implemented numerical algorithms are presented in the box below.

Nitric acid 'trapping'

The uptake of gaseous nitric acid by ice crystals growing, due to water vapor deposition, depends on the combined effect of all processes controlling the mass transfer like surface kinetics, gas diffusion toward the ice particles and limitations related to the burial processes. To take this into account the mass flux expression is multiplied with ε, which is defined as trapping efficiency (*Kärcher and Basko* (2004)).

$$\frac{dm_{HNO_3}}{dt} = 4 \cdot \pi \cdot D_{HNO_3} \cdot \frac{M_{HNO_3}}{R \cdot T} \cdot r_p \cdot \varepsilon(\gamma) \cdot (p_{HNO_3,\infty} - p_{HNO_3,s}) \tag{3.32}$$

where

D_{HNO_3}	– diffusion coefficient of gaseous nitric acid in $m^2 \cdot s^{-1}$ (see Eq. 3.13);
M_{HNO_3}	– molecular weight in $kg \cdot mol^{-1}$;
$\varepsilon(\gamma)$	– trapping efficiency;
γ	– uptake coefficient;
$p_{HNO_3,\infty}$	– partial pressure of HNO_3 far from the particle in Pa;
$p_{HNO_3,s}$	– vapor pressure at the curved particle surface in Pa (see Eq.3.19).

The uptake coefficient γ is defined as the ratio between the actual mass flux and the maximum kinetic mass flux. It depends on the combined effect of all processes controlling the mass transfer. It has lower values than the probability for molecular sticking (see accommodation factor α in Equation 3.11). A comparison of laboratory studies of nitric acid uptake coefficient on ice depending on temperature are described in *Gamblin et al.* (2007). An empirical fit for the data is used in the model:

$$\gamma = 0.635 - 0.00275 \cdot T \tag{3.33}$$

Kärcher and Voigt (2006) determined, based on field data, a parametrisation for the trapping efficiency, ε, as function of temperature (between 195 K and 240 K). By employing this parametrisation in sensitivity studies (Sections 3.3 and 4.3.2), the yielded trapping efficiencies of higher than 0.5 led very quickly to the complete nitric acid uptake on ice, in all created scenarios. This situation is unrealistic, compared with the observations.

Therefore, reduced trapping efficiencies $\varepsilon \approx 0.1$ are used in the simulations, in order to make the model results at least comparable with the observations.

The heterogeneous ice nucleation and the nitric acid uptake on growing ice crystals may significantly impact on the UT region (Chapter 2). Therefore, these processes have been lately implemented in MAID, to perform UT trajectory calculations.

3.1.3 Numerical techniques used in MAID

The condensation growth equations are solved very precisely by a finite difference method, according to the chosen representation of the particle size distribution and its time evolution. For the very small time steps used in this method, variations of parameters depending on temperature and particle size are also small. This circumstance together with an exact mass balance among phases provide most accurate solutions for the model simulations.

Interpolation for domains that are not distinctly specified in the parametrisations are solved numerically using spline functions (e.g. *Stör and Bulirsch* (1993)).

Mass balance

The boundaries of the simulated air parcel are considered closed. Cross-boundary fluxes of water, trace gases, particles or heat are not allowed. All processes described below conserve the mass of the aerosols components in different physical states.

When the temperature and pressure stay constant, the number density of molecules of a given species does not change, but it partitions between the gas and particulate (liquid + solid) phase. Along the atmospheric trajectory of an air parcel, the number densities of the different physical states change at each time step with temperature and pressure according to the ideal gas law.

Quantities balance

Different quantities are balanced among the solid, liquid and gaseous state. For instance the total number density of molecules of kkth component is:

$$n_{kk}^{tot} = n_{kk}^{g} + \sum_{k} n_{kk}^{l} + \sum_{k} n_{kk}^{s} \tag{3.34}$$

where

kk	– indices for the kkth component;
k	– indices for the kth size bin;
$n^{g/l/s}$	– total number density of molecules of kkth component in gas / liquid / solid phase in m^{-3}.

The quantities changes along a trajectory, caused by temperature and pressure changes are:

$$\frac{dn}{dt} = n \cdot \left(\frac{1}{p} \cdot \frac{dp}{dt} - \frac{1}{T} \cdot \frac{dT}{dt} \right) \tag{3.35}$$

The exact mass balance of the aerosols components in different physical states is a highlight of MAID, allowing to compute for each model step all parameters involved in the microphysical processes. The partitioning of water and nitric acid among gas / liquid / solid is therefore precisely determined.

Consequently, the model is very suitable to simulate the in-situ formation and evolution of a cirrus cloud. The very detailed handling of the diffusive growth of aerosol and ice parti-

cles allows comprehensive studies, like the investigation of cirrus microphysics sensitivity to the water accommodation coefficient.

Lagrangian time evolution of particle size distribution

The particles consist of a 'core' of non-volatile material (in this case H_2SO_4) and a 'shell' of relatively volatile material (H_2O and HNO_3), following a full – moving structure (*Jacobson* (2005)). This means, during condensation / evaporation of the volatile components, the particles are allowed to grow / shrink at a rate, which is consistent with the condensation growth law. In addition, the core volumes are preserved upon condensation / evaporation of the shell material (Figure 3.2). Under these circumstances, the particles do not leave the size bin that they started in. Consequently, numerical diffusion among bins in the time evolution of the particle size distribution may be eliminated.

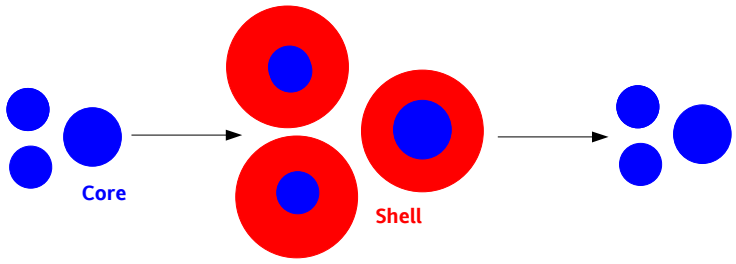

Figure 3.2: Preservation of aerosol material upon growth and evaporation in a 'full – moving structure'

The size distribution dynamics of the liquid and that of the frozen particles are treated separately within the simulation. The radius of an ice crystal as size coordinate signifies in the model the radius of a sphere with an equivalent volume.

The Lagrangian size distribution dynamics of a particle population is illustrated by the following test simulation, depicted in Figure 3.3. The initialized air parcel contains 100 aerosol particles /cm^3, in a size range 10 nm to 5 μm, distributed in 30 bins. Panel a of Figure 3.3 shows the thermodynamic history of the test parcel. The temperature and pressure evolutions are chosen to reproduce an ascending / descending movement of an atmospheric air parcel under very cold tropical UT conditions. The time evolution of aerosol and ice particles in the test air parcel (x axis represent the particle size, z axis

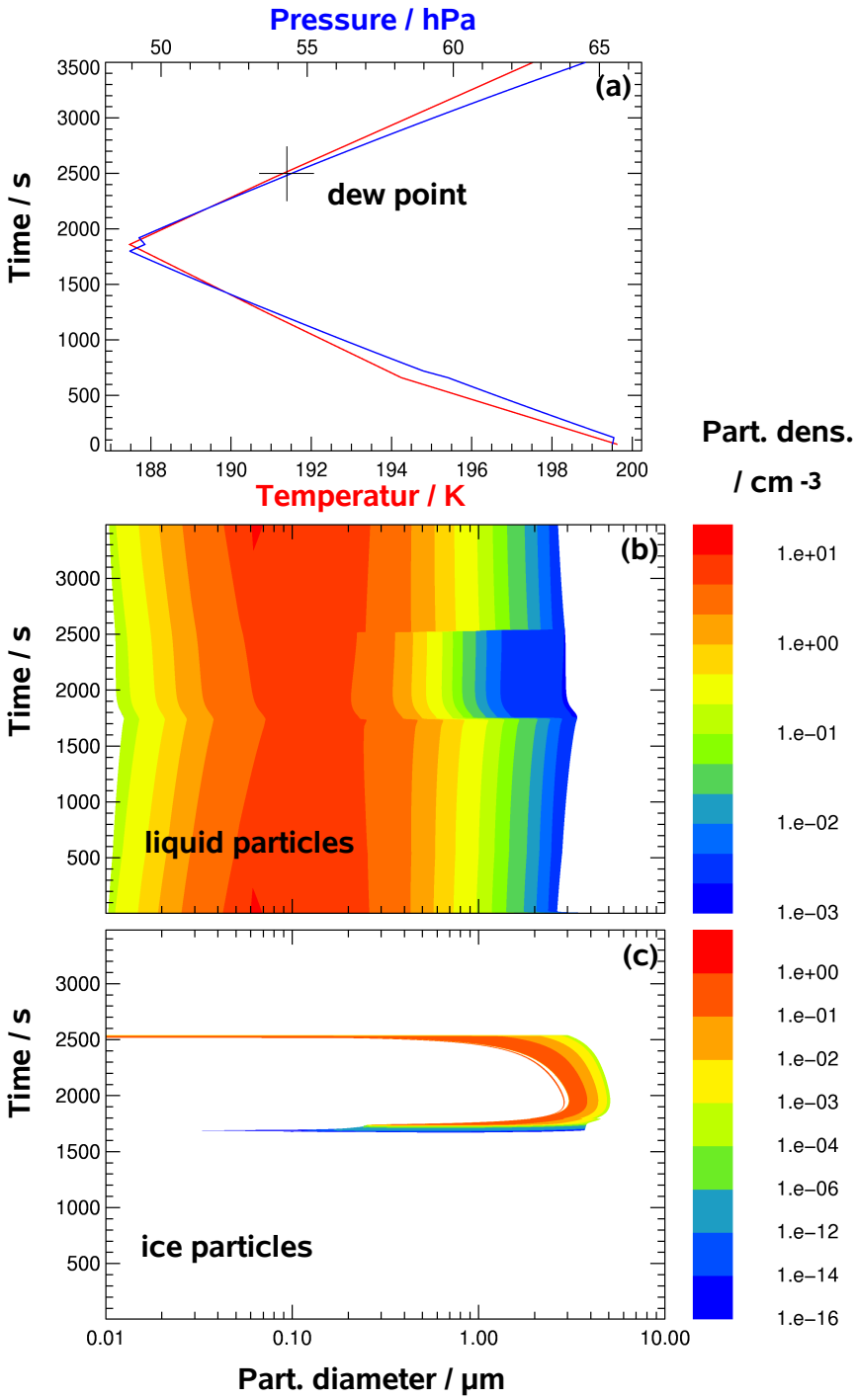

Figure 3.3: MAID test simulation (a: temperature–red and pressure–blue history of the air parcel; b, c: Lagrangian time evolution of the size distribution for liquid and ice particles, respectively; for details see text).

represent the particle number densities) is shown in the panels b and c. During the cooling period (in the first 1800 s of the test, T drops from 200 K to ≈187 K), a slight growth due to trace gases uptake of the aerosol particles is seen in panel b. After about 1700 s, ice nucleates first in bins situated near the 20^{th} bin, afterwards in all bins. The ice crystals grow very fast. The ice particle size distribution gets a sharp form, moving fastly to bigger sizes. In the second part of the test, the temperature increases to 200 K. The crystals live for a while, even after heating has started. When the ambient temperature exceeds the dew point at ≈2500 s (indicated by the cross in the Figure 3.3), the ice particles sublimate and the liquid aerosol size distribution reaches again its initial form.

3.2 MAID operational approach in sensitivity and closure studies

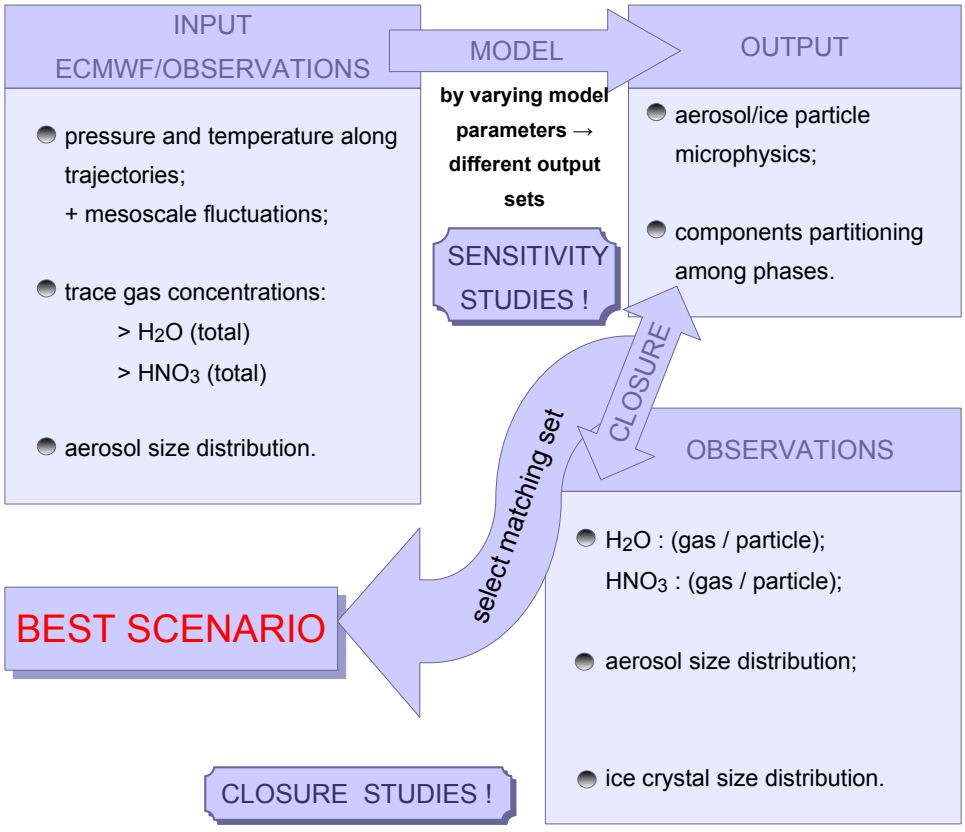

Figure 3.4: Operation scheme of MAID for sensitivity and closure studies.

The schematic shown in Figure 3.4 describes the operation of MAID as box model along atmospheric back trajectories, to perform sensitivity and closure studies. The model is initialized using observational data as described in the Sections 3.3.1 and 4.2. Initial temperature and pressure, information about the total (gas + particles) water and nitric acid, as well as the characterization of the aerosol particles are needed to calculate the particle population at the beginning of the simulations. Moreover, temperature and pressure history along the atmospheric trajectories constitutes the thermodynamic environment that determines the development of the particle population. By varying the input data, potential scenarios of the evolution of atmospheric microphysical processes are created. Such analyses are important to investigate the impact of different atmospheric parameters on the cloud formation and evolution (sensitivity studies). The simulations deliver for each model time step and each scenario detailed information sets, describing the particle microphysics and partitioning of chemical species among phases. Consequently, each model output set corresponds to the cloud development for a certain scenario. All output sets are finally compared with the airborne measurements (closure study). The closure matching data set is assigned to the 'best scenario', which most likely describes the formation and evolution of the probed cloud.

3.3 MAID validation: sensitivity studies of an Arctic cirrus cloud

The initialization of the simulations is based on measurements of water, nitric acid, aerosol and ice particles from instruments on-board the DLR – Falcon aircraft during the Polar Stratospheric Aerosol Experiment, POLSTAR–1. The model is forced by the temperature and pressure history of a single air parcel that moves along an atmospheric trajectory and reaches the flight path in the observed Arctic cloud layer on 24^{th} January 1997. MAID is employed to simulate the behavior of the aerosol population within this atmospheric parcel and the ice cloud formation, using two scenarios: in the first scenario, aerosol particles are exclusively allowed to freeze homogeneously, by blocking the heterogeneous ice nucleation, in the second scenario both, homogeneous and heterogeneous freezing may occur. The impact of different ice nucleation pathways on the microphysics, as well as on the H_2O and HNO_3 partitioning in the observed polar cirrus cloud is discussed in the following sections.

3.3.1 Model input

On 24^{th} January 1997 an Arctic cirrus cloud was observed in the tropopause region over the Atlantic, northwest of Scandinavia. This cloud was probed during POLSTAR–1 with the DLR Falcon aircraft, having on-board FZJ and DLR instruments to measure temperature, pressure, water, nitric acid, aerosol and ice particles. Details on measurements, in particular of the 24^{th} January flight, are provided elsewhere (e.g. *Feigl et al.* (1999), *Schiller et al.* (1999) and *Ziereis et al.* (2000)). The air parcel sampled in the cloud at

total water gas + particles	H_2O	10.3 ppmv
total nitric acid gas + particles	HNO_3	0.1445 ppbv
aerosol size distribution	N_{liq} $\bar{R}_{liq}$ σ_{liq}	$156\,cm^{-3}$ $0.05\,\mu m$ 2.25

Table 3.1: Parameters used to initialize the model simulations in the POLSTAR sensitivity studies

1200 UT is used to initialize the model (for initial parameters see Table 3.1). To determine the temperature history of the selected air parcel, a 3-days-backward trajectory is calculated with the 3-dimensional trajectory module of the Chemical Lagrangian Model of the Stratosphere (CLaMS, *McKenna et al.* (2002)). This module is driven by wind fields from ECMWF analyses. Trajectory temperatures had to be lowered by ≈ 12 K, so that the trajectory temperature at the Falcon sampling point matches the measured temperature. Finally mesoscale temperature fluctuations with an amplitude of 0.8 K are superimposed. The amplitude of the temperature fluctuations is calculated by using the parametrisation of *Gary* (2006), depending on the altitude, season, latitude and underlying substrates for the air parcel trajectory (see Section 4.2.1 for a detailed description of the approach used here). Since several recent studies showed that mesoscale vertical wind velocity may play the significant role in defining the microphysical properties of cirrus clouds, and not the synoptic-scale vertical wind, these superimposed mesoscale temperature fluctua-

tion are necessary for the UT calculations. The obtained temperature along the trajectory is plotted for a time range of - 2 h / + 3 h around the homogeneous ice cloud formation in Figure 3.5, panel a.

3.3.2 Sensitivity studies for the selected trajectory

Two scenarios of cloud formation are simulated along the selected trajectory:

- the aerosol particles freeze homogeneously ('hom' case);
- ice nucleates heterogeneously in the presence of soot particles coated with sulphuric acid ('het' case). The heterogeneous ice nuclei number density is set to 0.01 cm^{-3} (*Blake and Kato* (1995)). A subsequent homogeneous ice nucleation might occur.

The ice crystal number density N_{ice} throughout simulations is shown in panel b of Figure 3.5 (blue: homogeneous, red: heterogeneous case). The relative humidity evolution RH_{ice} is depicted in panel c, the nitric acid partitioning in liquid aerosol and ice in the panels e and f, respectively. The first ice crystals form heterogeneously earlier than in the 'hom' case (Figure 3.5: the red dashed line is more than one hour ahead of the blue dashed line), since the heterogeneous freezing threshold is lower than in the 'hom' case. Remarkably, in the 'het' case by further cooling a subsequent, homogeneous ice forming event occurs almost at the same time as in the pure 'hom' case.

$RH_{ice,het}$ is negatively correlated to the temperature fluctuations and has an increasing trend, until reaching the second nucleation step. This is attributable to the inefficient water vapor depletion by the few, heterogeneously nucleated ice crystals, which can not compensate the $RH_{ice,het}$ increase due to further cooling. High ice supersaturation persists for more than one hour. Both, $RH_{ice,het}$ and $RH_{ice,hom}$ drop after the homogeneous ice nucleation event and fluctuate around the saturation level. The amplitude of the $RH_{ice,het}$ fluctuations is slightly higher than that of $RH_{ice,hom}$. Since the integral ice particle size ($N_{ice} \cdot \bar{R}_{ice}$), as the parameter controling the RH_{ice}, is smaller in the heterogeneous than in the homogeneous case: $N_{ice,het} \cdot \bar{R}_{ice,het} < N_{ice,hom} \cdot \bar{R}_{ice,hom}$ (panel d of Figure 3.5), the water vapor deposition on ice crystals on the T descending / RH_{ice} ascending path of temperature fluctuations is slower in the heterogeneous case. The RH_{ice} increase is not so well compensated by the water depletion like in the homogeneous case, therefore the

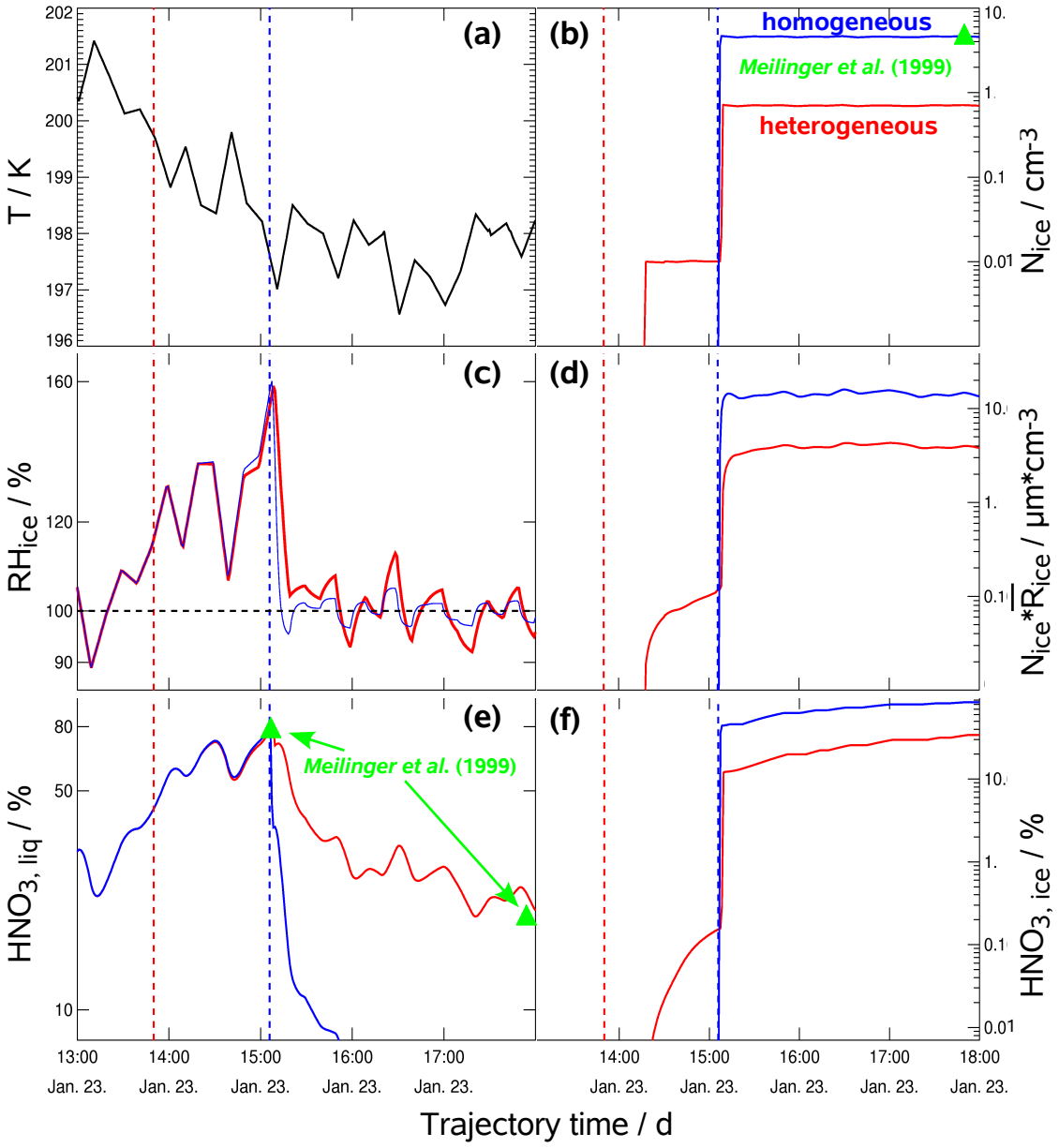

Figure 3.5: Evolution of an Arctic cirrus along an atmospheric trajectory, formed red: heterogeneously / blue: homogeneously (a: temperature – black; b: ice crystal number density; c: relative humidity with respect to ice; d: integral size of ice crystals; e: nitric acid in liquid aerosol; f: nitric acid in ice; dashed lines: appearance of first ice crystals; triangles: values presented by *Meilinger et al.* (1999), used in the MAID validation study).

higher RH_{ice}. The reverse processes on the T ascending / RH_{ice} descending path of temperature fluctuations explain the higher amplitude of $RH_{ice,het}$.

The uptake of nitric acid on liquid aerosol $HNO_{3,liq}$ (panel e) is sensitive to the evolution of RH_{ice} . Before homogeneous ice nucleation begins, up to 80 % nitric acid accommodates from the gas phase into the liquid particles. After the homogeneously formed cirrus appear, the most part of HNO_3 escapes from the interstitial particles again in the gas phase. This HNO_3 is trapped efficiently by the ice crystals. In the heterogeneous case, almost 40 % of the nitric acid remains in the interstitial particles one hour after the cloud formation (compared to less than 5 % in the homogeneous case) due to the persistent supersaturation. $RH_{ice,het}$ decreases under 100 % after 50 min, compared to 8 min in the homogeneous case.

The uptake of nitric acid on ice $HNO_{3,ice}$ (panel f) is also determined by the integral particle size $N_{ice} \cdot \bar{R}_{ice}$: nitric acid is slowly trapped by the few ice crystals formed heterogeneously. The nitric acid trapping on ice is more efficient after the homogeneous event, with a higher uptake of the available HNO_3 in the pure homogeneous case.

In a validation process, MAID was tested against *Meilinger et al.* (1999) conclusions and showed good agreement: in the homogeneous case, MAID yields similar results, concerning the ice number densities, as well as the partitioning of water and nitric acid directly after ice have formed. The nitric acid in the interstitial particles simulated with MAID do not agree with the *Meilinger et al.* (1999) study. There, the nitric acid in ice is represented only by the small amount retained upon the freezing of the aerosol particles. In the MAID simulation, higher nitric acid amounts partition into the ice, due to the HNO_3 trapping mechanism in the growing ice crystal. Corresponding, higher amounts of nitric acid than in *Meilinger et al.* (1999) escapes from the liquid particles. Therefore, lower nitric acid in the interstitial particles are simulated with MAID. However, MAID shows the advantage of the improved ice nucleation scheme, by allowing detailed investigations of the impact of different freezing mechanism on the cloud formation and evolution. These results show significant differences between the homogeneous and heterogeneous scenario in the water and nitric acid partitioning in an Arctic cirrus cloud at temperatures ≈ 200 K. These differences become more obvious at lower temperatures (T = 185 K, see CR–AVE study in Chapter 4).

Chapter 4

Tropical Cirrus: A Case Study

A detailed case study of a tropical sub-visible cirrus cloud is presented here. The sub-visible cirrus layer was observed on February 2nd 2006 near the tropical tropopause, few degrees north of the Equator and southwest of Costa Rica, during the Costa Rica Aura Validation Experiment (CR – AVE). The evolution of the relative humidity, ice microphysics and nitric acid partitioning in the cirrus cloud are investigated. The aim of this study is to reveal the origin of the very high supersaturation, frequently observed at typically low temperatures in the tropical UT region (see Section 2.2). Comprehensive sensitivity studies are performed by varying model parameters. In the closure study, all sensitivity runs are compared with the in-situ observations. The simulation yielding results next to the observations is selected as the most likely ('best') scenario for the microphysical and chemical processes that actually produced the observed cirrus (*Gensch et al.* (2008)).

4.1 Sketch of the 2nd February CR – AVE flight

The CR – AVE mission (http://cloud1.arc.nasa.gov/ave – costarica2/) was designed to explore the tropical UT region and to provide information for validation of satellite observations (e.g. for Aura satellite). A special scientific interest during CR – AVE was assigned to in-situ formed tropical sub-visible cirrus clouds. The in-situ sampling of very cold tropical tropopause layer (TTL) air in the vicinity and inside the thin cirrus layers were carried out with the complex instrumentation on-board the NASA high altitude research aircraft WB – 57. The WB – 57 flight track on 2nd February 2006 is shown in Figure 4.1. The sub-visible cirrus (red curve) was observed on the southbound leg of the WB – 57 flight from San Jose, Costa Rica, at an altitude of about 17000 m, over a broad geographic extent ($>$700 km). The observations show also clear air episodes in the cloud layer.

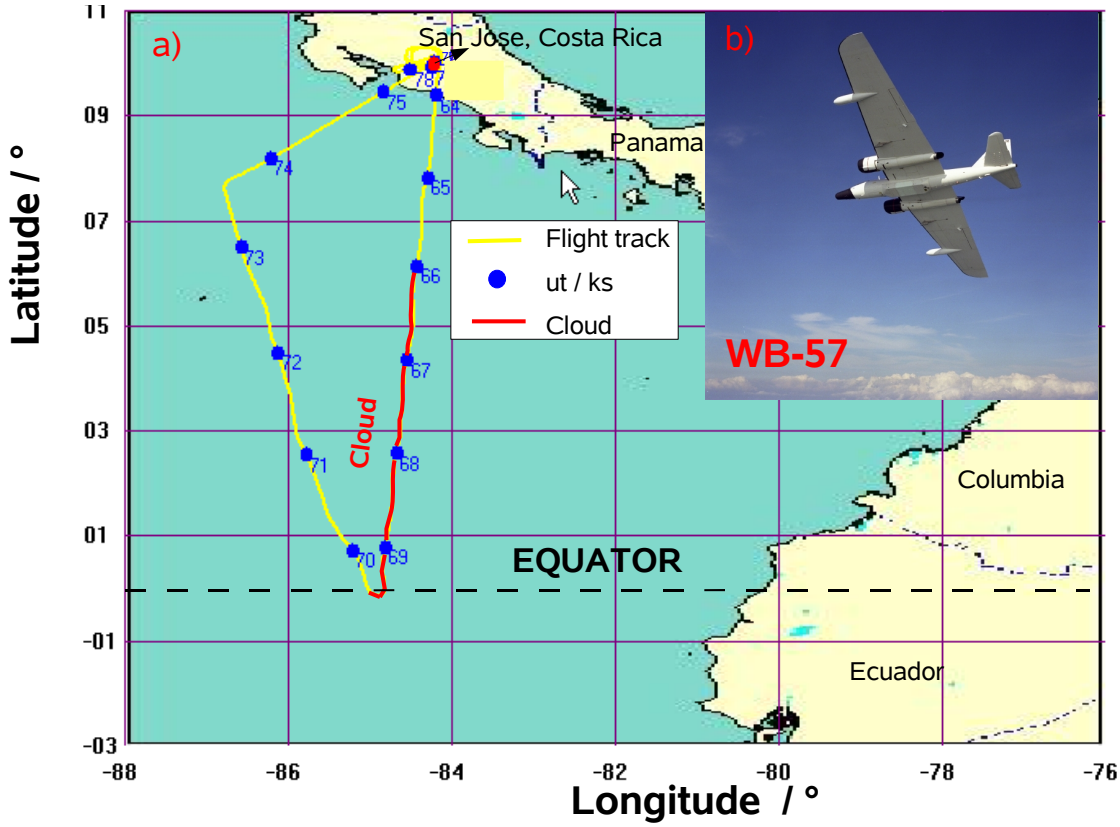

Figure 4.1: a: CR – AVE flight track on 2nd February 2006 (yellow line: flight track; red line: cirrus cloud; blue dots: universal time in ksec); b: NASA WB – 57 high altitude research aircraft.

The 5 – days – backward trajectories, shown in Figure 4.2, are determined with the 3 – dimensional trajectory module of the Chemical Lagrangian Model of the Stratosphere (CLaMS, *McKenna et al.* (2002)). This module is driven by wind fields from ECMWF analyses. The approach used here is to extract temperature and pressure every hour along the back trajectories, which start every three minutes at the WB – 57 flight path during the time period when the cloud was observed (1820 – 1920 ut). The analysis of the air parcel history and satellite GOES – 12 infrared pictures (Appendix A) show that the air sampled inside the cloud was not influenced by convection during the past few days. It generally came from subtropical regions and experienced a series of ascending/descending sequences. The cloud could have formed near the tropopause as the air was advected by equatorward – flowing limbs of the subtropical jet stream (Appendix B) into regions of anomalously low temperatures. These conditions suggest an in – situ cloud formation.

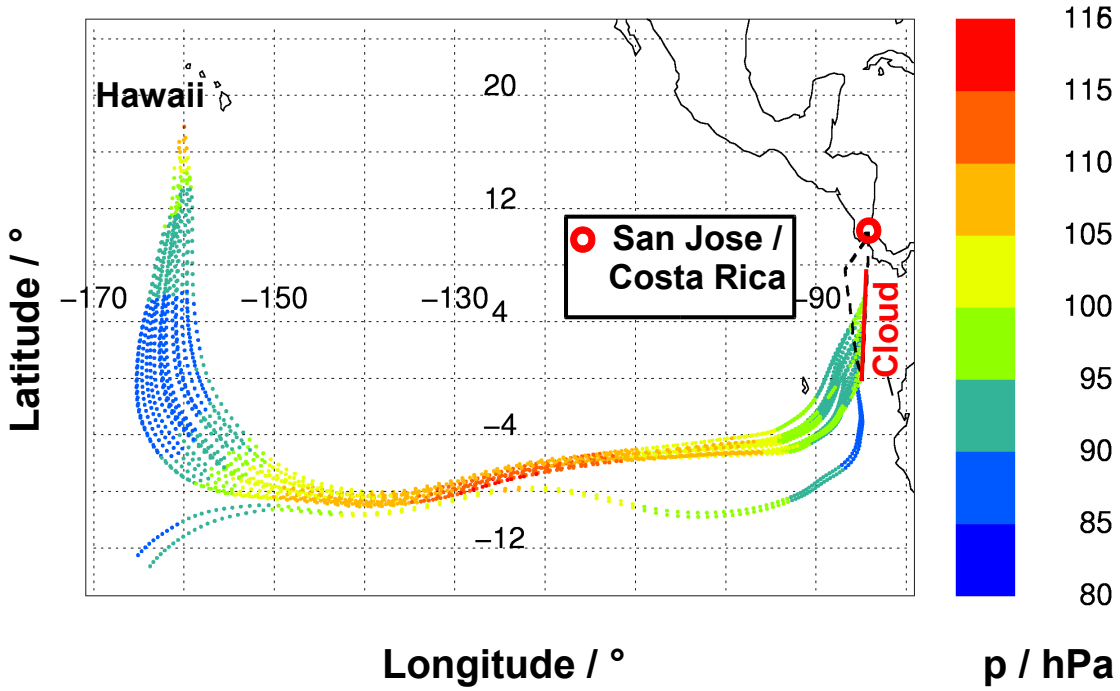

Figure 4.2: History of air parcels sampled in the cloud layer observed on 2nd February 2006: 20 isentropic 5 – days – backward trajectories calculated from ECMWF wind fields. The colors indicate the pressure levels of the air parcels along the trajectories (for details see text).

Since the target of this work is to reveal processes that impact on the formation and evolution of tropical, in – situ formed, very cold, sub – visible cirrus clouds (whose relevance was accentuated in 2.2), CR – AVE observation data sampled in such a cloud are simulated with an adequate theoretical instrument, MAID.

4.2 Model input

A variety of parameters have to be specified in the model input:

- temperatures and pressures along trajectories are calculated as described in Section 4.2.1;
- total (gas + particles) H_2O and HNO_3 are obtained from observations (Section 4.2.2);
- aerosol particle microphysics are initialized using the observations (Section 4.2.2).

Temperature, Pressure		
T, p	MTP[a], MMS[b]	*Denning et al.* (1989),*Scott et al.* (1990)
Water		
H_2O_{gas}	JLH[c]	*May* (1998)
H_2O_{gas}	HWV[d]	*Weinstock et al.* (1994)
H_2O_{total}	ALIAS[e]	*Webster et al.* (1994)
H_2O_{ice} (IWC)	CAPS[i]	see CAPS *
Nitric Acid		**used in the closure studies (Sections 4.3.2 and 4.3.3)
$HNO_{3,gas}$**, $HNO_{3,tot}$	CIMS[f]	*Neuman et al.* (2000, 2001), *Popp et al.* (2006)
Aerosol Microphysics		
N_{liq}, $\bar{R}_{liq}$	N−MASS[g] / FCAS II[h]	http://www.engr.du.edu/Aerosol/nmass.htm, *Jonsson et al.* (1995)
Ice Microphysics *		used in the closure studies (Sections 4.3.2 and 4.3.3)
N_{ice}, $\bar{R}_{ice}$	CAPS[i]	*Baumgardner et al.* (2001)

[a]MTP: Microwave Temperature Profiler;
[b]MMS: Meteorological Measurement System;
[c]JLH: Jet propulsion laboratory Laser Hygrometer;
[d]HWV: Harvard Water Vapor;
[e]ALIAS: Aircraft Laser Infrared Absorption Spectrometer;
[f]CIMS: Chemical Ionization Mass Spectrometer;
[g]N−MASS: Nucleation−Mode Aerosol Size Spectrometer;
[h]FCAS: Focused Cavity Aerosol Spectrometer;
[i]CAPS: Cloud Aerosol and Precipitation Spectrometer;

Table 4.1: WB−57 Instruments and parameters used in the CR−AVE case study as model input and for closure studies.

The WB – 57 payload included multiple instruments to register temperature, pressure, water vapor, nitric acid, as well as an unprecedented equipment to measure ice microphysics, in order to deliver detailed information on the atmospheric environment. Only a brief description of each instrument is given here, details are available in the cited literature. The instruments, as well as the parameters derived from the measurements, which are used as model input and for the closure studies (Sections 4.3.2 and 4.3.3), are listed in Tables 4.1,4.2 and described in Sections 4.2.1 – 4.3.1.

4.2.1 Thermodynamic environment: temperature and pressure

Temperature and pressure that force the model are gained in a three – step process:

- First an isentropic backward – trajectories analysis based on ECMWF wind fields is carried out in order to determine the temperature and pressure histories of air parcels ending up in the observed cloud (see Section 4.1).
- Second, the extracted temperatures and pressures are lowered by generally, ≈ 5 K (in some cases up to 11 K), to bring the trajectory values when reaching the flight path, to the same level with the detailed airborne MMS (*Scott et al.* (1990)) measurements.
- Finally, mesoscale temperature fluctuations are computed depending on season, latitude and underlying substrates (*Gary* (2006)) and superimposed on the synoptic scale parcel temperature and pressure histories. Inclusion of observed gravity wave temperature perturbations in the simulations is essential to reproduce the observed cloud properties. Considering the history of the air parcels reaching the flight path in the observed cloud, temperature fluctuations with an amplitude of 0.4 to 0.6 K are calculated from Equations 4.1 and 4.2 (see box below) and superimposed on the synoptic scale parcel temperature trajectories.

The result is a 'ceiling' of temperature/pressure versus time confining 20 trajectories, shown in Figure 4.3. The temperature history of the sampled air shows unusual very low temperatures, slightly higher around 1830 UT, corresponding to the two trajectories that start elsewhere (see Figure 4.2). During the cloud evolution, the temperature decreased to about 180 K and increased again shortly before the WB-57 sampling. The measurements are made probably near the end of the lifetime of the cloud, shortly before reaching the sublimation threshold.

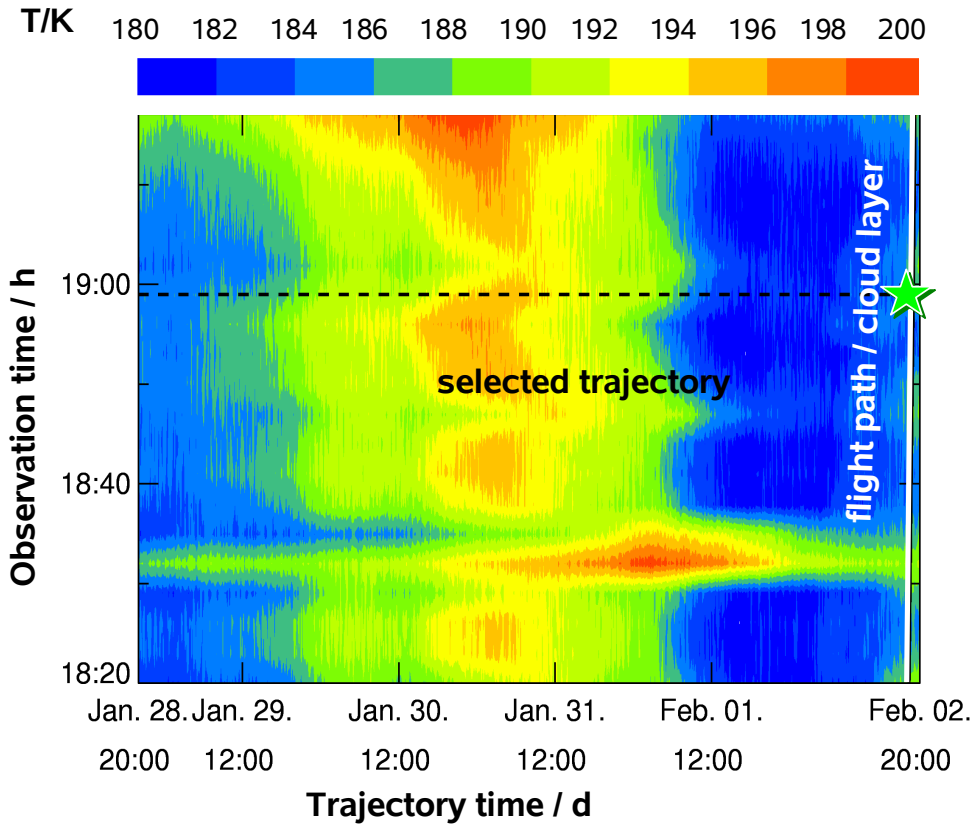

Figure 4.3: 5−days temperature histories of the air parcels ending in the cloud layer observed on 2^{nd} February 2006 (white solid line: flight path in the cloud layer; dashed line: example of a back−trajectory; green star: intersection air parcel trajectory / flight path).

Gary (2006) parametrisation for mesoscale temperature fluctuations

Isentrope altitude cross−sections, determined from airborne MTP measurements (*Denning et al.* (1989)), show differences compared with counterpart synoptic scale data, especially in the vicinity of jet streams (see Appendix B). These altitude variations give information on mesoscale temperature fluctuations that are not present in the synoptic scale temperature history of an air parcel. *Gary* (2006) examined in a study, based on hundreds of MTP temperature profile measurements, statistical properties of the vertical displacement of isentrope surfaces. He found that the magnitude of the mesoscale component of the temperature fluctuations varies with altitude, season, latitude and underlying substrates as follows:

$$MFA = (112 - 1.21 \cdot lat + 2.2 \cdot wint \cdot lat + 29 \cdot top) \cdot \left(\frac{p}{5885}\right)^{-0.4} \quad (4.1)$$

where

MFA – mesoscale fluctuation 'full – width' amplitude in m;
lat – latitude in °;
$wint$ – 'wintriness';
top – underlying topography roughness;
p – pressure in Pa.

The topography parameter varies from 0 for ocean to 1 for high continental mountains (see *Gary* (2006)). The 'wintriness' is the season parameter and vary also between 0 (one month after summer solstice) and 1 (one month after winter solstice), depending on the day of the year as follows:

$$wint = \frac{1}{2} \cdot \left(1 + \sin\left(2 \cdot \pi \cdot \frac{doy - 295}{365}\right)\right) \tag{4.2}$$

where

doy – day of the year.

The mesoscale fluctuation amplitude can be also expressed using temperature units, since under adiabatic conditions, a dry air parcel's change in altitude produces a temperature change at the rate of 1 K per 100 m.

Mesoscale pressure fluctuations, consistent with the air parcels movements, are superimposed on the synoptic scale pressure paths.

4.2.2 Water, nitric acid and aerosol measurements in model input

Water vapor mixing ratios

The Harvard Water Vapor (HWV, *Weinstock et al.* (1994)) instrument photodissociates H_2O molecules with Lyman – α radiation (121.6 nm) and detects the resulting photofragment fluorescence (OH^- at 315 nm). The Jet propulsion laboratory Laser Hygrometer (JLH, *May* (1998)) and the Aircraft Laser Infrared Absorption Spectrometer (ALIAS, - *Webster et al.* (1994)) are both high – resolution scanning tunable-diode – laser (TDL) spectrometers. While JLH is operated as open – path TDL that measures water vapor in the free-stream air flow external to the aircraft, ALIAS has a closed analysis cell and samples the ambient total (gas phase + ice) water content with an iso-kinetic, forward – facing inlet. Due to significant deceleration of the air when entering the inlet, ice particles are over – sampled with an enhancement ≈ 50, depending on altitude and cruising speed

of the aircraft. Corrections are applied in post−flight analyses. In addition, the ice water content, IWC, was measured by the Cloud Aerosol and Precipitation Spectrometer (CAPS) (for instrument details, see Section 4.3.1).

A discrepancy of 1 to 2.5 ppmv in the water vapor mixing ratio measured with JPL (JLH) and Harvard (HWV) instruments, was particularly obvious under the very dry conditions, registered during CR−AVE (panel a of Figure 4.4). This discrepancy was often observed between these two instruments, as well as in comparison to other water instruments (see panel b of Figure 4.4). Even if the JLH and HWV mean values (symbols) are alike in the comparison with HALOE (HALogen Occultation Experiment) measurements, it is also shown that in the indirect comparison, HWV measures higher water mixing ratios than JLH (horizontal lines). The discrepancies in the water measurements are for sure relevant in the modeling of cirrus clouds, because water is a determinant parameter in the cloud formation and evolution (*Jensen et al.* (2007)). Uncertainties in water measurements cause unreliable information on supersaturation in the atmosphere.

Therefore, an important issue of this study is to evaluate, which data set is in best agreement with the current understanding of the observed microphysics and RH_{ice}, as represented in the model studies (instrument assessment). This problematic aspect was treated in the present work by considering the two differing JLH / HWV water vapor mixing ratios as bases for different cloud scenarios. The approach used here was to compare the H_2O_{tot}, measured by the ALIAS instrument with total water mixing ratios, calculated from $H_2O_{gas,JLH/HWV} + IWC_{CAPS}$. Since this comparison shows mostly good agreement when using JLH data, the ALIAS data are not directly used in the input. Instead, the simulatios are initialized with total water derived from JLH and HWV and CAPS data, as follows (see Table 4.3):

$H_2O^{(b)}_{tot,input} = H_2O_{gas,JLH} + IWC_{CAPS}$

$H_2O^{(c)}_{tot,input} = H_2O_{gas,HWV} + IWC_{CAPS}$

Nitric acid

The Chemical Ionization Mass Spectrometer (*Neuman et al.* (2000, 2001) and *Popp et al.* (2006)), CIMS, has two independent detection channels, both configured for measurements of ambient nitric acid (HNO_3). The two sampling inlets are located in an airfoil−shaped inlet pylon, far beyond the aircraft boundary layer. One inlet is facing downward

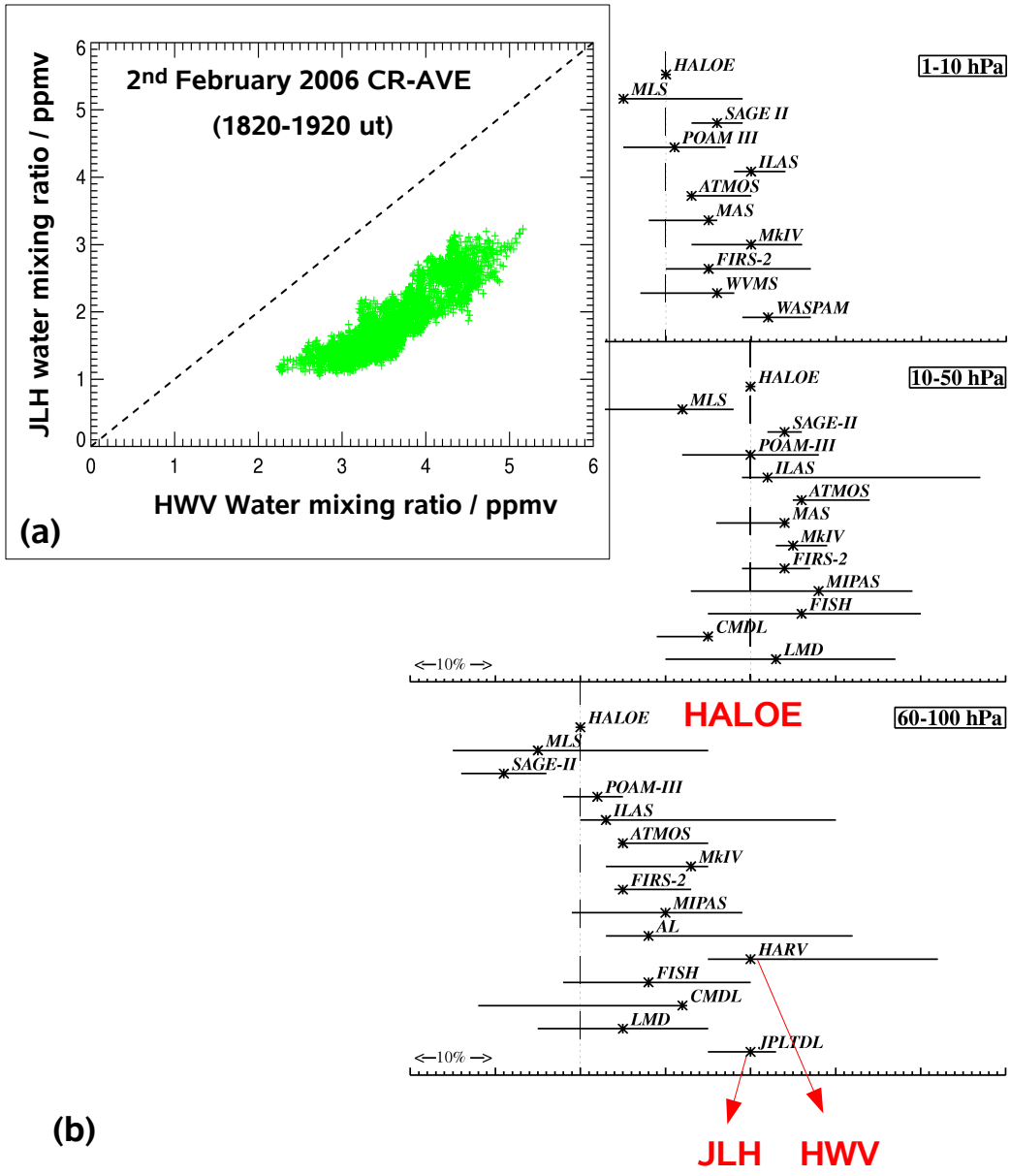

Figure 4.4: Discrepancies in the water measurements at high altitudes (a: water vapor mixing ratios measured by two different instruments, JLH and HWV, in the cloud on 2nd February 2006; b: summary of the relationship, in %, among water measurements at high altitudes; the symbols give the direct percentage difference from HALOE (HALogen Occultation Experiment), and the horizontal lines show the range of the indirect comparisons; each tick mark is 1 %, and the placement for HALOE is indicated by the dotted line; where no direct comparison was available, the symbols give the average of the indirect comparisons; source: *Kley et al.* (2000)).

and is sensitive to gas – phase HNO_3, the other inlet is facing forward and is sensitive to particulate HNO_3 as well (gas + particle = total nitric acid, which is used in the model input). The forward-facing inlet samples particles with an enhancement of ≈ 10 (see also 4.3.1).

Aerosol measurements

The Nucleation – Mode Aerosol Size Spectrometer (N – MASS) measures the concentration of particles as a function of diameter (4 – 60 nm). A sample flow is continuously extracted from the free stream using a decelerating inlet and is transported to the N – MASS. Within the instrument, the sample flow is carried to five parallel condensation nucleus counters (CNCs), which are tuned to measure the cumulative concentration of particles larger than a certain diameter (4.0, 7.5, 15, 30 and 55 nm).

A Focused Cavity Aerosol Spectrometer (FCAS II, *Jonsson et al.* (1995)) measures scattered light to count and size particles from 0.07 to 50 μm. The particles are sampled from the free stream with a nearly isokinetic sampler.

4.3 Sensitivity studies and closure

Cirrus clouds properties are very sensitive to a variety of initial parameters. To investigate the impact of these parameters on the formation and evolution of the observed cloud, the model has been repeatedly run by varying

- the freezing mechanism

as well as one of the input parameters characterizing the air parcels:

- water amount
- accommodation coefficient of water on ice
- heterogeneous ice nuclei type
- heterogeneous ice nuclei number density
- aerosol size distribution (geometrical mean radius and standard deviation)
- superimposed temperature fluctuations

Different scenarios of the evolution of the atmospheric state and the resulting cloud are thus created and named after the parameter, which has been varied. The simulated microphysics and the partitioning of water and nitric acid in the formed cloud are compared with the observations (see Section 4.2.2 for the total water, nitric acid and aerosol measurements and Section 4.3.1 for ice measurements). The scenario that gives the best match between modeled and observed cloud properties is entitled 'best scenario' (see MAID operational approach in Figure 3.4).

4.3.1 Measurements used in the closure studies

Nitric acid in ice

Nitric acid on ice particles is determined by the difference $HNO_{3,\mathrm{tot}}$ - $HNO_{3,\mathrm{gas}}$, reduced corresponding to the enhancement factor (Section 4.2.2), and is utilized first in the closure studies (Sections 4.3.2 and 4.3.3).

Ice microphysics measurements

The Cloud Aerosol and Precipitation Spectrometer (CAPS) provides extensive investigations of the ice crystal size distribution. The CAPS contains two particle probes, a Cloud and Aerosol Spectrometer (CAS), which measures forward and backward scattered light to count and size particles from 0.5 to 50 μm, and a Cloud Imaging Probe (CIP) that registers 25 μm / pixel images of particles between 25 and 1550 μm. Shattering is a special issue that should be discussed for the ice probing. Shattering (crushing) of big ice particles ($> 100\,\mu$m), which occurs by collision between ice crystals and probe housings, can produce a train of particles that could cause an overestimation of the ice crystal concentration (*Field et al.* (2006)). Since the ice particles analyzed on 2^{nd} February did not exceed 50 μm, particle shattering on probe inlets is not considered in this study (*Baumgardner et al.* (2006)).

4.3.2 Sensitivity studies and closure for a Selected Single Trajectory

The following sensitivity studies assess accurately the impact of different parameters on the microphysics inside an air parcel moving along a selected trajectory (dashed line in Figure 4.3).

The first scenario is initialized with the lower water amount (2.24 ppmv), corresponding to the JLH water vapor measurements and with full accommodation of water on ice. The freezing mechanism is set to heterogeneous. Other initial parameters to initialize the simulation along the selected trajectory are given in Table 4.2. This scenario, marked in reddish, represent the 'best' scenario (see above) and is discussed below.

total nitric acid gas + particles	HNO_3	0.0577 ppbv
aerosol size distribution	N_{liq}	$157.89\,cm^{-3}$
	$\bar{R}_{liq}$	$0.012\,\mu m$
	σ_{liq}	1.5

Table 4.2: Aerosol size distribution and total nitric acid used to initialize CR – AVE sensitivity studies along the selected trajectory.

Three additional scenarios, which produce features in the cloud development that can be relevant for the explanation of the 'supersaturation puzzle', like persistent very high relative humidities after the cloud formation, or a subsequent homogeneous ice nucleation after the heterogeneous cloud initiation, are selected for detailed sensitivity studies. These three scenarios grow out from the first 'best' scenario, by varying

- the freezing mechanism ('homogeneous' – blue).
- the water vapor mixing ratio ('more water' – burgundy),
- the accommodation factor of water on ice ('lower accommodation' – orange) and

A summary of the four scenarios are presented in Table 4.3. The other scenarios, which produce similar features in the cloud development like the selected scenarios for detailed studies (e.g. by enhancing the amplitude of the temperature fluctuations, or by lowering the ice nuclei number densities), or even have a minor influence on the cloud evolution (e.g. by changing the background aerosol properties) are shown in Appendix C.

The scenarios are analyzed only for the last two days of simulations, since only these are

Scenario / acronym	Freezing Mechanism	Water Mixing Ratio /ppmv	Accom-modation Factor water/ice	Line Color
'Best' 'heterogeneous'	heterogeneous[a]	2.24[b]	1.0	red
Homogeneous ice freezing 'homogeneous'	homogeneous	2.24[b]	1.0	blue
Higher water mixing ratio 'more water'	heterogeneous[a]	3.79[c]	1.0	burgundy
Lower water accom – modation on ice 'lower accommodation'	heterogeneous[a]	2.24[b]	0.005[d]	orange

[a] ice nuclei: soot particles coated with sulphuric acid; ice nuclei number of 0.01 / cm^3.
[b] observations ALIAS/JLH.
[c] observations ALIAS/HWV.
[d] *Magee et al.* (2006).

Table 4.3: Selected scenarios for formation and evolution of the cloud observed on 2^{nd} February 2006.

relevant for both, homogeneous and heterogeneous cloud formation, as shown in Figure 4.5. This depicts the corresponding slice of Figure 4.3, whereby the time of ice onset is indicated for both freezing mechanisms (red: heterogeneous, blue: homogeneous). Due to a lower freezing threshold, heterogeneous freezing initiates earlier than the homogeneous freezing.

Sensitivity studies of microphysics and ice supersaturation

The results of the sensitivity studies are summarized in Figure 4.6. Microphysics, supersaturation and the nitric acid partitioning in the simulated clouds are discussed below.

Ice microphysics in terms of number densities N_{ice} and size of the ice crystal $\bar{R}_{ice}$ is plotted vs. trajectory time in the panels a and b of Figure 4.6. The RH_{ice} time evolution is depicted separately for the four scenarios in the panels e – h. The observations in the cirrus cloud, probed by various instruments during the CR – AVE mission, are shown in the

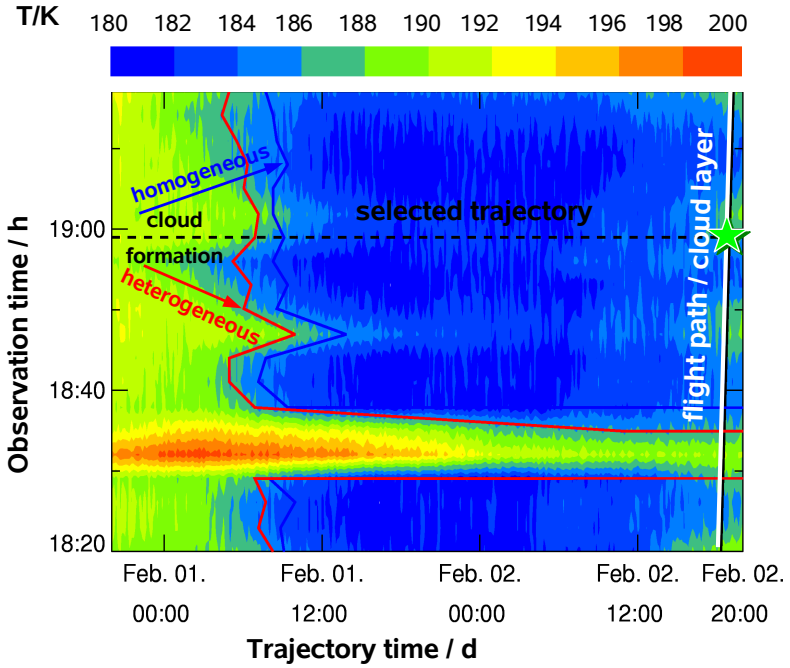

Figure 4.5: Past two days in the temperature histories of air parcels that end in the cloud layer observed on 2^{nd} February 2006 (white solid line: flight path in the cloud layer; dashed line: selected trajectory; green star: intersection air parcel trajectory / flight path; blue / red lines: appearance of the first ice crystals in the homogeneous / heterogeneous scenarios).

plots by greenish triangles. These values are compared with the model results along the selected trajectory at the moment of the observations.

In all scenarios RH_{ice} increases due to the cooling of the air parcels until reaching the freezing threshold, when the first ice crystals appear. The relative humidities increase steadily after the ice onset because of further air cooling, and resemble the temperature fluctuations. New ice nucleates, until the RH_{ice} increase is compensated by the water uptake on ice (see Figure 2.8).

As expected, the lowest number density (limited by the number density of heterogeneous ice nuclei) and the largest size of ice crystals are produced in the heterogeneous 'best scenario' (red lines). The water depletion by the ice crystals is not fast enough to fully compensate the RH_{ice} increase due to the further cooling of the air. This is the reason why high $RH_{ice,het}$ (red line in panel e) of 120 – 140 % can be measured for long periods of time after the cloud formation. The ice crystal observations (light green triangles for

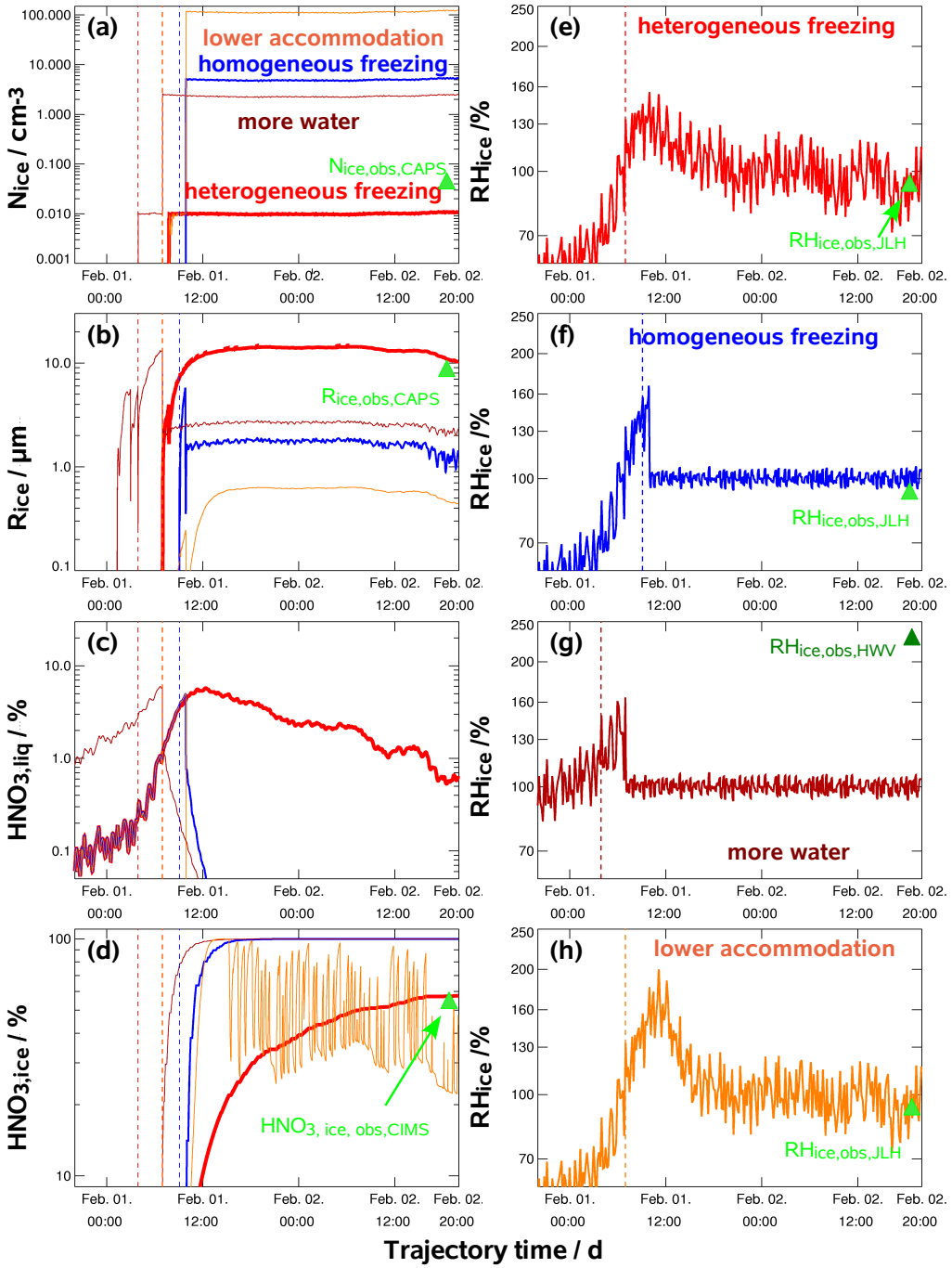

Figure 4.6: Single trajectory in detail (dashed lines: appearance of first ice crystals; greenish triangles: CR-AVE observations; a: ice crystal number density; b: ice crystal size; c: nitric acid in liquid aerosol; d: nitric acid in ice; e – h: relative humidity with respect to ice for the 'best' / 'homogeneous' / 'more water' / 'lower accommodation' scenarios).

CAPS measurements) and RH_{ice} from JLH measurements (light green triangles) match the best the red lines ('best' scenario).

The homogeneous ice nucleation (blue line) diverges from the 'best' scenario by the freezing mechanism. This scenario is very interesting for atmospheric investigations, since the homogeneous freezing is considered so far as most likely path for ice cloud formation. In this case, heterogeneous freezing is blocked, the cloud forms purely homogeneously. The scenario generates a higher number density of smaller crystals. More small ice crystals produced by homogeneous freezing (blue line in panel a) deplete the ambient gaseous water more efficently. The $RH_{ice,hom}$ drops sharply after the ice nucleation and fluctuates around saturation. The amplitude of the $RH_{ice,hom}$ fluctuations is lower than that of $RH_{ice,het}$ (see also Section 3.3.2). The agreement between the modeled and observed $RH_{ice,hom}$ is the same as for the heterogeneous scenario. The microphysical measurements do not match the 'homogeneous' simulations, the observed $N_{ice,hom}$ is much lower than the simulated one.

The scenario with 'more water' (burgundy line) is different to the 'best' scenario by the amount of water, which is now initiated with 3.79 ppmv, derived from the water measurements of HWV (Section 4.2.2). The relevance of this scenario was highlighted in 4.2.2. First ice crystals appear heterogeneously. Due to the higher initiated amount of water, the freezing threshold is exceeded ≈ 3 h earlier than in the first scenario (dashed burgundy line in panel a). Since a large amount of water is still available in the gas phase after the heterogeneous ice initiation, a subsequent homogeneous ice nucleation event occurs shortly after and produces a cloud with similar properties as in the homogeneous (blue) scenario. $RH_{ice,morewater}$ increases steadily in the cloud, as long as the ice crystal number is as low as in the heterogeneous case (see panel g). After the second freezing event $RH_{ice,morewater}$ behaves like $RH_{ice,hom}$ (blue). The observed $RH_{ice,morewater}$, derived from HWV water mixing ratios, is far higher than the simulated one.

The fourth scenario with 'lower accommodation' of water on ice (orange lines) diverges from the best scenario by the accomodation coefficient of water on ice α, which is set to 0.005, accordingly to recent laboratory studies of *Magee et al.* (2006). This scenario is also relevant for these sensitivity studies, since lower accommodation factors of water on ice seems to be one of the most intensly suggested solutions of the'supersaturation puzzle'. The heterogeneous ice nucleation occurs at the same time like in the 'best' scenario. Similarly to the 'more water' scenario, a subsequent, homogeneous freezing

event occurs, producing a very high number of very small ice crystals, extremely different from the in-situ observations (the orange line in panel a shows an almost 'complete' freezing of the aerosol particles). Due to a very unefficient water uptake on ice crystals (low α), very high supersaturation over a very long time period prevail in the cloud (panel h). The RH_{ice} fluctuation amplitudes are comparable with the 'heterogeneous' case.

Sensitivity studies of nitric acid partitioning

The amount of nitric acid in the liquid interstitial particles (panel c of Figure 4.6) ranges from 0.01 to 6 % of the total available HNO_3 and is determined by RH_{ice}: the higher the amount of water in the gas phase, the larger are the interstitial particles, containing more HNO_3. Consequently, HNO_3 resides longer in the interstitial particles in the first, heterogeneous (red) scenario due to higher $RH_{ice,het}$ inside the cloud. In the scenarios 'homogeneous' (blue) and with 'more water' (burgundy), HNO_3 escapes from the liquid into the gas phase rapidly after RH_{ice} has dropped, due to shrinking of interstitial particles. In the fourth scenario with 'lower accommodation' of water on ice (orange), the fraction of the total available HNO_3 residing in the interstitial particles is negligible due to the nearly 'complete' freezing of the aerosol particles.

The range of the nitric acid fraction on ice is very broad for the different scenarios (panel d of Figure 4.6). The lowest HNO_3 uptake in the first, heterogeneous (red) scenario, is caused by the lower number density of big crystals and shows good agreement with the observations (green triangle). More small crystals in the second (hom., blue) and third (more water, burgundy) scenarios can trap the HNO_3 more efficiently. Almost all available HNO_3 resides in ice at the end of these simulations. The evolution of HNO_3 partitioning on ice in the fourth scenario with 'lower accommodation' of water on ice (orange) is different from the other scenarios: the amplitudes of $HNO_{3,\mathrm{ice,loweraccom}}$ fluctuation with the temperature are very high. This can be explained as follows: concerning the large RH_{ice} fluctuation amplitudes (see above), the fourth scenario is similar to the 'best' scenario (red). Large variations in the amount of gaseous water, which is available to deposit on the crystals influence the accompanying nitric acid trapping process. The same amount of water condensing on the much smaller ice crystals formed in the fourth scenario (with 'lower accommodation' of water on ice) burries more HNO_3 ad-layers. The consecutive phases uptake/release of $HNO_{3,\mathrm{ice}}$, accompanying deposition/sublimation of water on ice, appear in the orange line more pronounced than in the red line ('best' scenario) on

panel d. This feature does not appear in the blue and burgundy line because of the low amplitudes of $RH_{ice,hom}$ and $RH_{ice,morewater}$ in the clouds formed homogeneously in the scenarios 'homogeneous' and with 'more water'.

Summary for the single trajectory

The comparison of the four diffferent scenarios to each other contributes to get insight in the evolution of microphysical processes under different conditions, before and after a cirrus cloud forms.

The first scenario ('best' – red) shows similarities to the fourth scenario (with 'lower accomodation ' – orange), concerning the inefficient water depletion in the cloud and consequently, the higher supersaturation directly after the cloud formation. The explanation of this high water amount available in the gas phase is different for the two cases: in the first scenario ('best' – red) there is the low number density of ice crystals, in the fourth scenario (with 'lower accomodation' – orange) there is the lower accommodation coefficient of water on ice that delays the water deposition on ice. Also at later times, both scenarios show high amplitudes of the RH_{ice} fluctuations (for explanation, see Section 3.3.2). The evolution of HNO_3 partitioning on ice is different in the two scenarios, due to the different microphysical properties of the simulated clouds (see above).

A very efficient water depletion in the ice cloud, associated with a high number density of small ice crystals, is shown again in two of the described scenarios: the pure 'homogeneous' scenario (blue), when the heterogeneous freezing is not allowed, and the scenario with 'more water' (burgundy), when the second freezing determines the decisive cloud microphysics (Section 4.3.2).

The subsequent homogeneous ice nucleation can have another origin than the high amounts of ambient water vapor from the scenario with 'more water'. The long-lasting vapor excess that is not depleted by the ice crystals, formed in the first heterogeneous freezing, can be caused by the 'lower accomodation' of water on ice (orange). Higher amplitudes of temperature fluctuations can also lead to a second freezing event because of the higher cooling rates. This is discussed in more detail in Appendix C. The origin of cooling rates that initiate the second freezing event can be also the randomly created superimposed temperature fluctuations (*Hoyle et al.* (2005)). In order to investigate how frequently the initial heterogeneous freezing from the 'best' scenario might be followed

by a secondary homogeneous freezing, the simulations for the selected trajectory were repeated many times, using multiple temperature histories. These histories diverge from each other only by the randomly created superimposed temperature fluctuations (see 4.2.1). The result, presented in Figure 4.7, shows undoubtedly that the 'pure' heterogeneous freezing is most probably the pathway for the formation of the cloud observed on 2nd February 2006, under the described conditions. 90 % of the the simulations do not contain an additional homogeneous freezing event.

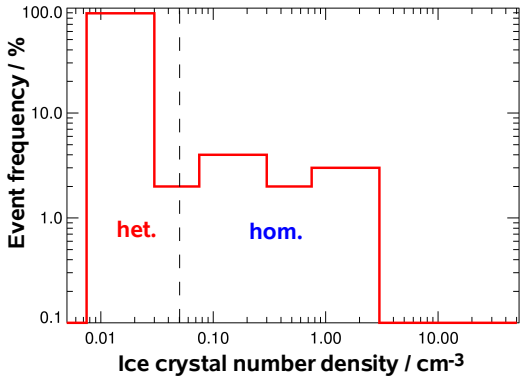

Figure 4.7: Frequency of heterogeneous / homogeneous freezing in simulations using randomly created temperature fluctuations with the amplitude of 0.6 K: distribution of ice crystal number densities.

By evaluating the scenarios of possible cirrus evolution against the observations in a closure for the selected trajectory, the first scenario (red), representing pure heterogeneous ice nucleation, with lower amount of water and full accommodation of water on ice, is2nd February 2006 found to best match the observations of microphysics, as well as water vapor and nitric acid partitioning.

Another major result of the closure is the assessment of the trapping efficiency used in MAID to be 0.1. Higher efficiency values, given by *Kärcher and Voigt* (2006) in the parametrisation of trapping efficiency for the temperature range T=195 – 240 K, would yield an unrealistic overestimation of HNO_3 uptake on ice.

4.3.3 Overall closure for all trajectories

Simulations using the same scenarios analyzed in Section 4.3.2 have been performed for all 20 back−trajectories of sampled air parcels (calculated as described in Section 4.2.1). In an overall closure study, the simulated variables at the moment when the trajectories meet the flight path are compared with the observations. The results are depicted in Figure 4.8. Different scenarios that yield similar modeling results due to equivalent microphysical processes are handled as one. The 'pure' and the subsequent homogeneous freezing are marked simply as 'homogeneous'. The simulations for the scenario with lower water accommodation on ice, producing a totally different cloud from the observed one are not considered in Figure 4.8. Excepting panel c, for the RH_{ice} comparison, the plots depicting the microphysics of the cloud (panels a and b), as well as the $HNO_{3,ice}$ (panel d), contain less than 20 points. This can be explained as follows: two trajectories of the analyzed air parcels have a different origin than the majority, coming from tropical regions (see Figure 4.2). These trajectories correspond to clear air episodes in the obsevations, i.d. no ice. In addition, two other cases show in the simulations that the cloud is near the end of its lifetime (see Section 4.2.1). Consequently, in these cases, most of the particles had already sublimated and thus, N_{ice}, $\bar{R}_{ice}$ and $HNO_{3,ice}$ are not anymore in the depicted range.

The first scenario (red: heterogenous freezing, lower water amount, full accommodation of water on ice) is found to reproduce best the in-situ observations not only for the selected trajectory but for almost all simulations: N_{ice} (panel a), $\bar{R}_{ice}$ (panel b), RH_{ice} (panel c) and $HNO_{3,ice}$ (panel d of Figure 4.8). Four from 20 'heterogeneous' (red) trajectories produce a subsequent homogeneous freezing event (explanation see above). These (red encircled stars) and the homogeneous scenarios (blue stars) produce too many small ice crystals (panels a and b).

The simulated RH_{ice} generally fluctuates around ice saturation (100 %) at the end of all trajectories for all scenarios (panel c). As shown in Figure 4.5, the cloud existed for ≈ 40 hours prior to the observations. None of the scenarios can maintain a very high supersaturation over such a long period (see the burgundy stars, corresponding to HWV measurements). The simulations show very high supersaturation only in younger, heterogeneously formed ice clouds.

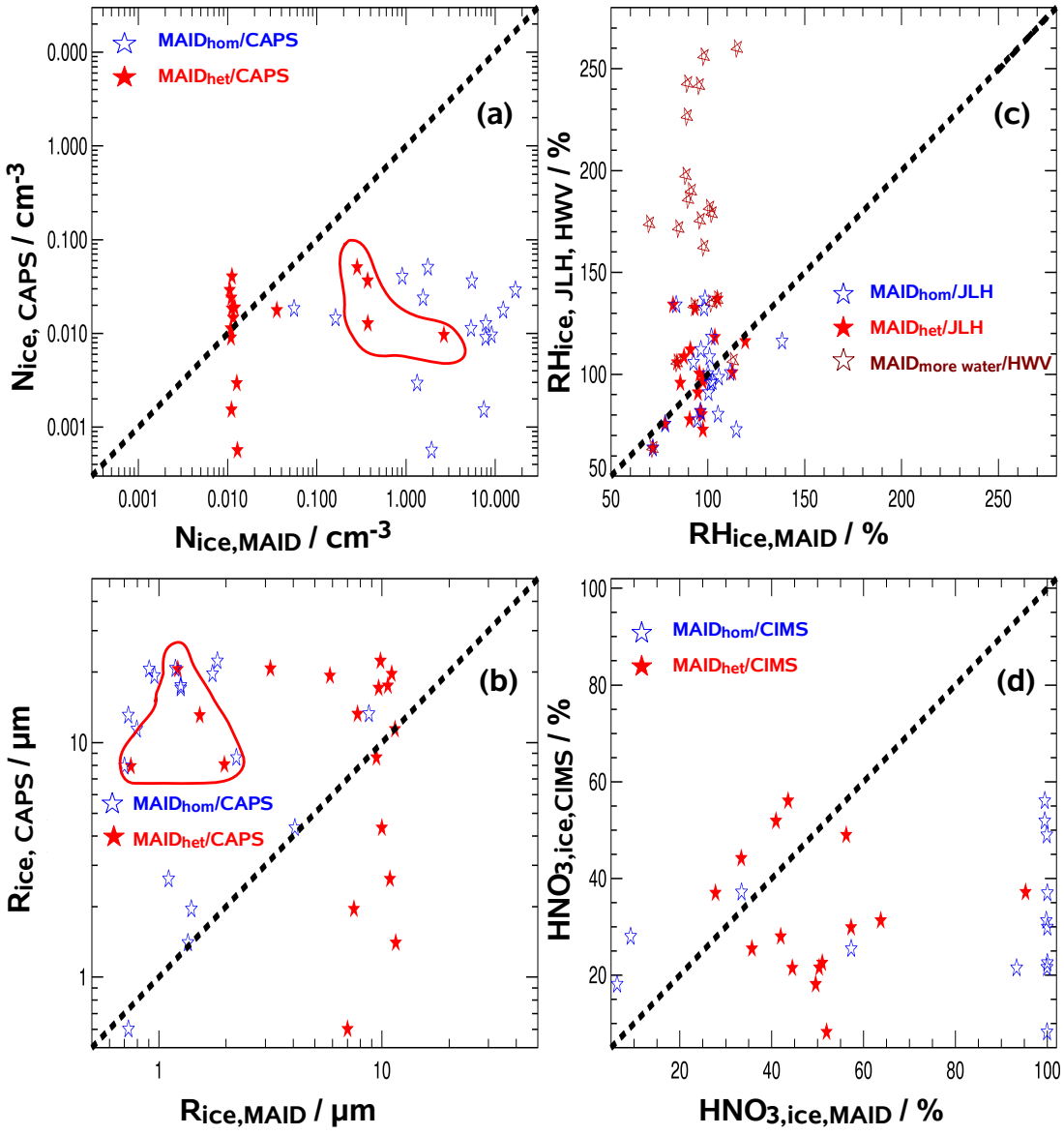

Figure 4.8: Overall closure – comparison of MAID results with in-situ observations (stars: MAID results for 'best' – red, 'homogeneous' – blue, and 'more water' – burgundy vs. observations for a: ice crystal number density; b: ice crystal size; c: relative humidity with respect to ice; d: nitric acid in ice; encircled red stars represent the four trajectories that contain a subsequent homogeneous freezing event, see text).

Observations are in good agreement with the simulated nitric acid residing in the heterogeneously formed cloud particles (panel d). Simulations following homogeneous scenarios lead to almost total incorporation of nitric acid in ice and this differs from the observations.

The first attempt to use microphysical modeling studies to interpret the observations was done by *Khvorostyanov et al.* (2006). The dominance of either heterogeneous or homogeneous nucleation in tropopause cirrus is investigated using a detailed bin – resolving and a bulk microphysics model, to simulate cirrus clouds observed during CRYSTAL – FACE 2002 (Cirrus Regional Study of Tropical Anvils and Cirrus Layers – Florida Area Cirrus Experiment). Their conclusions are partially similar to those presented in this work, despite the different approaches to simulate the formation of cirrus clouds. Though, they cannot conclude, whether the cloud formed homogeneously or heterogeneously, both pathways produce results similar to the observations: 'the simulated cloud microphysical properties are similar to observations, suggesting that tropopause cirrus may potentially form as a result of heterogeneous immersion freezing of internally mixed aerosols serving as ice nuclei (IN)', but 'simulations using homogeneous nucleation theory are also able to produce comparable microphysical properties if the heterogeneous mode is turned off'.

The overall closure using MAID shows that the pure heterogenous freezing alone can produce an ice cloud with such a low number of ice crystals in the size range of the observations. Variation of the freezing process, the accommodation coefficient or the amount of available water would have produced a cloud with completely different microphysical properties.

Another MAID advantage consist in the involvation of the air parcel histories in the calculations. This and the exact balancing of trace gases and other aerosol components along the back-trajectories allow the accurate determination of the freezing point, and so of the cloud 'age'. Information on relaxation times and cloud age help to predict the RH_{ice} values at the end of the trajectory. This can be of importance when assessing instrument performances.

Chapter 5

Summary and outlook

The aim of this work was to contribute to the explanation of the 'supersaturation puzzle' (*Peter et al.* (2006)) by answering the open questions presented in Chapter 1:

- Can MAID reproduce observed 'in-cloud' supersaturation by solely using the conventional ice cloud microphysics?
- Is it possible to reassess airborne instrument performances by comparing the observations with MAID simulations?

Therefore, the microphysical model MAID was developed and tested to simulate upper tropospheric aerosols and ice clouds. The exact mass balancing of chemical species among different physical states at each time step makes the model suitable for detailed process studies of cirrus clouds evolution.

5.1 Summary

Two different airborne measurements of cirrus clouds provided information for sensitivity and closure studies with MAID: an Arctic cirrus cloud observed during POLSTAR–1 1997 and a tropical cirrus cloud observed during CR–AVE 2006. Similarities and also differences in the development of these cirrus types were investigated.

The POLSTAR–1 simulations had been designed to validate MAID with and to extend the results of *Meilinger et al.* (1999), who simulated the same cirrus cloud using a different ice nucleation scheme. MAID shows advantages due to its ability to treat separately the homogeneous and heterogeneous freezing and therewith, to investigate the impact of different ice nucleation pathways on the microphysics and consequently, on the water and nitric acid in the cloud. The ice nucleation used by *Meilinger et al.* (1999) was

similar to *Koop et al.* (2000); the results from the two models agree well, when MAID simulates the homogeneous freezing mechanism. A closure study between model results and observations was not planned for the POLSTAR–1 cloud. Still, the validation process suggests that the observed and the MAID 'homogeneous' cloud are very alike. The homogeneously formed cloud contains higher number density of ice crystal with lower sizes than in the heterogeneous case. The relative humidity drops immediately after the cloud formation and fluctuates a little around saturation, due to the temperature fluctuations. More nitric acid resides in the ice crystals, compared to the heterogeneous cloud.

In the CR–AVE study, beside the freezing mechanism, multiple model parameters are varied to create realistic atmospheric scenarios for the development of the observed cloud: the ambient water amount, the accommodation of water on ice, the aerosol size distribution and chemical composition, as well as temperature mesoscale fluctuations. By comparing the observations with the MAID simulation results for various scenarios, the most likely way ('best scenario') of cloud formation is determined. In this case the cloud forms heterogeneously (whereas the ice nuclei are soot particles embedded in sulphuric acid, $N_{IN} = 0.01$ cm^{-3}), with less water and full accommodation of water on ice crystals. The observed microphysical properties and the partitioning of water and nitric acid are fairly well reproduced in the 'best' scenario cloud.

The low ice crystal number densities at low temperatures and the resulting long-lasting ice supersaturation, supported by this scenario, are in agreement with the in-situ observations and could be an explanation of the observed climatology of high frequency of ice supersaturation in cirrus (*Krämer et al.* (2008b)). All other scenarios, implying an imposed or a subsequent homogeneous ice nucleation produce a cloud very different to the observations. Hence, the homogeneous freezing pathway in case of this observed thin very cold TTL cloud appears very unlikely.

All scenarios show that the CR-AVE cloud is existing for ≈ 40 hours. Very high supersaturation can be simulated in young, heterogeneously formed clouds and these can persist for some hours. But no scenario can simulate RH_{ice} exceeding 130 % after 40 hours. This may be of importance when assessing instrument performances, since the Harvard (HWV) instrument measures RH_{ice} higher than 200 % in this old cloud.

Even if the sensitivity studies of both, Arctic and tropical cirrus clouds show similarities concerning the impact of the composition of the freezing aerosol on the microphysics in the cloud, they also emphasize the different pathways of ice cloud development under

different background conditions. The most likely freezing mechanism for the tropical cirrus, forming in a dry, very cold environment, was shown to be the heterogeneous one. The Arctic cloud seems to have formed homogeneously in a 'warmer' and wetter environment. Due to the higher amount of water, the particle population prior to ice formation is characterized by larger mean sizes. Therefore, the partitioning of nitric acid on the aerosol particles is $\approx 80\,\%$, compared with less than 10 % in the CR-AVE study.

The questions referring to the 'supersaturation puzzle' (see above) can now be answered:

for the POLSTAR Arctic 'warmer' cirrus cloud ($T > 200\,K$)

- yes, RH_{ice} behavior can be well described with the conventional ice cloud microphysics.

for the CR-AVE tropical 'cold' cirrus cloud ($T < 200\,K$)

- yes, significant 'in-cloud' supersaturation can be simulated by solely using the conventional ice cloud microphysics, when assuming heterogeneous freezing of soot coated with sulphuric acid;
- if knowing the cloud age and relaxation time, it is possible to predict RH_{ice} values at the end of the trajectory. These in turn provide information about the water partitioning in the observed cloud. In this way water instrument performances can be reassessed.

5.2 Outlook

A key in the explanation of the 'supersaturation puzzle' may be the assumption that subvisible TTL cirrus clouds potentially form as a result of heterogeneous freezing of internally mixed aerosols, with total accommodation of water on ice. The supersaturation in these clouds can be then well explained, new microphysics is not necessary. But still then, the question, **how plausible is it to consider heterogeneous freezing as the major process in the cold UT region**, remains open.

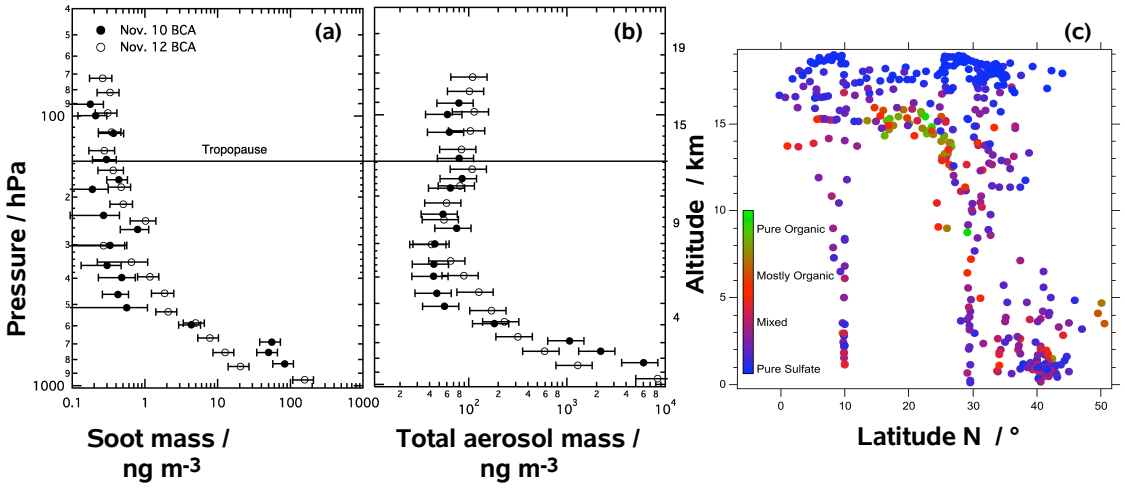

Figure 5.1: Vertical profiles of soot and total aerosol mass concentration, fraction of organics in the total aerosol (a: vertical profile of the soot mass concentration; b: vertical profile of the total aerosol mass (*Schwarz et al.* (2006)); c: an altitude - latitude cross-section of the organic fraction in the total aerosol (*Murphy et al.* (2006))).

Before trying to answer this questions, some issues must be discussed:

- until recent times, homogeneous ice nucleation was considered the most likely freezing pathway in the cirrus cloud formation (*Jensen and Toon* (1994)). Supercooled ternary solution particles, which potentially freeze homogeneously, are believed to represent the main part of the UT aerosol (Section 2.1). In addition, it seems very likely that the homogeneous freezing threshold is frequently reached (*Hoyle et al.* (2005));
- the heterogeneous freezing of aerosol particles, containing soot with sulphuric acid coating produces big ice crystals, which can be removed after a while through sedimentation. Yet, such a washing out process was not validated by in-situ soot measurements (panel a and b in Figure 5.1, adapted from *Schwarz et al.* (2006)). Vertical profiles of soot as function of altitude show no significant variance of the mass concentration in the tropopause region, where the cirrus cloud formation is expected. Thus, soot should not be the ice nucleus that initiates the cirrus cloud formation.

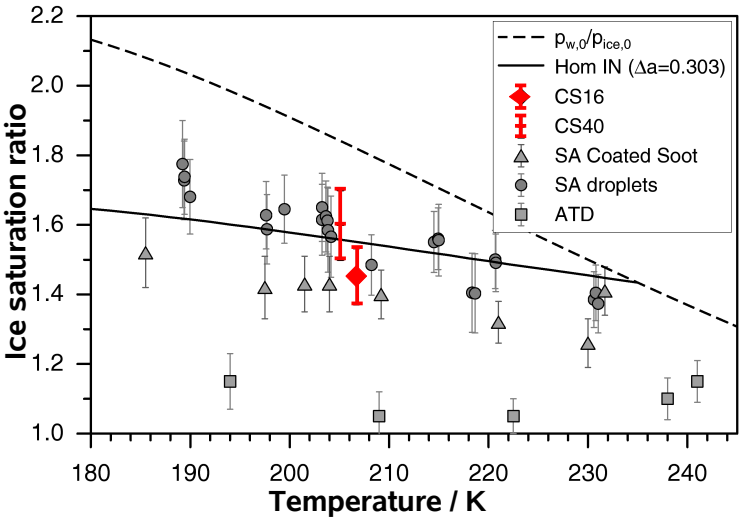

Figure 5.2: Ice saturation ratios for ice nucleation onset on soot coated with 16 % (red diamond) and 40 % (red panel) organic coating (*Möhler et al.* (2005)).

Recent hypotheses aim to clarify these issues. *Shilling et al.* (2006) showed that the cubic ice, as the dominant ice form when solution droplets freeze below ≈ 190 K, is one contributing factor for persistent supersaturation inside cirrus clouds. Another investigation track is the suppression of the ice nucleation by organics. In this case, supersaturation exceeding even the homogeneous freezing threshold (Figure 2.7) could be well explained. *Murphy et al.* (2006) showed already that a major part of the UT aerosol contains organic species (panel c in Figure 5.1). Laboratory experiments in the aerosol chamber AIDA indicated that by increasing the fraction of organic coating on soot, the heterogeneous ice nucleation might be suppressed (Figure 5.2). This can be explained by the delayed water deposition in the presence of surfactant monolayers. But the organics may play an important role also in the homogeneous ice nucleation of liquid aqueous aerosol particles by lowering the equilibrium water content at a given relative humidity. Since the aerosols need a certain 'dilution' to freeze, the droplets remain liquid in the presence of organic solutes (*Cziczo et al.* (2007)). A very different hypothesis, supporting the suppression of the homogeneous ice nucleation due to organics, was proposed by *Koop and Marcolli* (2007). They suggest that at low upper tropospheric temperatures, aerosol particles containing organic solutes can transform from the liquid into a 'glassy' phase. The ice nucleation as well as ice crystal grow may be significantly reduced, or even inhibited in these glasses.

An overarching completion, encompassing all questions and hypotheses mentioned above, is that **the 'supersaturation puzzle' may turn into a 'freezing puzzle'!**

Following challenges, essential for the 'freezing puzzle' explanation, have to be considered in the future atmospheric research:

- further field and laboratory studies are required to identify the phase and composition of ice nuclei, as well as the efficiency at which they nucleate ice. The modes of ice nucleation in the UT region could be clarified by the chemical analysis of cirrus ice residues obtained over localized regions. Freezing behavior of different ice nuclei should be investigated in the laboratory, and the results should be compared to previous parameterizations and verified against observations.
- measurements in the upper troposphere must improve, despite the generally hostile (very dry and cold) conditions encountered in this region. Reliable sampling and analysis techniques are a challenge for the numerous semi-volatile species (specially water) in particles.
- process-models have to be evaluated against the observations to better understand and represent the microphysical processes leading to cirrus clouds formation. Parametrisations derived from the validated process-models should be further incorporated into complex climate models, which can better derive global scale impacts and also test the future system solutions.

Appendix A

Satellite Infrared Imagery GOES12

The geostationary operational environmental satellites GOES is one of the NOAA's (National Oceanic and Atmospheric Administration's) operational weather satellite system. GOES provides the kind of continuous monitoring necessary for intensive data analysis and is used to monitor storm development. The GOES12 Infrared Imagery (http://bocachica.arc.nasa.gov/CRAVE_06/movies/index.html) is employed here to locate possible convection systems.

The region interesting for this work is captured in GOES12 Infrared Imagery pictures beginning with 1st February 2006, which are illustrated in Figures A.1 – A.3. This time period is relevant for the cloud developement (Section 4.2.1). The pictures, depicted in Figures A.1 – A.3 show temperatures at top of the cloud in 20 km altitude. Generally, very low temperatures prevail in this region ($T < 200$ K). The green spots, showing $T \approx 208$ K, indicate possible strong updraft air movement, bringing warmer air from lower troposphere layers. Since these spots do not apear near the track of the analysed air parcels (turquoise dashed arrow), it is considered that the air sampled on 2nd February 2006 in the cirrus cloud was not influenced by convection on their ascending pathway (Section 4.1).

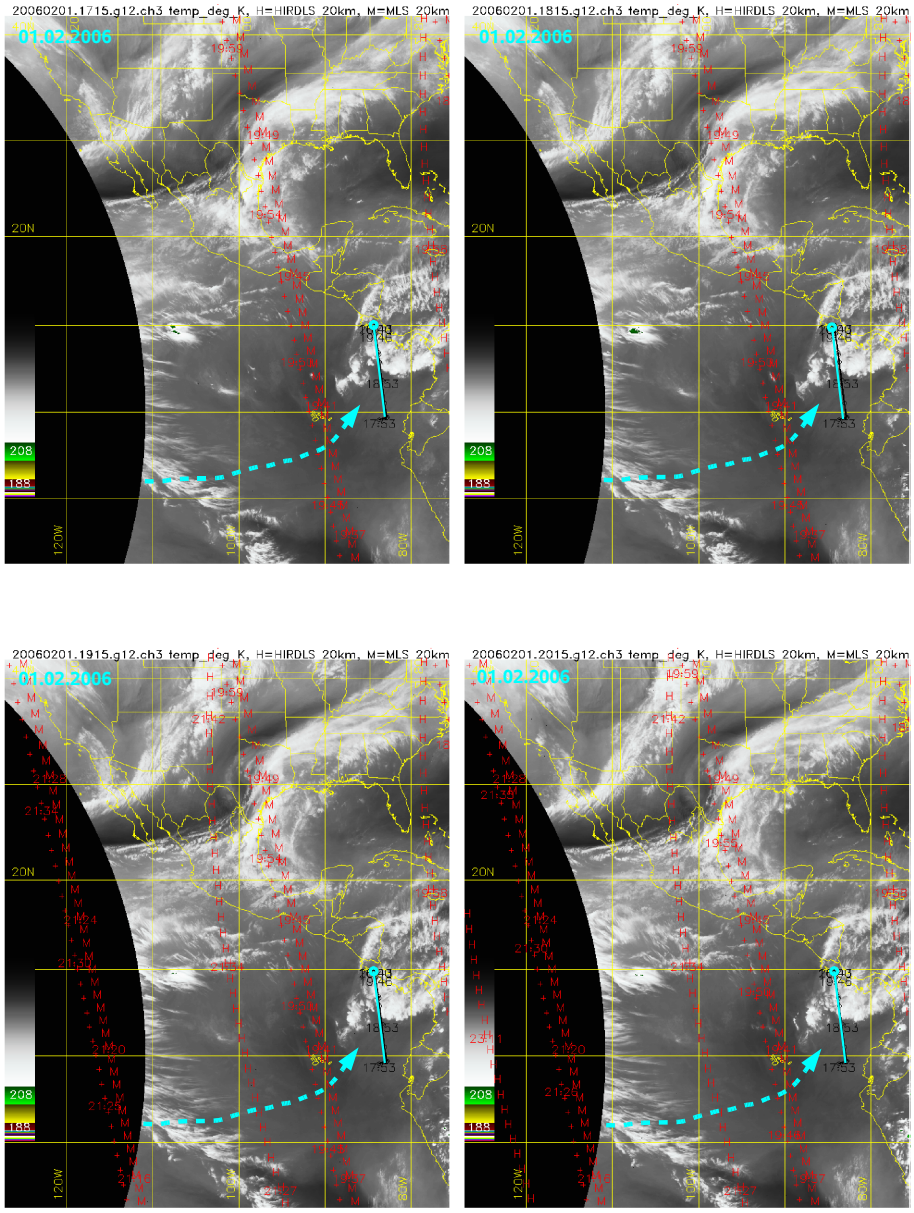

Figure A.1: GOES–12 satellite infrared imagery on 1st February 2006 (colored bars: temperatures at top of clouds; greenish spots: convective systems; yellow contours: american continent; turquoise line: CR–AVE flight paths, corresponding to the depicted days; turquoise dashed arrow: track of sampled air parcels; capture time is given above each picture).

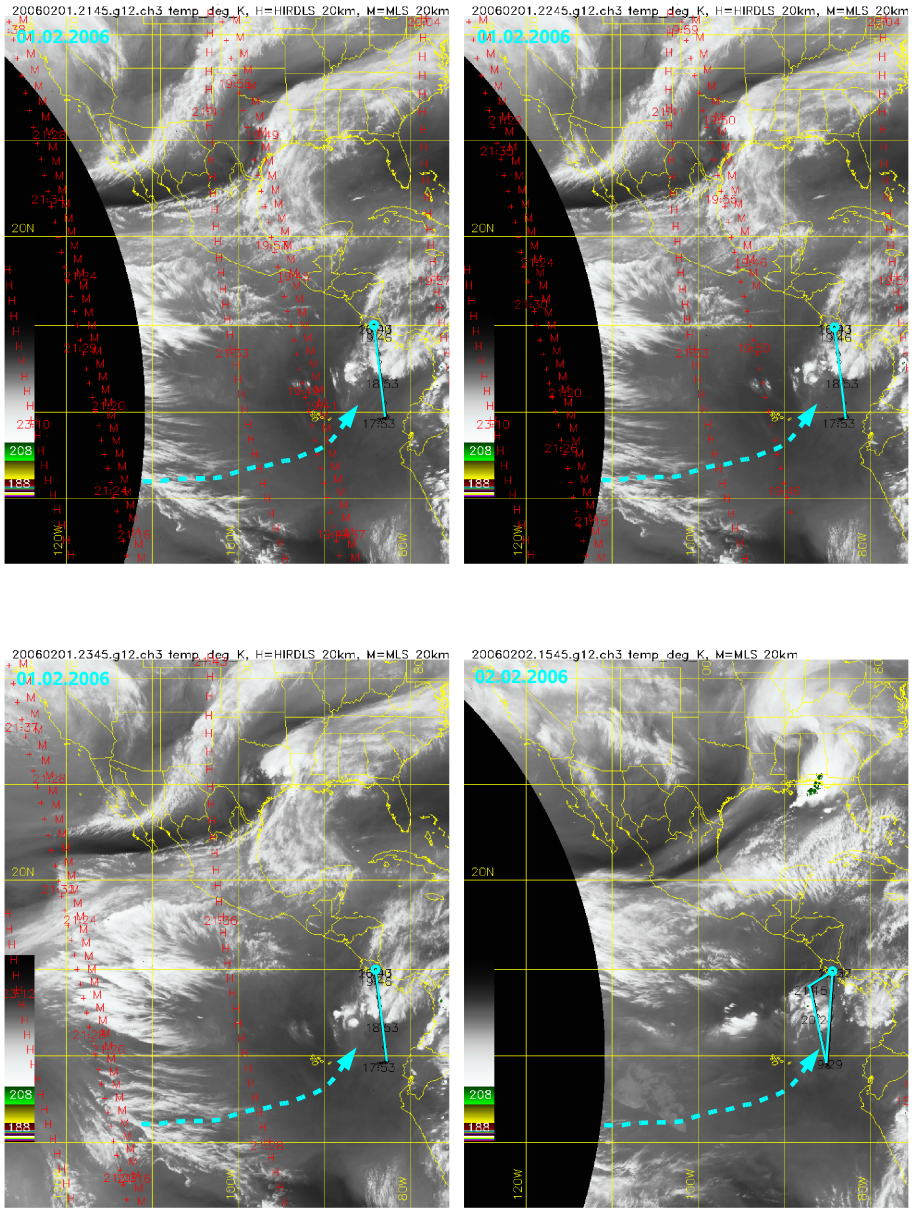

Figure A.2: GOES–12 satellite infrared imagery on 1st and 2nd February 2006 (colored bars: temperatures at top of clouds; greenish spots: convective systems; yellow contours: american continent; turquoise line: CR–AVE flight paths, corresponding to the depicted days; turquoise dashed arrow: track of sampled air parcels; capture time is given above each picture).

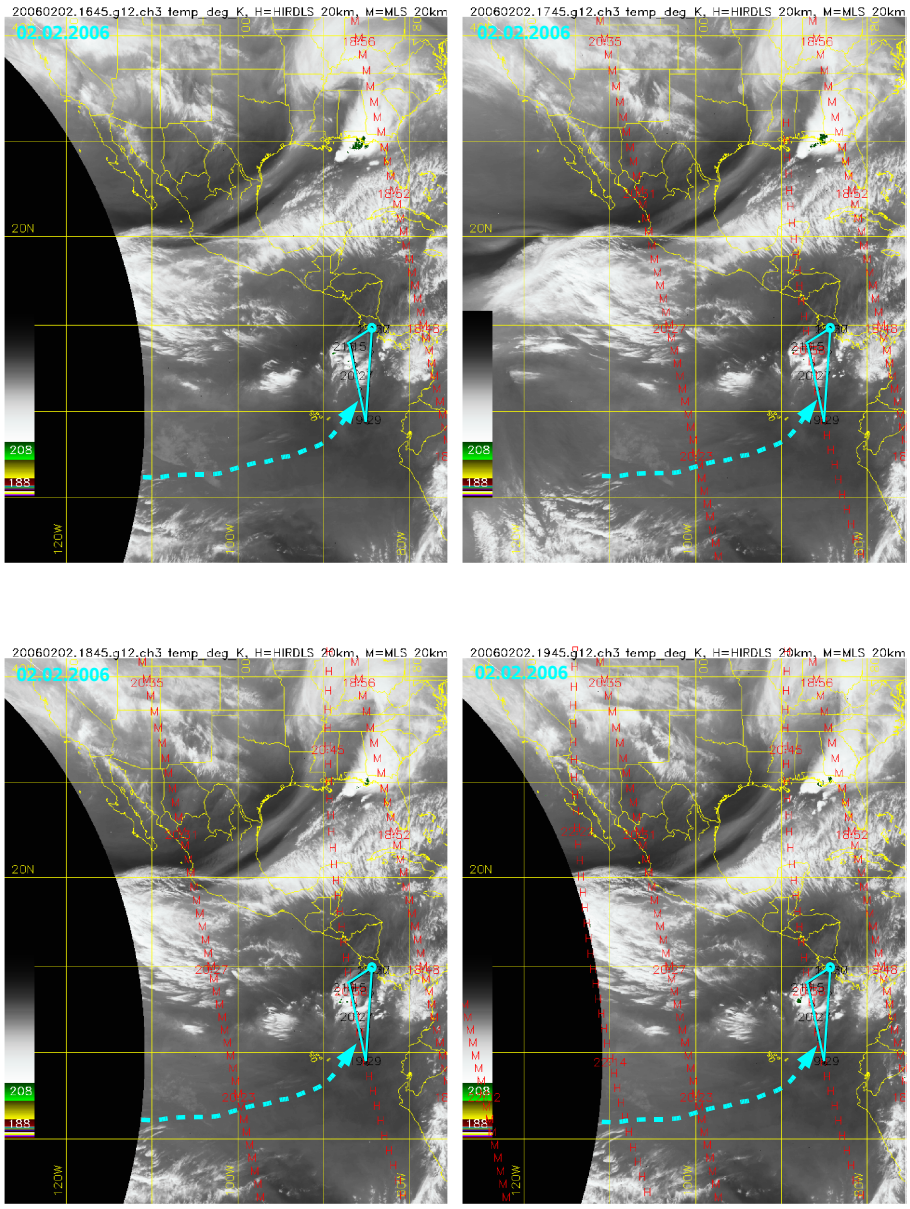

Figure A.3: GOES–12 satellite infrared imagery on 2nd February 2006 (colored bars: temperatures at top of clouds; greenish spots: convective systems; yellow contours: american continent; turquoise line: CR–AVE flight paths, corresponding to the depicted days; turquoise dashed arrow: track of sampled air parcels; capture time is given above each picture).

Appendix B

Subtropical Jet Stream

The subtropical jet stream is a band of relatively strong winds concentrated between 20° and 40° latitude in the middle and upper troposphere.

The analysis of the subtropical jet stream pattern on the 28–29th January 2006 shows good agreement with the history of the air parcels sampled on 2nd February in the cirrus cloud layer (Figure 4.2, see Section 4.1). The analysed air parcels start on 28th January above the Hawaii Islands (around 160W longitude and 20N latitude). The wind direction is towards south. The weakening of the subtropical jet stream (black arrows) may be the reason for the initiation of mesoscale waves, which are translated in the air parcel histories by the superimposed temperature fluctuations (Section 4.2.1).

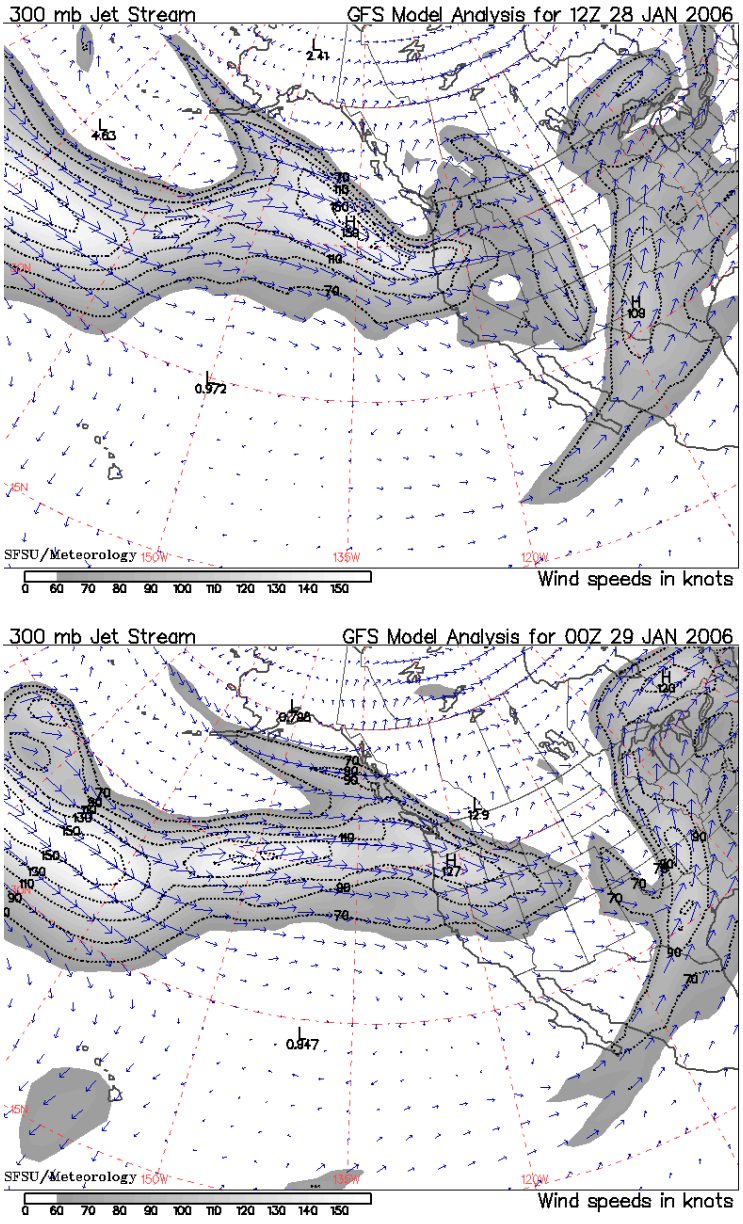

Figure B.1: Subtropical Jet Stream patern on 28–29th January 2006 (source: http://squall.sfsu.edu/crws/jetstream.html).

Appendix C

Extra CR – AVE sensitivity studies along the selected trajectory

Different scenarios of the formation and evolution of the very cold sub-visible tropical cirrus cloud on 2nd February 2006 were created by varying the model parameters as described in Section 4.3.

Four significant scenarios to illustrate the high sensitivity of microphysical processes to changes in the characterization/history of the described air parcel were selected and presented in detail in the Section 4.3.2. The first scenario ('best') simulated heterogeneous ice nucleation of soot coated with sulfuric acid ($N_{IN} = 0.01\,cm^{-3}$), with low amount of water and total accommodation of water on ice. The used amplitude of the superimposed temperature fluctuations is 0.6 K (Section 4.2.1). The other three scenarios diverge from the 'best' scenario by the freezing mechanism ('homogeneous'), available water amount ('more water') and accommodation coefficient α of water on ice ('lower accommodation'). The size distribution of the initialized aerosol, used in these scenarios, was characterized by $\bar{R}_{liq} = 0.01\,\mu m$ and $N_{liq} = 157\,cm^{-3}$ for the selected trajectory.

A variety of other scenarios are presented here (violet lines), which diverge from the 'best' scenario (red) by:

- the ice nuclei type – Mineral dust is considered the ice nucleus, initiating the heterogeneous freezing, and the scenario is named 'mineral dust' scenario;
- the amplitude of superimposed temperature fluctuations – The temperature fluctuations have an amplitude of 1.2 K and the scenario is named 'higher temperature fluctuations' scenario;
- the ice nuclei number density – Two scenarios are analysed for $N_{IN} = 0.001\,cm^{-3}$ and $N_{IN} = 0.1\,cm^{-3}$. The scenarios are named 'lower ice nuclei' / 'higher ice nuclei' scenario, respectively;

- the aerosol mean size – A mean radius of 0.1 μm (ten times bigger than the observed one) is initialized to describe the aerosol size distribution and the scenario is named 'bigger aerosol' scenario;
- aerosol number density – The tenth part of the probed aerosol number density is initialized (16 cm^{-3}) and the scenario is named 'few aerosol' scenario.

These scenarios are compared to the 'best' scenario. Temperature history is showed in the panel a of Figures C.3 – C.6. The ice crystal number density N_{ice} is shown in panels b (red: heterogeneous case, violet: other scenario). The relative humidity evolution RH_{ice} is depicted in panels c, the nitric acid partitioning in liquid aerosol and ice in the panels e and f, respectively. In panels d the integral ice particle size ($N_{ice} \cdot \bar{R}_{ice}$) is shown, as the parameter controlling the RH_{ice}.

Most of these scenarios contain a subsequent homogeneous freezing event. In these cases, the formed clouds show microphysical properties, time evolution of relative humidity and nitric acid partitioning similar to the 'homogeneous' case, discussed in Section 4.3.2: higher N_{ice}, smaller $\bar{R}_{ice}$. Since the integral ice particle size ($N_{ice} \cdot \bar{R}_{ice}$), as the parameter controlling the RH_{ice}, is higher than in the 'best' scenario (panels d), the water vapor depletion by the ice crystals is more efficient in the homogeneous case, so that RH_{ice} drops immediately after the secondary homogeneous ice nucleation event and fluctuates with the temperature fluctuations around saturation. After the abrupt RH_{ice} decrease, the interstitial particles shrink and nitric acid escapes in the gas phase (panels e). The 'homogeneous' clouds contain more nitric acid in ice (panels f). Because of these similarities among the scenarios, only differences and special features are discussed in the next sections.

C.1 The 'mineral dust' scenario

This scenario corresponds to the 'best' scenario, but simulates the deposition heterogeneous freezing on mineral dust particles. Mineral dust is a very efficient ice nuclei. The ice cloud form at lower RH_{ice} than in the 'best' scenario ($\approx$ 102 %, violet line in panel c of Figure C.1). Because of less water in the gas phase, less ice crystal appear (panel b). The water depletion is in the heterogeneously formed cloud less efficient than in the 'best' scenario. Thus, a subsequent ice nucleation event occurs, forming an ice cloud with the properties of the 'homogeneous cloud' (blue line in Section 4.3.2).

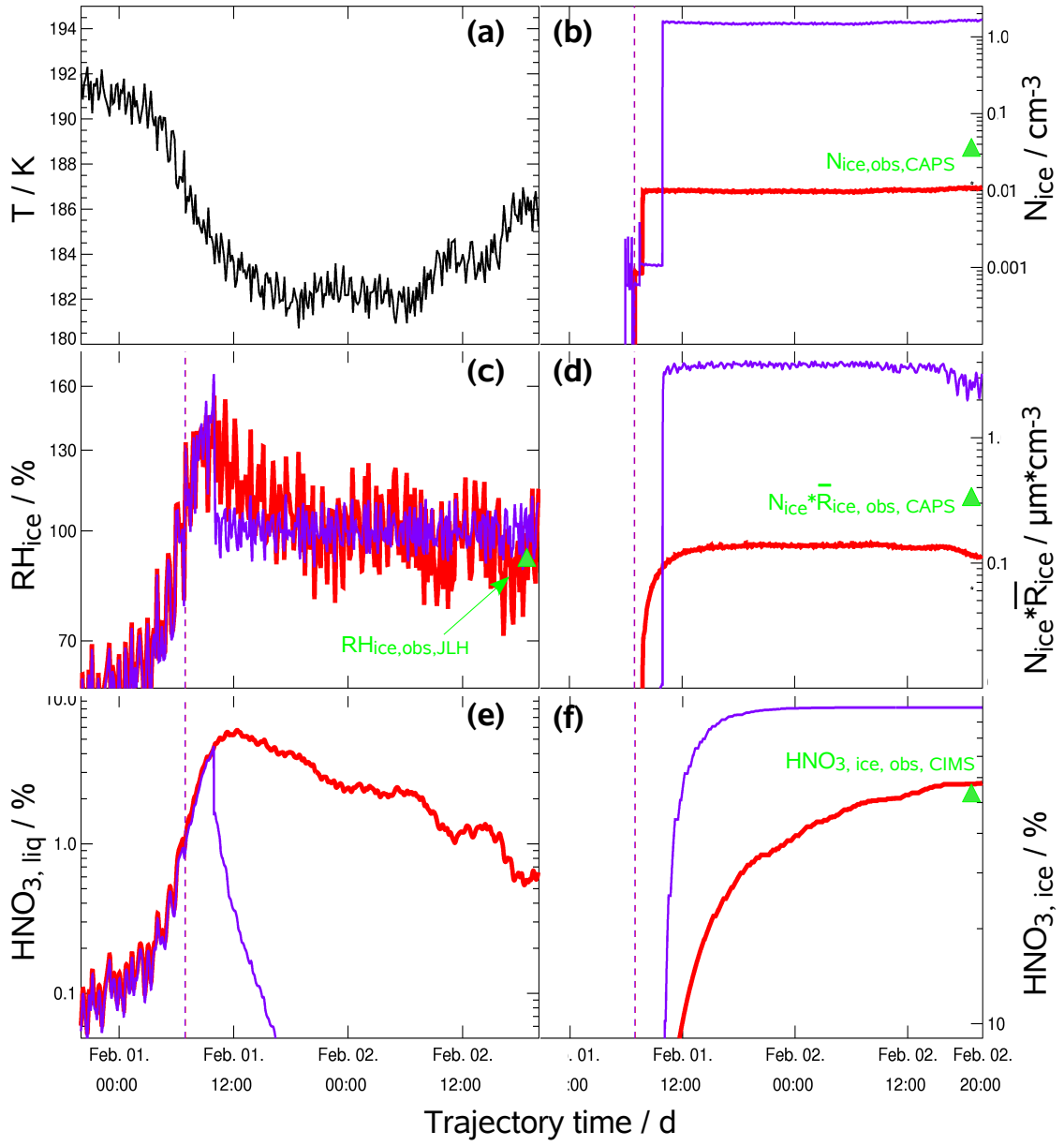

Figure C.1: Evolution of the CR-AVE cirrus along the selected trajectory in the 'mineral dust' scenario compared to the 'best' scenario(red: 'best', violet: 'mineral dust' scenario; a: temperature; b: ice crystal number density; c: relative humidity with respect to ice; d: number density · size of ice crystals; e: nitric acid in liquid aerosol; f: nitric acid in ice; dashed lines: appearance of first icThis scenario corresponds to the 'best' scenario, but the number densities of the ice nuclei are set to $N_{IN} = 0.001, 0.1\,cm^{-3}$. e crystals; green triangles: observations).

C.2 The 'higher temperature fluctuations' scenario

This scenario diverges from the 'best' scenario by the amplitude of the superimposed temperature fluctuations in the temperature history of the air parcel along the selected trajectory. The temperature history of the air parcel is determined in this case as described in 4.2.1, by superimposing temperature fluctuations with the amplitude of 1.2 K instead of 0.6 K like in the 'best' scenario. Consequently, after the initial heterogeneous ice cloud formation, higher cooling rates cause a subsequent homogeneous ice nucleation (see panel b of Figure C.3). Afterwards, the cloud acquires the microphysical properties of a 'homogeneous' cloud. The RH_{ice} fluctuations around 100 % have a higher amplitude than in the other 'homogeneous' scenarios due to the higher amplitude of the temperature fluctuations,

In order to evaluate the impact of the mesoscale temperature fluctuations on the freezing mechanism, multiple simulations are performed using randomly created variations. By increasing twofold the amplitude of the temperature fluctuations, the weight of the prevailing freezing mechanism moves from 90 % heterogeneously to 90 % homogeneously (Figure C.2).

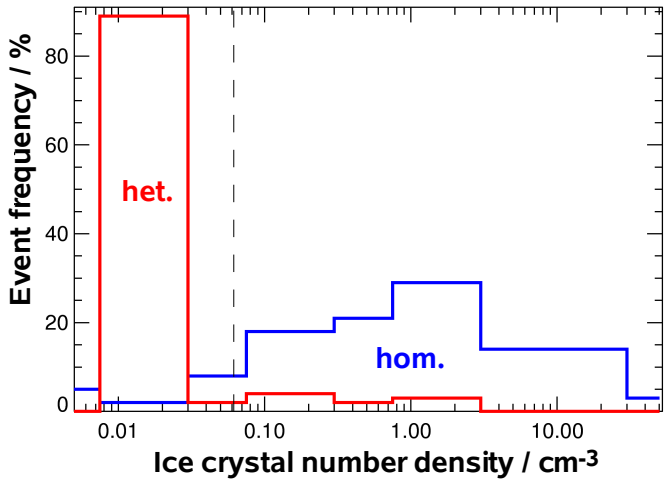

Figure C.2: Frequency of heterogeneous / homogeneous freezing in simulations using randomly created temperature fluctuations: distribution of ice crystal number densities; for details see Section 4.2.1; (temperature fluctuation amplitude red: 0.6 K, blue: 1.2 K)

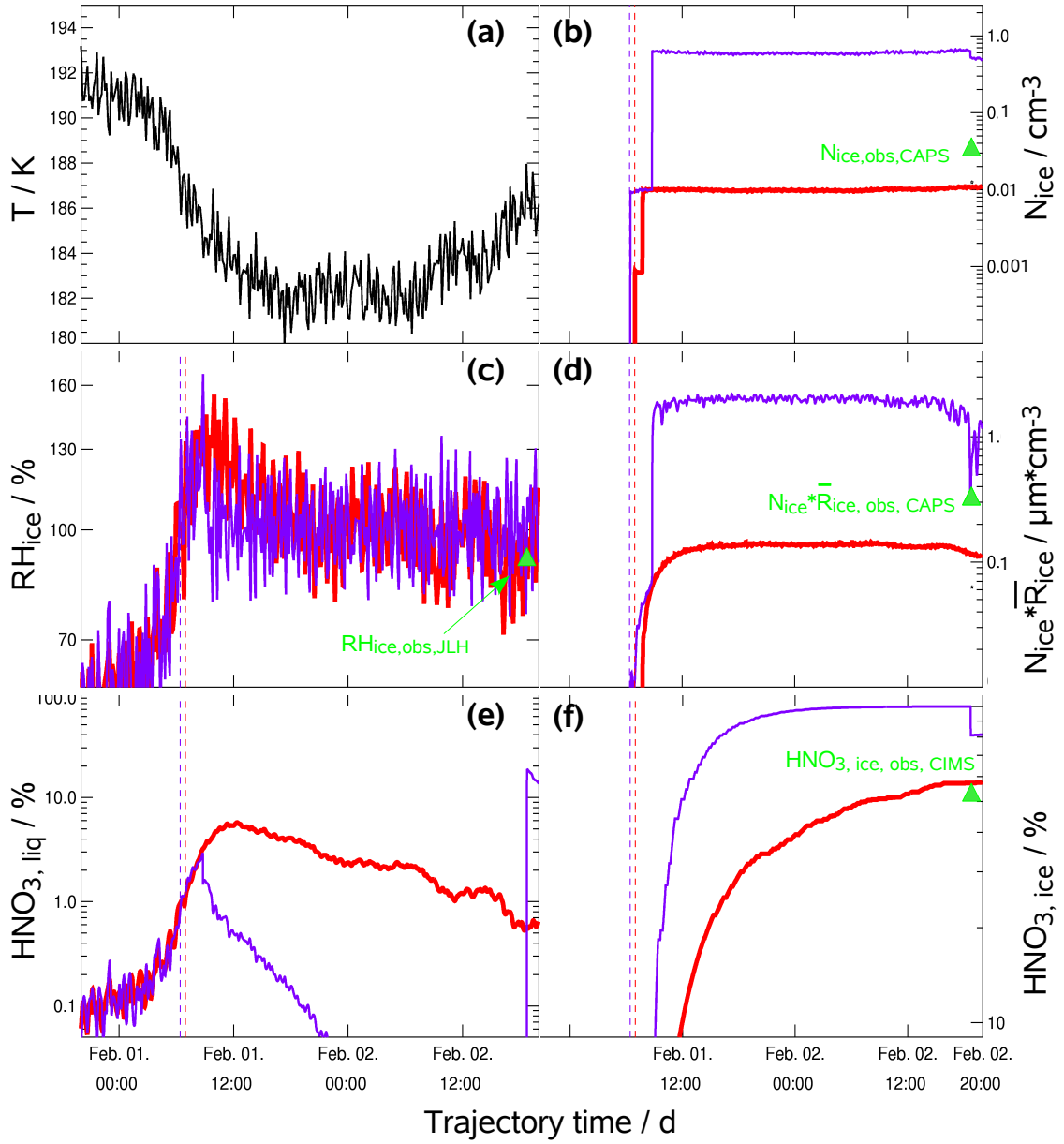

Figure C.3: Evolution of the CR-AVE cirrus along the selected trajectory in the 'higher temperature fluctuations' scenario compared to the 'best' scenario (red: 'best', violet: 'higher temperature fluctuations' scenario; a: temperature; b: ice crystal number density; c: relative humidity with respect to ice; d: number density · size of ice crystals; e: nitric acid in liquid aerosol; f: nitric acid in ice; dashed lines: appearance of first ice crystals; green triangles: observations).

C.3 The 'lower ice nuclei' / 'higher ice nuclei' scenario

This scenario corresponds to the 'best' scenario, but the number densities of the ice nuclei are set to $N_{IN} = 0.001,\ 0.1\,cm^{-3}$.

In the case of fewer available ice nuclei, a 'heterogeneous' cloud containing less ice crystals forms (violet line in panel b). The water depletion by the few ice crystals is inefficient, therefore higher RH_{ice} exist in the young cloud (violet line in panel c). After exceeding the homogeneous freezing threshold, the subsequent homogeneous freezing occurs. The cloud character changes from 'heterogeneous' to 'homogeneous' (Section C.1).

In the case of 'higher ice nuclei' (orchid), all $0.1\,cm^{-3}$ available ice nuclei freeze heterogeneously. In the formed cloud, the water depletion is effective enough, so that the increasing of RH_{ice} due to further cooling is compensated by the crystal growth. The conditions for a second homogeneous ice nucleation are not fulfilled. The simulated microphysics is comparable in this case with the observations. The simulated nitric acid partitioning in ice and interstitial particles is on the other hand very different from the observations. The microphysical properties of the cloud formed with $0.1\,cm^{-3}$ ice nuclei (orchid), as well as the partitioning of water and nitric acid are situated between the 'best' (red) and 'lower ice nuclei' (violet).

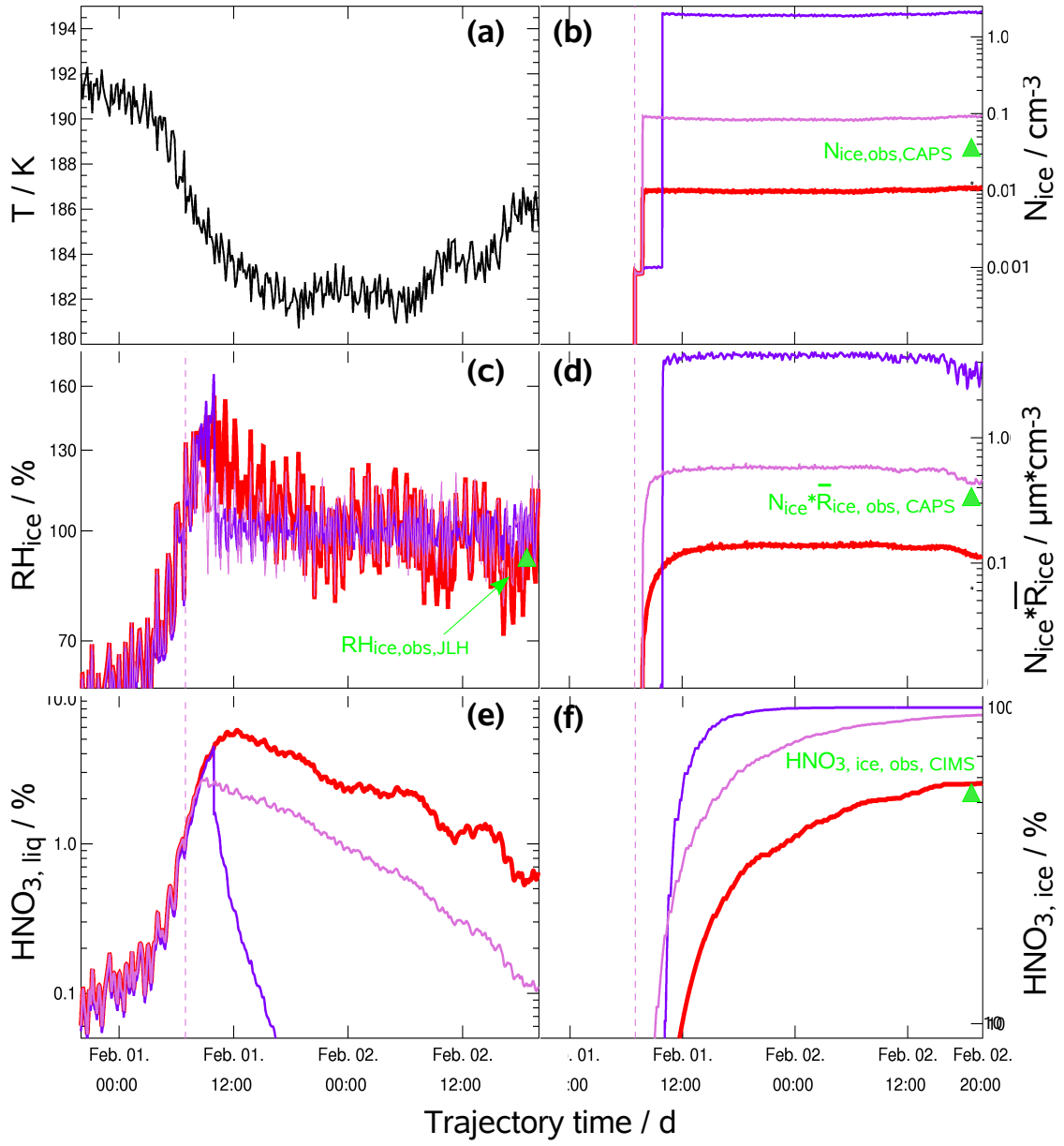

Figure C.4: Evolution of the CR-AVE cirrus along the selected trajectory in the 'lower ice nuclei' / 'higher ice nuclei' scenario compared to the 'best' scenario (red: 'best', violet: 'lower ice nuclei', orchid: 'higher ice nuclei'; a: temperature; b: ice crystal number density; c: relative humidity with respect to ice; d: number density · size of ice crystals; e: nitric acid in liquid aerosol; f: nitric acid in ice; dashed lines: appearance of first ice crystals; green triangles: observations).

C.4 The 'bigger aerosol' scenario

This scenario corresponds to the 'best' scenario, but the mean aerosol size used in the initialization is ten times bigger than the observed one (0.1 μm).

Since the probability of droplet freezing is proportional to the droplet volume (2.2), ice nucleation occurs some minutes earlier in aerosol of bigger mean sizes. In this case, no subsequent homogeneous freezing event follows. The microphysical properties, water and nitric acid are very similar to the 'best' scenario (panels b–f of Figure C.5. The interstitial particles contain more nitric acid because they are bigger (more water).

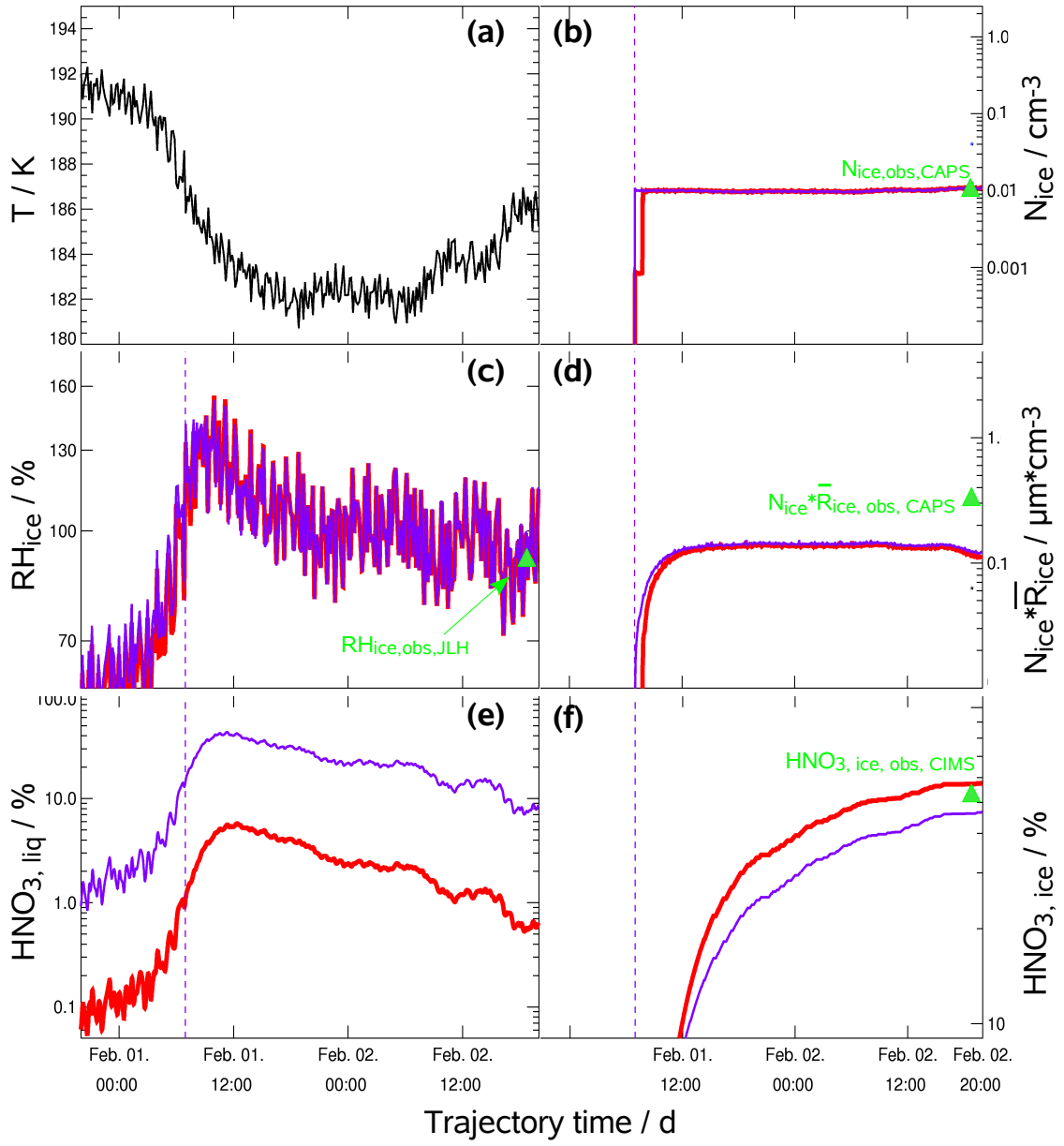

Figure C.5: Evolution of the CR-AVE cirrus along the selected trajectory in the 'bigger aerosol' scenario compared to the 'best' scenario (red: 'best', violet: 'bigger aerosol' scenario; a: temperature; b: ice crystal number density; c: relative humidity with respect to ice; d: number density · size of ice crystals; e: nitric acid in liquid aerosol; f: nitric acid in ice; dashed lines: appearance of first ice crystals; green triangles: observations).

C.5 The 'few aerosol' scenario

This scenario corresponds to the 'best' scenario, but the number density of background aerosol is set to the tenth part of the observed:

$$N_{liq,fewaerosol} = \frac{N_{liq}}{10} \tag{C.1}$$

Variation in the number density of background aerosol do not impact on the formation and evolution of the cloud (Figure C.6). The only difference between the two scenarios is the fraction of total nitric acid in the interstitial particles (panel e). This is lower in the 'few aerosol' scenario, because of the lower number density of aerosol particles.

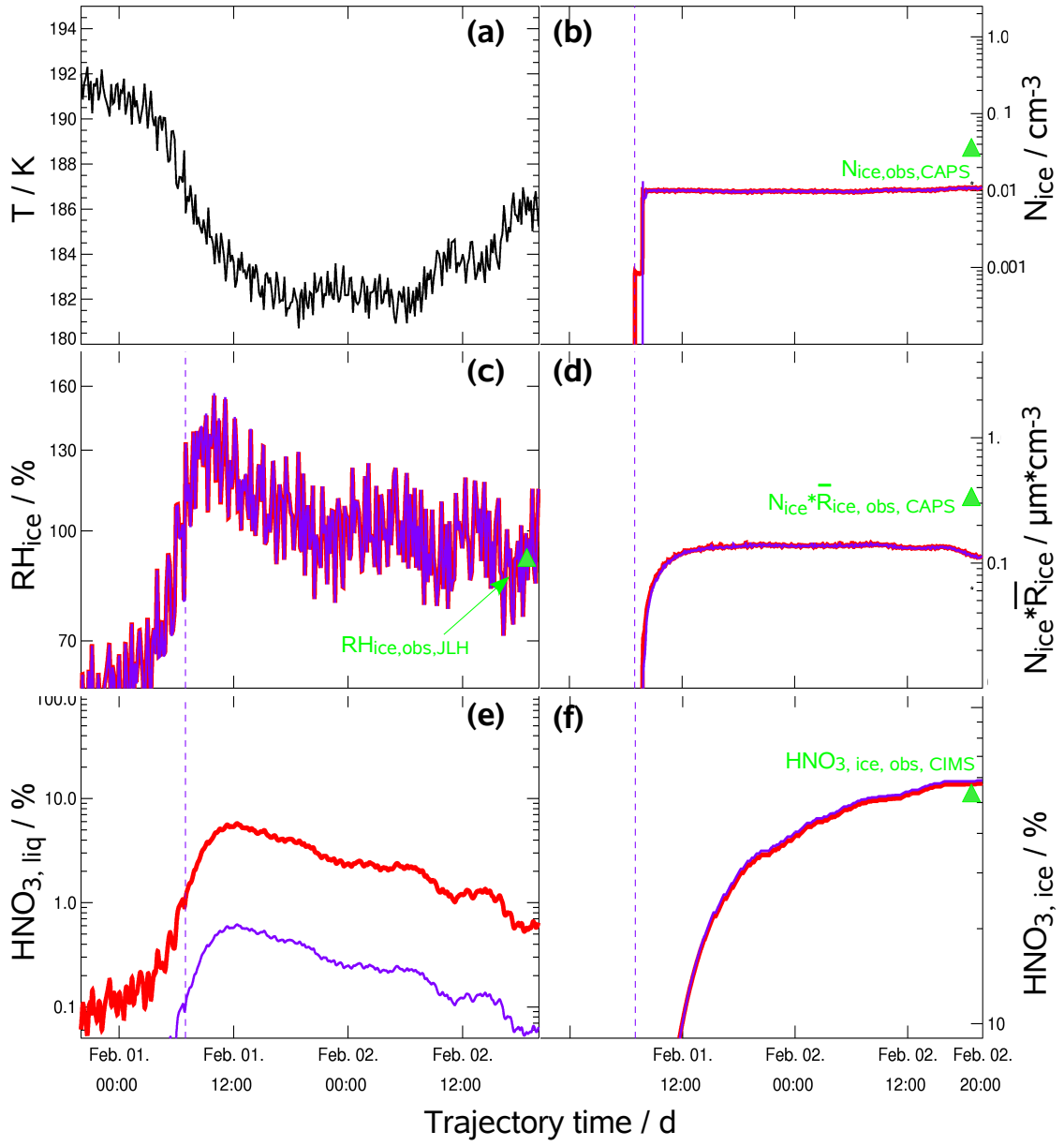

Figure C.6: Evolution of the CR-AVE cirrus along the selected trajectory in the 'few aerosol' scenario compared to the 'best' scenario (red: 'best', violet: 'few aerosol' scenario; a: temperature; b: ice crystal number density; c: relative humidity with respect to ice; d: number density · size of ice crystals; e: nitric acid in liquid aerosol; f: nitric acid in ice; dashed lines: appearance of first ice crystals; green triangles: observations).

Summary of the extra scenarios

As shown in Chapter 4, MAID simulations of the microphysics and H_2O / HNO_3 partitioning in a cloud formed heterogeneously, with low amount of water and total accommodation of water on ice, using as ice nuclei 0.01 cm^{-3} soot particles coated with sulfuric acid, the measured aerosol distribution and the amplitude of 0.6 K for the superimposed mesoscale temperature fluctuations on the temperature history, shows good agreement with the observations from 2nd February 2006. By changing the ice nuclei type and number density or the amplitude of the superimposed mesoscale temperature fluctuations, cloud form, which are very different to the probed cloud. The size distribution of the background aerosol do not influence dramatically the development of the cirrus cloud.

Bibliography

Anderson, B., et al. (1999), An assessment of aircraft as a source of particles to the upper troposphere, *Geophys. Res. Lett.*, *26*(20), 3069 – 3072.

Baumgardner, D., H. Jonsson, W. Dawson, D. O'Connor, and R. Newton (2001), The cloud, aerosol and precipitation spectrometer: a new instrument for cloud investigations, *Atmos. Res.*, *51*(1), 251 – 264.

Baumgardner, D., G. Kok, T. Garrett, E. Jensen, M. Krämer, and J. Mace (2006), The small particle dilemma: fracture or fiction?, Personal comunication on the AGU Fall Meeting, San Francisco, USA, 11–15 December.

Blake, D., and K. Kato (1995), Latitudinal distribution of black carbon soot in the upper troposphere and lower stratosphere, *J. Geophys. Res.*, *100*(D4), 7195 – 7202.

Borrmann, S., S. Solomon, L. Avallone, D. Toohey, and D. Baumgardner (1997), On the occurrence of ClO in cirrus clouds and volcanic aerosol in the tropopause region, *Geophys. Res. Lett.*, *24*(16), 2011 – 2014.

Bunz, H., and R. Dlugi (1991), Numerical studies on the behaviour of aerosols in smog chambers, *J. Aerosol Sci.*, *22*(4), 441 – 465.

Bunz, H., S. Benz, I. Gensch, and M. Krämer (2008), MAID: a model to simulate UT / LS aerosols and ice clouds, *Environ. Res. Lett.*, *3*, doi 10.1088/1748-9326/3/3/035001.

Carslaw, K., S. Clegg, and P. Brimblecombe (1995), A thermodynamic model of the system $HCl-HNO_3-H_2SO_4-H_2O$, including solubilities of HBr, from less than 200 to 328 K, *J. Phys. Chem. A*, *99*, 11,557 – 11,574.

Cziczo, D., P. DeMott, S. Brooks, A. Prenni, D. Thomson, D. Baumgardner, J. Wilson, S. Kreidenweis, and D. Murphy (2004a), Particle analysis by laser mass spectrometry

(PALMS) studies of ice nuclei and other low number density particles, *Geophys. Res. Lett.*, *31*(12).

Cziczo, D., D. Murphy, P. Hudson, and D. Thomson (2004b), Single particle measurements of the chemical composition of cirrus ice residue during CRYSTAL – FACE, *J. Geophys. Res.*, *109*(D4).

Cziczo, D., D. Thomson, T. Thompson, P. DeMott, and D. Murphy (2006), Measurements of the concentration and composition of nuclei for cirrus formation, *Proceedings of the National Academy of Sciences of the United States of America*, *100*(25), 14,655 – 14,660.

Cziczo, D., P. DeMott, D. Thomson, and D. Murphy (2007), Organic species and atmospheric ice formation, Personal comunication on the International Workshop on Upper Tropospheric Humidity, Karlsruhe, Germany, 12–15 JUN 2007.

Dahneke, D. (1983), *Theory of Dispersed Multiphase Flow*, chap. Simple kinetic theory of Brownian diffusion in vapors and aerosols, pp. 97 – 133, Academic Press, New York.

DeMott, P., D. Cziczo, A. Prenni, D. Murphy, S. Kreidenweis, D. Thomson, R. Borys, and D. Rogers (2003), Measurements of the concentration and composition of nuclei for cirrus formation, *Proceedings of the National Academy of Sciences of the United States of America*, *100*(25), 14,655 – 14,660.

Denning, R., S. Guidero, G. Parks, and B. Gary (1989), Instrument description of the airborne Microwave Temperature Profiler, *J. Geophys. Res.*, *94*(D14), 16,757 – 16,765.

Feigl, C., H. Schlager, H. Ziereis, J. Curtius, F. Arnold, and C. Schiller (1999), Observation of NO_y uptake by particles in the Arctic tropopause region at low temperatures, *Geophys. Res. Lett.*, *26*(14), 2215 – 2218.

Field, P., A. Heymsfield, and A. Bansemer (2006), Shattering and particle interarrival times measured by optical array probes in ice clouds, *J. Atmos. Ocean. Technol.*, *23*(10), 1357 – 1371.

Gamblin, B., et al. (2007), Nitric acid condensation on ice: 2. Kinetic limitations, a possible 'cloud clock' for determining cloud parcel lifetime, *J. Geophys. Res. – Atmos.*, *112*.

Gary, B. L. (2006), Mesoscale temperature fluctuations in the stratosphere, *Atmos. Chem. Phys.*, *6*, 4577 – 4589.

Gayet, J., F. Auriol, A. Minikin, J. Strom, M. Seifert, R. Krejci, A. Petzold, G. Febvre, and U. Schumann (2002), Quantitative measurement of the microphysical and optical properties of cirrus clouds with four different in situ probes: Evidence of small ice crystals, *Geophys. Res. Lett.*, *29*(24).

Gayet, J.-F., J. Ovarlez, V. Shcherbakov, M. Ström, U. Schuhmann, A. Minikin, F. Auriol, A. Petzold, and M. Monier (2004), Cirrus cloud microphysical and optical properties at southern and northern midlatitudes during the INCA experiment, *J. Geophys. Res.*, *109*.

Gensch, I., et al. (2008), Supersaturations, microphysics and nitric acid partitioning in a cold cirrus cloud observed during CR – AVE 2006: an observation-modelling intercomparison study, *Environ. Res. Lett.*, *3*, doi 10.1088/1748-9326/3/3/035003.

Gettelman, A., and D. Kinnison (2007), The global impact of supersaturation in a coupled chemistry – climate model, *Atmos. Chem. Phys*, *7*, 1629 – 1643.

Gierens, K., U. Schumann, M. Helten, H. Smit, and A. Marenco (1999), A distribution law for relative humidity in the upper troposphere and lower stratosphere derived from three years of MOZAIC measurements, *Ann. Geophys.-atmos. Hydros. Space Sci.*, *17*(9), 1218 – 1226.

Hendricks, J., B. Kärcher, A. Döpelheuer, J. Feichter, U. Lohmann, and D. Baumgardner (2004), Simulating the global atmospheric black carbon cycle: a revisit to the contribution of aircraft emissions, *Atmos. Chem. Phys.*, *4*, 2521 – 2541.

Hoyle, C., B. Luo, and T. Peter (2005), The Origin of High Ice Crystal Number Densities in Cirrus Clouds, *J. Atmos. Sci.*, *62*(7), 2568 – 2579.

IPCC (1999), Aviation and the Global Atmosphere., Cambridge University Press, UK.

IPCC Fourth Assessment Report (2007), Fourth Assessment Report, Working Group I, The Physical Science Basis of Climate Change, http://ipcc – wg1.ucar.edu/wg1/wg1 – report.html.

IPCC Second Assessment Report (2001), Climate Change 2001: The Scientific Basis, http://www.grida.no/climate/ipcc_tar/index.htm.

Jacobson, M. (2005), *Fundamentals of atmospheric modeling*, 2 ed., Cambridge University Press, New York.

Jänicke, R. (1998), *Atmospheric Particles*, chap. Atmospheric aerosol size distribution, pp. 1 – 28, John Wiley & Sons, New York.

Jensen, E., and O. Toon (1994), Ice nucleation in the upper troposphere - sensitivity to aerosol number density, temperature, and cooling rate, *Geophys. Res. Lett.*, *21*(18), 2019 – 2022.

Jensen, E., et al. (1998), Ice nucleation processes in upper tropospheric wave – clouds observed during SUCCESS, *J. Geophys. Res.*, *25*, 1363 – 1366.

Jensen, E., et al. (2005), Ice supersaturations exceeding 100% at the cold tropical tropopause: implications for cirrus formation and dehydration, *Atmos. Chem. Phys.*, *5*, 851 – 862.

Jensen, E., et al. (2007), Formation of large ($\simeq$100 μm) ice crystals near the tropical tropopause, *Atmospheric Chemistry and Physics Discussions*, *7*, 6255 – 6292.

Jonsson, H., et al. (1995), Performance of a focused cavity aerosol spectrometer for measurements in the stratosphere of particle size in the 0.06 – 2.0 μm diameter range, *J. Atmos. Ocean. Technol.*, *12*(11), 115 – 129.

Kärcher, B., and M. Basko (2004), Trapping of trace gases in growing ice crystals, *J. Geophys. Res.*, *109*(22).

Kärcher, B., and U. Lohmann (2002a), A parameterization of cirrus cloud formation: Homogeneous freezing of supercooled aerosols, *J. Geophys. Res.*, *107*(D2).

Kärcher, B., and U. Lohmann (2002b), A parameterization of cirrus cloud formation: Homogeneous freezing including effects of aerosol size, *J. Geophys. Res.*, *107*(D23).

Kärcher, B., and U. Lohmann (2003), A parameterization of cirrus cloud formation: Heterogeneous freezing, *J. Geophys. Res.*, *108*(D14).

Kärcher, B., and C. Voigt (2006), Formation of nitric acid/water ice particles in cirrus clouds, *Geophys. Res. Lett.*, *33*(8).

Kärcher, B., O. Möhler, P. J. DeMott, S. Pechtl, and F. Yu (2007), Insights into the role of soot aerosols in cirrus cloud formation, *Atmos. Chem. Phys.*, *7*(16), 4203 – 4227.

Khvorostyanov, V., H. Morrison, J. Curry, D. Baumgardner, and P. Lawson (2006), High supersaturation and modes of ice nucleation in thin tropopause cirrus: Simulation of

the 13 July 2002 Cirrus Regional Study of Tropical Anvils and Cirrus Layers case, *J. Geophys. Res. – Atmos.*, *111*(D2).

Kley, D., J. Russell III, and C. Phillips (2000), 2nd sparc report: Sparc assessment of upper tropospheric and stratospheric water vapour, *Tech. rep.*, SPARC – Stratospheric Processes And their Role in Climate.

Koop, T., and C. Marcolli (2007), The effects of organics on atmospheric ice nucleations, Personal comunication on the International Workshop on Upper Tropospheric Humidity, Karlsruhe, Germany, 12–15 JUN 2007.

Koop, T., B. Luo, A. Tsias, and T. Peter (2000), Water activity as the determinant for homogeneous ice nucleation in aqueous solutions, *Nature*, *406*, 611 – 614.

Krämer, M., C. Schiller, C. Voigt, and H. Schlager (2008a), An in-situ climatology in arctic, mid-latitude and tropical cirrus. a view on HNO_3 partitioning, submitt. Quart. J. Roy. Meteorol. Soc.

Krämer, M., et al. (2008b), Supersaturations in arctic, mid-latitude, tropical and artificial cirrus, submitt. Atmos. Chem. Phys.

Lohmann, U., B. Kärcher, and C. Timmreck (2003), Impact of the Mount Pinatubo eruption on cirrus clouds formed by homogeneous freezing in the ECHAM4 GCM, *J. Geophys. Res.*, *108*(D18).

Luo, B., K. Carslaw, T. Peter, and S. Clegg (1995), Vapor pressures of H_2SO_4/HNO_3 /HCl/HBr/H_2O solutions to low statospheric temperatures, *Geophys. Res. Lett.*, *22*(3), 247 – 250.

Luo, Z., W. Rossow, T. Inoue, and C. Stubenrauch (2002), Did the eruption of the Mt. Pinatubo Volcano affect cirrus properties?, *J. Climate*, *15*(19), 2806 – 2820.

Lynch, D., K. Sassen, D. O. Starr, and G. Stephens (Eds.) (2002), *CIRRUS*, Oxford University Press.

Magee, N., A. Moyle, and D. Lamb (2006), Experimental determination of the deposition coefficient of small cirrus – like ice crystals near – 50 degrees C, *Geophys. Res. Lett.*, *33*(17).

Mangold, A., R. Wagner, H. Saathoff, U. Schurath, C. Giesemann, V. Ebert, M. Krämer, and O. Möhler (2005), Experimental investigation of ice nucleation by different types of aerosols in the aerosol chamber AIDA: implications to microphysics of cirrus clouds, *Meteorol. Z.*, *14*(4), 485 – 497.

Marti, J., and K. Mauersberger (1993), A survey and new measurements of ice vapour pressure at temperatures between 170 K and 250 K, *Geophys. Res. Lett.*, *20*, 363 – 366.

Martin, E., C. George, and P. Mirabel (2000), Densities and surface tensions of $H_2SO_4/HNO_3/H_2O$ solutions, *Geophys. Res. Lett.*, *27*(2), 197 – 200.

May, R. (1998), Open – path, near – infrared tunable diode laser spectrometer for atmospheric measurements of H_2O, *J. Geophys. Res.*, *103*(D15), 19,161 –.

McKenna, D., P. Konopka, J.-U. Grooss, G. Günther, R. M"uller, R. Spang, D. Offermann, and Y. Orsolini (2002), A new Chemical Lagrangian Model of the Stratosphere (CLaMS) 1. Formulation of advection and mixing, *J. Geophys. Res.*, *107*(D16), art. No. 4309.

Meilinger, S., B. Kärcher, R. von Kuhlmann, and T. Peter (2001), On the impact of heterogeneous chemistry on ozone in the tropopause region, *Geophys. Res. Lett.*, *28*(3), 515 – 518.

Meilinger, S., et al. (1999), HNO3 partitioning in cirrus clouds, *Geophys. Res. Lett.*, *26*(14), 2207 – 2210.

Minikin, A., A. Petzold, J. Strom, R. Krejci, M. Seifert, P. van Velthoven, H. Schlager, and U. Schumann (2003), Aircraft observations of the upper tropospheric fine particle aerosol in the northern and southern hemispheres at midlatitudes, *Geophys. Res. Let.*, *30*(10).

Minnis, P., J. Ayers, R. Palikonda, and D. Phan (2004), Contrails, cirrus trends, and climate, *J. Climate*, *17*(8), 1671 – 1685.

Möhler, O., C. Linke, H. Saathoff, M. Schnaiter, R. Wagner, A. Mangold, M. Krämer, and U. Schurath (2005), Ice nucleation on flame soot aerosol of different organic carbon content, *Meteorologische Zeitschrift*, *14*(4), 477 – 484.

Möhler, O., et al. (2005), Effect of sulfuric acid coating on heterogeneous ice nucleation by soot aerosol particles, *J. Geophys. Res.*, *110*(D11).

Murphy, D., et al. (2006), Single – particle mass spectrometry of tropospheric aerosol particles, *J. Geophys. Res.*, *111*(D23).

Murphy, D. M., D. J. Cziczo, P. K. Hudson, and D. S. Thomson (2007), Carbonaceous material in aerosol particles in the lower stratosphere and tropopause region, *J. Geophys. Res.*, *112*(D4).

Neuman, J., et al. (2000), A fastresponse chemical ionization mass spectrometer for in situ measurements of HNO3 in the upper troposphere and lower stratosphere, *Rev. Sci. Instrum.*, *71*, 3886 – 3894.

Neuman, J., et al. (2001), In situ measurements of HNO_3, NO_y, NO, and O_3 in the lower stratosphere and upper troposphere, *Atmos. Environ.*, *35*, 5789 – 5797.

Ovarlez, J., J. Gayet, K. Gierens, J. Strom, H. Ovarlez, F. Auriol, R. Busen, and U. Schumann (2002), Water vapour measurements inside cirrus clouds in Northern and Southern hespheres during INCA, *Geophys. Res. Lett.*, *29*(16).

Peter, T., C. Marcolli, P. Spichtinger, T. Corti, M. Baker, and T. Koop (2006), When dry air is too humid, *Science*, *314*(5804), 1399 – 1401.

Popp, P., et al. (2004), Nitric acid uptake on subtropical cirrus cloud particles, *J. Geophys. Res. – Atmos.*, *109*(D6).

Popp, P., et al. (2006), The observation of nitric acid – containing particles in the tropical lower stratosphere, *Atmos. Chem. Phys.*, *6*, 601 – 611.

Pruppacher, H., and J. Klett (1997), *Microphysics of Clouds and Precipitation*, 2nd ed., Kluwer Academic.

Ramanathan, V., P. Crutzen, J. Kiehl, and R. D. (2001), Aerosols, Climate, and the Hydrological Cycle, *Science*, *294*(5549), 2119 – 2124.

Richardson, M., et al. (2007), Measurements of heterogeneous ice nuclei in the western United States in springtime and their relation to aerosol characteristics, *J. Geophys. Res.*, *112*(D2).

Schiller, C., et al. (1999), Ice particle formation and sedimentation in the tropopause region: A case study based on in situ measurements of total water during POLSTAR 1997, *Geophys. Res. Lett.*, *26*(14), 2219 – 2222.

Schlicht, S. (2006), Untersuchungen zur Wasser–Partitionierung in Zirruswolken, Doctoral thesis, Bergische Universität Wuppertal.

Schwarz, J., et al. (2006), Single-particle measurements of midlatitude black carbon and light-scattering aerosols from the boundary layer to the lower stratosphere, *J. Geophys. Res.*, *111*(D16).

Scott, S., T. Bui, K. Chan, and S. Bowen (1990), The meteorological measurement system on the NASA ER – 2 aircraft, *J. Atmos. Ocean. Technol.*, *7*(4), 525 – 540.

Seifert, M., J. Strom, R. Krejci, A. Minikin, A. Petzold, J. Gayet, U. Schumann, and J. Ovarlez (2003), In-situ observations of aerosol particles remaining from evaporated cirrus crystals: Comparing clean and polluted air masses, *Atmos. Chem. Phys.*, *3*, 1037 – 1049.

Shilling, J. E., M. A. Tolbert, O. B. Toon, E. J. Jensen, B. J. Murray, and A. K. Bertram (2006), Measurements of the vapor pressure of cubic ice and their implications for atmospheric ice clouds, *Geophys. Res. Lett.*, *33*(17).

Solomon, S., S. Borrmann, R. Garcia, R. Portmann, L. Thomason, L. Poole, D. Winker, and M. McCormick (1997), Heterogeneous chlorine chemistry in the tropopause region, *J. Geophys. Res.*, *102*(D17), 21,411 – 21,429.

Stör, J., and R. Bulirsch (1993), *Introduction to Numerical Analysis*, 2 ed., Springer, New York.

Tabazadeh, A., O. Toon, and E. Jensen (1997), Formation and implications of ice particle nucleation in the stratosphere, *Geophys. Res. Lett.*, *24*(16), 2007 – 2010.

Tabazadeh, A., O. Toon, and E. Jensen (1999), A surface chemistry model for nonreactive trac gas adsorption on ice: Implications for nitric acid scavenging by cirrus, *Geophys. Res. Lett.*, *26*(14), 2211 – 2214.

Ullerstam, M., and J. Abbatt (1997), Interaction of HNO_3 with water – ice surfaces at temperatures of the free troposphere, *Geophys. Res. Lett.*, *24*(12), 1479 – 1482.

Ullerstam, M., and J. Abbatt (2005), Burial of gas-phase HNO_3 by growing ice surfaces under tropospheric conditions, *Phys. Chem. Chem. Phys.*, *7*(20), 3596 – 3600.

VDI–Wärmeatlas (2006), Vdi–gesellschaft verfahrenstechnik und chemieingenieurwesen (gvc), Springer, Berlin, chapter: Berechnungsmethoden fuer Stoffeigenschaften.

Voigt, C., et al. (2006), Nitric acid in cirrus clouds, *Geophys. Res. Lett.*, *33*(5).

von Hobe, M. (2008), Chlorine activation on cirrus clouds in the tropical UTLS, *submitt. Geophys. Res. Lett.*

Webster, C., R. May, C. Trimble, R. Chave, and J. Kendall (1994), Aircraft (ER – 2) Laser Infrared Absorption Spectrometer (ALIAS) for In-situ Stratospheric Measurements of HCl, N_2O, CH_4, NO_2, and HNO_3, *Appl. Opt.*, *33*(3), 454 – 472.

Weinstock, E., E. Hintsa, A. Dessler, J. Oliver, N. Hazen, J. Demusz, N. Allen, L. Lapson, and J. Anderson (1994), New fast response photofragment fluorescence hygrometer for use on the NASA ER – 2 and the Perseus remotely piloted aircraft, *Rev. Sci. Instrum.*, *65*(12), 3544 – 3554.

Wexler, A., and S. Potukuchi (1998), *Atmospheric Particles*, chap. Kinetics and thermodynamics of tropospheric aerosols, pp. 203 – 231, John Wiley & Sons, New York.

Yin, Y., K. Carslaw, and D. Parker (2002), Redistribution of trace gases by convective clouds – mixed – phase processes, *Atmos. Chem. Phys.*, *2*, 293 – 306.

Ziereis, H., H. Schlager, H. Fischer, C. Feigl, P. Hoor, R. Marquardt, and V. Wagner (2000), Aircraft measurements of tracer correlations in the Arctic subvorter region during the Polar Stratospheric Aerosol Experiment (POLSTAR), *J. Geophys. Res.*, *105*(D19), 24,305 – 24,313.

Abreviations

AIDA Aerosol-Interaktionen und -Dynamik in der Atmosphäre

ALIAS Aircraft Laser Infrared Absorption Spectrometer

CAPS Cloud Aerosol and Precipitation Spectrometer

CIMS Chemical Ionization Mass Spectrometer

CLaMS Chemische LAGRANGE'sche Modell der Stratosphäre

CR–AVE Costa Rica – Aura Validation Experiment

CRYSTAL–FACE Cirrus Regional Study of Tropical Anvils and Cirrus Layers – Florida Area Cirrus Experiment

DLR Deutsches Zentrum für Luft- und Raumfahrt

ECMWF European Centre for Medium-Range Weather Forecasts

FCAS Focused Cavity Aerosol Spectrometer

FZJ Forschungszentrum Jülich

FZK Forschungszentrum Karlsruhe

GOES Geostationary Operational Environmental Satellites

HALOE HALogen Occultation Experiment

HWV Harvard Water Vapor instrument

ICG Institut für Chemie und Dynamik der Geosphäre

IMK Institut für Meteorologie und Klimaforschung

IN Ice Nuclei

ISSR Ice SuperSaturated Regions

IWC Ice Water Content

IPCC Intergovernmental Panel of Climate Change

JLH JPL Laser Hygrometer

JPL Jet Propulsion Laboratory

MAID Model for Aerosol and Ice Dynamics

MMS Meteorological Measurement System

MTP Microwave Temperature Profiler

NASA National Aeronautics and Space Administration

NH Northern Hemisphere

N–MASS Nucleation–Mode Aerosol Size Spectrometer

ppbv parts per billion by volume

ppmv parts per million by volume

POLSTAR POLar STratospheric AeRosol Experiment

RH_{ice} Relative Humidity with respect to ice

STS supercooled ternary solution

SH Southern Hemisphere

SVC Sub-Visible Cirrus

TDL Tunable Diode Laser

TTL Tropical Tropopause Layer

UT Upper Troposphere

ut universal time

We shall not cease from exploration
and the end of all our exploring will be to arrive where we started...
and know the place for the first time.

Thomas Stearns Eliot (1888 – 1965))

Jül-4286
Januar 2009
ISSN 0944-2952